MULTIPLE JET CHARACTERISTICS

by

Mrinal Kaushik

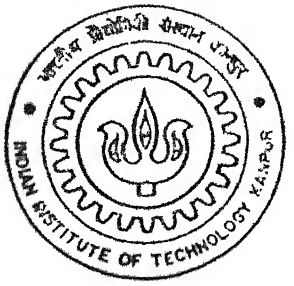

DEPARTMENT OF AEROSPACE ENGINEERING

Indian Institute of Technology Kanpur

DECEMBER, 2002

MULTIPLE JET CHARACTERISTICS

A Thesis Submitted in Partial Fulfillment of the Requirements
for the Degree of

MASTER OF TECHNOLOGY

by

MRINAL KAUSHIK

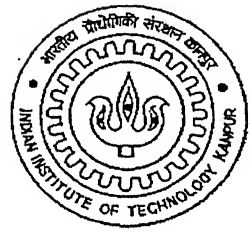

Department of Aerospace Engineering
Indian Institute of Technology Kanpur, India
December 2002

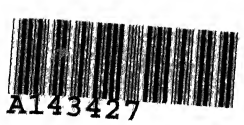

Dedicated to my

Mentor

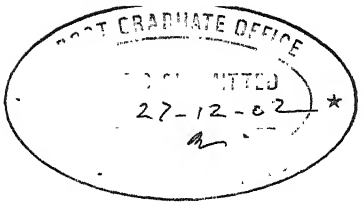

CERTIFICATE

It is certified that the work contained in the thesis entitled "**MULTIPLE JET CHARATERISTICS**" by Mrinal Kaushik, has been carried out under my supervision and that this work has not been submitted elsewhere for a degree.

Prof. E. Rathakrishnan
Department of Aerospace Engineering
Indian Institute of Technology Kanpur

December 27, 2002

ACKNOWLEDGEMENT

I record my deep sense of gratitude to Prof. E. Rathakrishnan for his great guidance, full freedom, constant encouragement, immense patience and benevolence. It was a privilege to be associated with him, which was a rich, memorable and cherishing experience.

I must acknowledge with lot gratitude, the spontaneous assistance and co-operation extended by Mr. Suresh Mishra, Mr. Sharad Chauhan and Mr. Shishupal Singh of High Speed Aerodynamics Laboratory, Dept. of Aerospace Engg.

I thank Mr. S. S. Chuahan, Incharge of Aerospace workshop and his technical team for fabricating the models of my work.

I thank Mr. Girish, the photographer, Maa Jaanaki Studio, Kalyanpur Road, Kanpur for recording all the visualization and experimental setting of this thesis.

I want to thank my friends who helped me in various stages and for their mental support. The blessings of my parents and my family members have been an invaluable source of inspiration.

Mrinal Kaushik.

Abstract

The aerodynamic mixing characteristics of triple jet, with different Mach numbers of core and surrounding jets, was investigated experimentally. The multijet decays much faster than the individual jets. The shock cell length for the multijet is significantly lower than the individual jets. The entrainment of the jet depends strongly on the level of expansion (NPR).

CONTENTS

List of Figures

Nomenclature

NPR	Nozzle Pressure Ratio (P_0/P_a)
PRV	Pressure Regulating Valve
M	Nozzle exit Mach number
M_1	Mach number upstream of the shock
P	Centerline Pitot Pressure
P_a	Ambient Pressure
P_0	Stagnation Pressure in the settling chamber
m_j	Total mass flow at j^{th} Location
m_{exit}	Mass flow at Nozzle exit
B	Local cross sectional half width of the Jet
B_{max}	Total cross sectional half width of the Jet
U	Local velocity in the jet field
U_{max}	Centerline velocity of the Core Jet
D_e	Core nozzle exit diameter
X	Co-ordinate perpendicular to nozzle exit plane
Y	Transverse Co-ordinate (See Page no. 64)
Z	Transverse Co-ordinate (See Page no. 64)
P_{01}	Upstream stagnation pressure (Before shock)
P_{02}	Downstream stagnation pressure (After shock)
γ	Specific heat ratio of air
L_s	Length of the shock cell

Chapter 1

Introduction

Multijet phenomenon in the regime of supersonic Mach numbers is the subject of investigation for a large number of investigators over a long period. This finds application in many engineering problems of practical interest, like flow field of a booster motor in spacecraft. Voluminous literature is available for both subsonic and supersonic jet propagation, analyzing mixing phenomenon of multijet, bringing out the decay, spread and the entrainment characteristics. But most of the researchers focused their attention on multijets configurations, which are of academic interest only. Further, other than the jet features, they hardly have focused their attention on the base pressure field. This base pressure field in the case of rockets and missiles plays a vital role from drag point of view and also due to the fact that the high temperature plumes exciting the nozzle will get attracted towards the base region when the base pressure is at low sub atmospheric level. This causes concern, since the heated base might affect the electronic devices, which are housed inside the rocket shell. Therefore, care must be taken to ensure that the base pressure is kept at reasonably high level so that the base heating can be prevented. The base flow is dictated by the merging location and the entrainment characteristics. A multijet which decays faster and entrains the mass from the surrounding atmosphere and the base region which strongly influence the base pressure. If the entrainment is large just after nozzle exit, the base will experience very low pressure this will cause the hot stream coming out of the nozzle to get deflected towards the base and the associated thermal radiations due to large temperature difference between hot jet and the environment will result in severe heating of the base. Therefore, a deep and thorough understanding of the merging, decay and influence characteristics of multijet is needed. Understanding the performance of practical configurations will be of high technical value for the launch vehicle applications. With these in mind the present study, with a configuration similar to that of GSLV Mark II is studied in the present work.

1.1 Multijet offer the following advantages

- Requires less total nozzle length in comparison to a single exhaust nozzle.
- Controllability in pitch, yaw and roll by swiveling the individual nozzles.
- Additional thrust at higher altitudes and in space gained by increasing the base pressure of rocket vehicles.
- Significant thrust increase from use of common multijet-nozzle shroud which have a similar effect as an increase of the area ratio of nozzles.
- Thrust augmentation of shrouded cluster nozzles gained by adapting atmospheric air to the exhaust flow at low and medium altitudes.

By keeping above points in mind, in the present investigation multijet configuration as shown in Figure.1, has 3 jets cluster has been studied experimentally. The parameters considered in the study are; number of jets, jet configurations and level of expansion. The jet Mach number considered in the study for the core nozzle is 1.6 and for strapon 2.5. All the nozzles were convergent-divergent axisymmetric nozzles. The attention was mainly focused on centerline decay of individual nozzle as well as multijets. Mass entrainment effects are also studied for various combinations of nozzles with different level of expansion.

1.2 Aim of the Present Investigation

The present investigation is mainly concentrated on studying the following aspects of the multijet flow field,

1. Overall centerline decay for different NPRs (i.e. Nozzle pressure ratios).
2. Mass entrainment for different configurations of nozzles with various NPRs.
3. Velocity profiles at various NPRs for Multijet.
4. Optical flow visualization for all nozzles.

1.3 Literature Survey

The literatures directly associated with the present investigation are reviewed briefly in this section.

Twin, triple and four jet configurations with Laval nozzles at supersonic Mach numbers has been studied by **Rathakrishnan** [1]. In this investigation, the analysis has been done by varying the inter nozzle spacing between the jets. The entrainment characteristics and the jet decay for different combination of configurations and flow parameters have been studied. However, the base pressure has not been investigated in this study.

Moustaffa and Rathakrishnan [2] have studied the flow field of multijet with square configuration issuing from axisymmetric Laval nozzles. The result highlights the strong influence of pressure ratio on the jet decay. However, the inter-nozzle spacing is found to be of only marginal effect on centerline decay. The nozzle configuration plays a dominant role on the mixing process.

Tam et al [3] studied the turbulent mixing noise from supersonic jets, and compared the calculated and measured noise directivity, for different Strouhal numbers. At lower jet Mach numbers and temperatures, the propagation speeds of the instability waves are greatly reduced. The Mach wave noise generation mechanism would become less efficient.

Raman et al [4] studied experimentally (both singles and doubles bevel) supersonic jets from beveled rectangular nozzles for jet mixing and noise production. They observed that for reduction of peak mixing noise for the doubled beveled convergent-divergent nozzle operated at design pressure ratio. All beveled geometries provided screech noise reduction for under expanded jets and an upstream mixing noise directivity shift which would be beneficial for improved acoustics treatment performance of a shrouded system.

Norum et al [5] studied the screech in supersonic jets (under-expanded). They observed that, for a given configuration and operating condition, existing of multiple stages of screech shows a large scale changes which occur randomly with time. A small

modification on external surface of the tube at the jet exit had a large effect on the process.

Raman et al [6] studied the jet mixing control using excitation from miniature oscillating jets. They observed that the jets velocity decay more rapidly for the forced than the unforced. The normalized mass flux ratio was higher for the forced than for the unforced and both the methods of jet excitation produced approximately the same increase in the mass flux ratio.

1.3.1 Synopsis:

From the above literature it is evident that almost all the available literature on multijet is on the collective nature of the combined jets from multiple nozzles. Further, mass entrainment phenomenon is hardly looked into. Hence there is a need for studying the multiple jets focusing attention on the effect of neighboring jets on the center jet and mass entrainment from surroundings into the combined multiple jets. Since the mixing process and the shock structure (shock strength and core length) has a dominant effect on the jet noise, investigation relating the jet noise through sound level measurement is of importance.

Chapter 2

Experimental Setup and Procedure

2.1 Experimental Setup

The experimental facility consists of the following components.

- Jet test setup
- Compressed air tanks
- Compressor
- Pressure measuring system
- Optical flow visualization system

2.1.1 Jet Test Facility

Setup of the jet test facility is shown in Figure. 2a. It consists of a settling chamber, with a provision to mount the jet nozzles on its end plate. The settling chamber is fed with the compressed dry air at high pressure through PRV (Pressure Regulating Valve) which controls the settling chamber pressure at any desired level. The settling chamber is provided with wire mesh screens to control the flow entering it to attain settled equilibrium before expansion through the jet nozzles.

2.1.2 Compressed Air Tanks

The storage system consists of 3 vessels of volume 1000 cubic foot each. The compressed air stored in these tanks at a pressure of about 250 psi is used to drive the jets.

2.1.3 Compressor

A reciprocating compressor with a discharge of 360 cfm, driven by 150 hp electrical motor, is used to charge the storage tanks. Compressed air from the compressor is passed through a filter unit to remove the impurities and oil contamination, and then passed through drier units containing silica gel with electrical heating before reaching the storage tank.

2.1.4 Pressure Measuring System

It has dial type bourdon pressure gauge for the rough monitoring of settling chamber pressure, multi-tube water manometries and 16 channels PSI (Pressure System International) make pressure transducer with 300-psi range. The pressure probe used is pitot in the jet field a rigid 3-D traverse with 6 degrees of freedom (3 translation and 3 rotational) and having the least count of 0.10 mm in linear motion and 0.5 degree in angular motion is used.

2.1.5 Optical Flow Visualization System

It consists of an arc lamp source with provision to vary the intensity, two parabolic eight-inch diameter concave mirrors with a focal length of 1.75 m and a screen. Direct shadow was used for the measurement of core length. To facilitate the direct measurement of core length, the image of specially made pointer mounted on the traverse is captured on the screen along with the shock structure. The shadow graphic views of shock cell structures are shown in Figures 2b to 2j.

2.2 Experimental Models

Two convergent-divergent nozzles of Mach number 1.6 and 2.5 shown in Figure 2k, were used. The exit diameter of core nozzle (Mach number 1.6) was 2.4 cm. The exit diameter of strapon nozzle (Mach number 2.5) was 1.3 cm. The strapon was mounted with 6 degree outward canting with reference to core nozzle axis on the common base block.

2.3 Experimental Procedure

2.3.1 Center line Pressure Decay

The models were mounted on the settling chamber and all the joints were leak tested. The required pressure in the settling chamber (P_0) was maintained by controlling the PRV (Pressure Regulating Valve). The pressure tap at the settling chamber was connected to a port of PSI system and P_0 was monitored continuously. The pitot probe mounted on the traverse was aligned to face the jet axis at the nozzle exit and the pitot pressure was recorded by connecting the pitot tube to another port of the PSI system. Since the jet Mach number is supersonic, the pitot pressure [P_{02}] measured is the pressure downstream of the bow shock at the pitot probe mouth. Using the normal shock relation given below the jet Mach number has been calculated.

$$\frac{P_{02}}{P_{01}} = \left(1 + \frac{2\gamma}{(\gamma+1)}(M_1^2 - 1)\right)^{\frac{-1}{(\gamma-1)}} \left\{\frac{(\gamma+1)M_1^2}{(\gamma-1)M_1^2 + 2}\right\}^{\frac{\gamma}{(\gamma-1)}}$$

where γ is the specific heat ratio of the air and M_1 is the upstream Mach number. The probe is moved along the core jet axis and positioned at different stations from the nozzle exit, at intervals of 1 mm from 0 to $2D_e$, 2 mm from $2D_e$ to $5D_e$, 5 mm from $5D_e$ to $10D_e$ and 10 mm beyond $10D_e$. The jet field centerline pitot pressure at these points was recorded for a settling chamber pressure. Upon completing one measurement set, the settling chamber pressure was changed to the next NPR (Nozzle Pressure Ratio) level and the measurement was repeated.

2.3.2 Jet Pressure Field

After completing the centerline pressure distribution, the pressure grid measurements were made. For this, one quadrant of the jet cluster has been chosen. At a given axial location pressure at different grid points in the quadrant has been surveyed by positioning the pitot probe with the help of the traverse at the grid points. The grid co-ordinates used for pressure survey is given in Table 2.1.

Axial location	ΔX	ΔY	ΔZ
$0D_e$ - $5D_e$	2 mm	1 mm	1 mm
$5D_e$ - $10D_e$	5 mm	3 mm	3 mm
$10D_e$ - $15D_e$	10 mm	5 mm	5 mm

Table 2.1: Table for grid points in jet pressure field

Grid measurements were made for all the levels of settling chamber pressure tested. Upon completing the centre line pressure and the jet pressure field measurements, the next model was mounted on the settling chamber and similar measurements were done.

2.4 Experimental Precautions

During the experimental runs the following precautions were observed. The nozzle centre line was aligned longitudinally for every model.

- The settling chamber was kept in a horizontal position to align the flow in the horizontal direction.
- The model was carefully adjusted and checked with a sprit level to keep the measuring plane in the desired position.
- The probe was aligned with the flow direction facing the nozzle exit.
- Before the experimental runs, the leakage test was performed so that the experimental setup was leak free even at the maximum working pressure.
- The apparatus was placed in a large room with constant ambient temperature.
- The arc lamp was carefully adjusted so as to keep it in the focal point of the mirror.
- The stagnation pressure and the air flow rate in the settling chamber was kept constant during the experiments by adjusting the PRV.

2.5 Data Accuracy

The possible source of error of the present investigation is due to,

- Linear movement of the traverse along X, Y, and Z direction.
- Settling chamber stagnation pressure measuring pressure transducer.
- Error in the measurement of pitot pressure in the jet field.
- Possible inaccuracies in the nozzle dimensions

The traverse is provided with a vernier scale of 0.1 mm. Hence, all the length dimensions measured were accurate upto 0.1 mm. The pressure measuring transducers and manometers were provided with graduations with a resolution of 1 mm. The variation of the temperature throughout on set of experimental run was less than 2%.

All the pressures measured were found to be repeatable within ±3 %. The maximum uncertainty involved in the pitot pressure was estimated to be ±3.5 %.

Chapter 3

Results and Discussion

3.1 Introduction

Aerodynamic and aeroacoustics characteristics are two important characteristics to be understood thoroughly for an efficient utility of jets in general and multijets in particular. Multijets are used invariably in all launched vehicles in present days. The school of thought among launch vehicle researchers was that only underexpanded jets were efficient thrust produces and hence only they were used in the launch vehicle motors. But this thinking has changed and overexpanded, in fact highly overexpanded jets are used for launch vehicles. For example in our GSLV both the core and all the four strapon motors were operated at highly underexpanded conditions. Further it is a common practice to use core and strapon of different supersonic Mach numbers in the launch vehicle operation. It is proposed to use a core and two strapons in a row in ISRO's augmented GSLV (Mark II) unlike one core and four strapon in the GSLV. Even though GSLV multijet acoustics characteristics were studied by several people extensively but the aerodynamic characteristics was hardly looked into. It is the aim of present investigation to gain and insight into the aerodynamic characteristics of a core and two strapons with outward canting of 6 degrees, similar to augmented GSLV configuration. Attention is focused on the wave structures in the jet core, the jet propagation in the combined mode, highlighting the merging and confluence of the individual jets and overexpanded conditions. In addition to this the entrainment of the mass is also quantified with the present investigation. The Mach numbers of the core and strapons are 1.6 and 2.5 respectively. Measurements were made at NPR 4, 5 and 7 in order to there level of overexpansion with varying degrees of adverse pressure gradient. Measurements of center line decay, velocity profiles in the transverse plane (i.e. normal to all the three jet axis) and pressure measurements at predecided grid points, in the jet field to estimate the mass flow at various axial location were carried out in the present investigation.

3.2 Centerline decay

Centerline pressure decay for the Mach 1.6 (core jet) decay at NPR 4, 5 and 7 are compared in the Figure.3.1. Typical of supersonic jets in the pressure plots exhibits shocks and expansion fans in the core with the strongest first shock (minimum point in the pressure plot) for NPR 7 are seen. The shock in the subsequent cells become stronger with increase of NPR as seen from the figure also the longest core (the extent of supersonic zone along with the jet axis) is for NPR 7 and the shortest one for NPR 4 which is typical of supersonic free jet. After that core jet decay is similar to subsonic jet.

The results for Mach 2.5 strapon jet (both the strapons are identical) are shown in Figure 3.2. Compared to the core jet, core length for the strapon is much shorter for all NPRs. This is because the Mach number of the strapon being much higher than that of core and the shocks in the core become much stronger than for that core jet, in order to overcome the higher adverse pressure gradient and to come to an equilibrium with the surrounding environment.

The centerline decay for the multijet is shown in Figures 3.4 to 3.6, respectively for NPR 4, 5 and 7. The individual decay of core and strapon jets are also included in these plots for comparison.

The results of NPR 4 in Figure 3.7 shows that the core length of the multijet is slightly shorter than core length of the core nozzle also after the first shock cell the subsequent cells are made significantly weaker for the multijet. This is a significant advantage from both mixing and acoustics point of view. The shocks strength in the jet core can result in significant attenuation of shock associated noise which is a higher desirable feature in the launch vehicle operations [15].

Also the reduction in the core is the direct measure of efficient mixing of the jet with environment. This efficient mixing can enhance the stealth capabilities of missiles or fighter jet since the hot core zone is the direct source of infrared signals to the radars for detecting these vehicles.

When the NPR 5 (Figure 3.5) the behaviour of the combined jet is almost identical to NPR 4. This may be because even though adverse pressure gradient, in the jet fields is much smaller than NPR 4, may not be sufficient to introduce the drastic change in the behaviour.

When the NPR is increased to 7 the decay of combined jet is drastically different from NPR 4 and 5. Unlike NPR4 and 5 the adverse pressure gradient is reduced significantly and hence the shocks in the core not forced to increase the jet pressure to the extent of NPR 4 and 5. Because of this the shocks in the cells upto about $X/D_e = 7$ are of significant strength but compared to core nozzle jet the multijet experiences a reduction in core at about two times D_e, this can be regarded as significant advantage of multijet. The physical reasoning for this behaviour is that the strapons offers a shielding to the core jet propagation which restricts the main jet to regain its energy in the subsequent cells when strapon jets are flowing.

The centerline decay of multijets at NPRs 4, 5 and 7 are compared in Figure 3.6. As in the case of single jets, here also the shocks cells become stronger and core length increased with increase of NPR, however, one the jets becomes subsonic the decay is fastest for the highest NPR this is because of the stronger shocks in the core. The jet at the NPR 7 is having much less momentum when it becomes subsonic compared to lower NPRs this makes the subsonic part of the jet to decay faster.

3.3 Velocity profiles of multijet

The measured pitot pressures in the jet axis plane were converted to velocity by using the following normal shock and isentropic relation.

1. ***Normal shock relation***:

$$\frac{P_{02}}{P_{01}} = \left(1 + \frac{2\gamma}{(\gamma+1)}(M_1^2 - 1)\right)^{\frac{-1}{(\gamma-1)}} \left\{\frac{(\gamma+1)M_1^2}{(\gamma-1)M_1^2 + 2}\right\}^{\frac{\gamma}{(\gamma-1)}}$$

2. ***Isentropic relation***:

$$\frac{P_0}{P} = \left(1 + \frac{(\gamma-1)}{2}M^2\right)^{\frac{\gamma}{\gamma-1}}$$

3. ***Velocity:***

$$U = M\sqrt{\gamma RT}$$

It is important to note here that in the wave dominated complex field like the jet field in the present study what the pitot probe measures is P_{02}, the total pressure behind a normal shock at its nose (the actual shock at the nose is detached bow shock but the portion of the bow shock can be approximated as normal shock) but it is a common practice among jet researchers to use this P_{02} for calculating the local Mach numbers with the stagnation chambers pressure, P_{01} as the stagnation pressure of the normal shock [16]. Even though calculated value of Mach number and velocity with the measured pitot pressure is not accurate but good enough for analyzing the jet structure.

The calculated local velocity (U) in the jet field were made nondimensional with the local centerline velocity (centerline of the main jet velocity) U_{max}. The results are presented in the form of B/B_{max} verses. U/U_{max}, where B is the local off width and the B_{max} is the total off width (Figure 3.10).

The velocity profiles at axial stations X/D_e = 1 to 15 for NPR 4 are shown in Figure 3.7. At X/D_e = 1.0, it is seen that the jets are retaining individual characteristics even though they show a tendency to merge, exhibiting a nominal value of slightly more than 10% of the centerline velocity at the merging point. At X/D_e = 2.0, the jets are merged and the velocities have gone upto as high as 27% of merging location, under the same time the maximum velocity ratio of the strapon jets which was 0.6 at X/D = 1.0 has come down to 0.5 at X/D_e = 2.0. As the jet travels downstream the strapon slowly losses their identity showing a tendency to mix with the core nozzle jet this is exhibited the progressive reduction in the velocity ratio of the strapon jet continuously with increase of the velocities of the merged zone. At X/D_e = 5.0 the strapons losses their individual identity and the combined jet is tending towards the nature of the single jet. This process continues and at X/D_e = 15.0 the field has become as that of a single jet.

The velocity profiles are NPR 5 at different axial locations shown in Figure 3.8. From these results it is seen that at X/D_e = 1.0 the jets behave independently and merging is yet to take place unlike NPR 4. At X/D_e = 2.0 the peak value of strapon jet decreased and the merging is on. As the jet proceeds downstream the peak value of velocity comes down and velocity at merging location progressively increases. In this process upto X/D_e = 8.0 jets slightly looses their identity but the jet is yet to become like a single jet. This

tendency continues the jet confluences completely beyond $15D_e$, which is slightly downstream compared to NPR 4 case.

Velocity profiles for NPR 7 are shown in Figure 3.9. Unlike the lower NPRs at NPR 7 the jet remains its identity over a long distance as high as $12D_e$. At $13D_e$ individual jets looses their identity to become similar to a single jet at a downstream station beyond $15D_e$, which is far downstream compared to NPR 5.

The velocity profiles discussed above should be understood as only qualitative, since the present case of strapons with outward canting, a combined effect of canting and differential overexpansion (higher for strapon jets and lower for core nozzle jet) make the jets to behave in peculiar manner as in the present case. The differential overexpansion compels the strapons to get deflected toward the main jet whereas the outward canting forces the strapon moves away from the central jet. A closer look at the individual jet suggest that U/U_{max} closer to the nozzle exit should be more than one for strapon jet but the actual values (though not accurate) are much less than one. This behaviour opens a new direction for multijet research. It is worthwhile to investigate deep into this to understand the combined effect of canting and overexpansion.

3.4 Mass entrainment

The induction of the surrounding mass into the jet field by the eddies at the jet periphery is termed as *entrainment* (i.e. entrained mass from zero momentum surrounding zone). When moved into the jet field acquires momentum from the jet flow thereby reducing the momentum of original fluid, since momentum is conserved. The mass entrainment as a direct influence on the jet decay through the momentum exchange process. Higher the entrainment faster the decay.

The mass at different cross sections of the jet field (m_j), is computed from the measured pitot pressure at different grid points. The difference between m_j and m_{exit}, which is mass flow at nozzle exit, is made nondimensional with m_{exit}. The variation of $(m_j-m_{exit})/m_{exit}$ along the axial distance (X/D_e) for the core nozzle at NPR 4, 5 and 7 are shown in Figure 3.11. It is seen that at all axial stations the entrainment increases with increase of NPR. However, the mass entrainment gets augmented faster with increase of NPR in the far field beyond $10D_e$ for NPR 4 and 5, beyond $7D_e$ for NPR 7. This is

because the shocks in the core becomes progressively stronger with increase of NPR which makes the jet to become subsonic early for higher NPR, also the cross sectional area in the subsonic zone for the higher NPR cases are larger than for lower NPRs. The combination of lower Mach number and higher periphery available for entrainment makes large entrainment in the far field. The entrainment result for strapon nozzle is shown in Figure 3.12. Here again behaviour is similar to that for core nozzle. Exhibiting steep increase in the entrainment in the far field.

The mass entrainment for the multijet for NPR 4, 5 and 7 are considered in Figure 3.13. Increase of NPR results in increase entrainment at all axial stations. This was the nature observed for the individual jets also.

The entrainment for the core alone, strapon alone and the multijet are compared in Figure 3.14. Here the reference mass flow is taken as the mass flow due to all the three jets in multijet configuration, m_{total}. The advantage of multijet configuration is evident from this figure. The multijet entrains considerably high mass from the some of the individual entrainment (entrainment for the core jet and entrainment of two strapon jets) in the far field. This causes the multijet to decay faster than the individual jet as it was shown in the discussion on centerline decay.

The mass entrainment results of NPR 5 are shown in Figure 3.15. Once again highlighting superiority of multijets over individual jet. It is Interesting to note that multijet enjoys enhanced mixing compared to individual jets both in the near and far field, unlike NPR 4 case where mixing enhancement done to multijet configuration only marginal in near field.

3.5 Flow visualization

To quantify the effect of multijet configuration on the shock cells in the jet core, the flow fields of individual and multijets are visualized by shadowgraph for all NPRs of the present study.

3.5.1 Core jet

The flow patterns in the jet core of the main jet are shown in Figure 2, for NPR 4, 5 and 7. It is seen that the shock cells grow in size with increase of NPR, specially the first

three cells are strongly influenced by NPR. The size of Mach disc decreases with increase of NPR.

3.5.2 Strapon jet

The shock cells in the core of strapon jet are shown in Figure 2. Here again the shock cell length increase with increase of NPR.

3.5.3 Multijet

The visualization pictures for multijet are shown in Figure 2. The gross features of the shock cells for the multijet are similar to individual jets. But comparison of shock cell length of the core jet alone and that of core jet in multijet mode, reveals the distinct benefits of multijet configuration.

The following table compares the length of the first cell for the core alone (L_{s1}) and core in the multijet (L_s).

$$\% \text{ Reduction shock cell length} = \frac{(L_{s1} - L_s)}{L_{s1}} \times 100$$

NPR	L_{s1} (Core alone)	L_s (Core in Multijet)	% Reduction
4	12.0	10.5	12.5
5	16.0	15.0	6.25
7	26.0	24.0	7.7

Table 3.1: Comparison shown for % reduction of first shock cell length

From the above table it is seen that the shock cell length are getting reduced because of multijet configuration, which can be regarded as a definite advantage from acoustics point of view. Since a reduction in core length results in reduction of shock associated noise of the jet [6]. Further reduction in the core can be viewed as increase of mixing. Thus both from aerodynamic mixing and acoustics point of view multijets are beneficial over corresponding individual jets.

Chapter 4

Conclusions

Main conclusions from the experimental study on multijets with differential Mach numbers are the following.

- The decay of multijets are faster than the decay of individual jets for all the NPRs of present study.
- With increase of NPR the decay becomes faster in the subsonic zone of both individual and multijets. The entrainment of multijet is superior to the individual jets combined entrainment at all axial stations for all NPRs.
- The reduction of shock cell length in multijet compared to their individual counterpart can offer advantage from jet acoustics point of view.

Appendix

5.1 Program for calculation of stagnation pressure ratios

```
c     For Calculating Ptotal/Pchamber for all the nozzles
      DIMENSION X(100),P02(100),PTR(100)
      REAL NX
      OPEN(1,FILE ='file1')
      OPEN(2,FILE ='file2')

C     WRITE(*,*)'NUMBER OF ROWS FOR NX'
      READ(1,*)NX

      DO I = 1,NX
      READ(1,*)X(I),P02(I)
      ENDDO

      PATM = 'Atmospheric pressure'
      TATM = 'Atmospheric temperature'
      P01  = 'Stagnation chamber pressure'
      DIA  = 'Diameter of core nozzle'

      DO I = 1,NX
      PTR(I)= (P02(I)+PATM)/(P01+PATM)
      WRITE(2,1000)X(I)/DIA,PTR(I)
      ENDDO


1000  FORMAT(2F12.4)

      STOP
      END
```

5.2 Program for calculation of velocity profiles

```
c      For Calculating  Mach Number for all the nozzles

       PARAMETER (N=100)
      DIMENSION X(N),PTR(N),P02(N),T1(N),V1(N)
      DIMENSION P1(N),RHO(N)
      REAL NX,M,MACH(N),P,RHOTOTAL
      OPEN(1,FILE ='p10d4')
```

```
      OPEN(2,FILE ='V10d4')
      OPEN(3,FILE ='v10d4')

C      WRITE(*,*)'NUMBER OF ROWS FOR NX'
       READ(1,*)NX

      DO I = 1,NX
      READ(1,*)X(I),P02(I)
      ENDDO

      PATM = 'Atmospheric pressure'
      TATM = 'Atmospheric temperature'
      P01  = 'Stagnation chamber pressure'
      DIA  = 'Diameter of core nozzle'
      G    = 1.4
      R = 'Gas constant'

         DO I = 1,NX
         IF(I.LE.0)THEN
         write(*,*)I
           M    = 1.0
           PTR(I)=(P02(I)+PATM)/(P01+PATM)
           VA =G+1
           VB =G-1
             DO ITER = 1,10000
             VC = 1+(2*G*(M*M-1))/VA
             VD =(VA*M*M)/((VB*M*M)+2)
             VE = VC**(-1.0/VB)
             VF = VD**(G/VB)
             SU =(VE*VF) - PTR(I)
              IF(SU.LE.0.00001) THEN
               MACH(I) = M
               T1(I)= TATM/(1.0+VB/2*MACH(I)**2)
               V1(I)= MACH(I)*SQRT(G*R*T1(I))
               VG = (2.0*G*MACH(I)**2.0)/VA
               VH = VB/VA
               VI = (VA*MACH(I)**2)/2.0
               VK = (VG-VH)**(1.0/VB)
               VL = VI**(G/VB)
               P     = ((P02(I)+PATM)*VK)/VL
               P1(I) = (P*101325)/29.92
               RHO(I)= P1(I)/(R*T1(I))
               GO TO 100
              ELSE
               M = M + 0.001
              ENDIF
             ENDDO

        ELSE
         A = G-1
         B = A/G
```

```
            C = 2./A
            D = A/2.0
             MACH(I)   = SQRT((((P02(I)+PATM)/PATM)**B
     1      1.0)*C)
            T1(I)   = TATM/(1.0 + D * MACH(I) * MACH(I))
            V1(I)   = MACH(I) * SQRT(G*R*T1(I))
            P       = (P02(I)+PATM)/(1.0+D*MACH(I)**2)**(G/A)
            P1(I)   = (P*101325)/29.92
c           RHOTOTAL = (PATM*101325)/(29.92*R*TATM)
c           RHO(I) = RHOTOTAL/(1.0+D*MACH(I)**2)**(G/A)
            RHO(I) = (PATM*101325)/(29.92*R*T1(I))
            GO TO 100
           ENDIF

100         WRITE(2,1000)X(I),X(I)/DIA,MACH(I),P1(I),
      1     T1(I),V1(I),RHO(I)
            WRITE(3,2000)V1(I),RHO(I)
            ENDDO

1000        FORMAT(7F12.4)
2000        FORMAT(2F12.4)

 STOP
 END
```

5.3 Program for calculation of mass entrainment

```
   c     For Calculating  entrainment for all the nozzles

          PARAMETER (N=100)
          DIMENSION X(N),DELTA_MASS(N)
          REAL NX,m(N),INITIAL_MASS
          OPEN(1,FILE ='total_mass')
          OPEN(2,FILE ='entrain_mass')

          DO I = 1,15
          READ(1,*)X(I),m(I)
          ENDDO
          INITIAL_MASS = 0.3176
          DO I = 1,15
         DELTA_MASS(I) = (m(I)-INITIAL_MASS)/(INITIAL_MASS)
          WRITE(2,1000)X(I),DELTA_MASS(I)
          WRITE(*,*)X(I),DELTA_MASS(I)
          ENDDO
 1000     FORMAT(2F12.4)
          STOP
          END
```

References

[1] Abramovich G N, 1963, The Theory of Turbulent Jets.M.I.T.press,MA, USA

[2] Schlichting H, 1959, Boundary Layer Theory, McGraw Hill, New York.

[3] Rathakrishnan E, 1995, Gas Dynamics, Prentice-Hall of India Pvt. Ltd., New Delhi.

[4] Glass D R, 1968, "Effects of Acoustics Feedback on the Spread and Decay of Supersonic Jets", *AIAA Journal*, Vol. 6, No. 10, pp. 1890-1897.

[5] Rice J and Raman G, 1993, "Supersonic Jets from Beveled Rectangular Nozzles", ASME Paper 93-WA/NCA-26.

[6] Tam C K W 1995, "Supersonic Jet Noise", *Annual Review of Fluid Mechanics*, Vol. 27, pp. 17-43.

[7] Tam C K W and Chen P, 1994, "Turbulent Mixing Noise from Supersonic Jets", *AIAA Journal*, Vol. 32, No. 9, pp. 1774-1780.

[8] Tam C K W , 1975, "Supersonic Jet Noise Generated by Large Scale Disturbances", Journal of Sound and Vibration, Vol. 38, pp. 51-79.

[9] K.K. Ahuja, "Mixing enhancement and jet noise reduction through tabs plus ejector", *AIAA Journal* 93-4347 (1993).

[10] Navin Kumar Singh and Rathakrishnan E, "Effect of Tab Geometry on Sonic Jet Characteristics" accepted in 22nd International Symposium on Space Technology and Science, Morioka, Japan, May 28- June 3, 2000.

[11] Moustafa G. H. and Rathakrishnan E., "Studies on the flowfield of multijet with square configuration", *AIAA Journal*, Vol. 31, pp. 1189-1190, 1993.

[12] Mustafa Rajan K.S.M. and Rathakrishnan E.,"Numerical analysis of Supersonic multijets", *Journal of Aircraft*, Vol. 30, pp. 801-802, 1993.

[13] Rathakrishnan E. Reddy V. and Padmanaban K., "Some studies on twin Jet Propagation", *Mechanics Research Communications*, Vol. 16, pp. 279-287, 1989.

[14] Rathakrishnan E., "Instrumentation, Measurements and Experiments in Fluids", Book to be published.

[15] Verma S B and Rathakrishnan E, "Mixing enhancement and noise attenuation in notched elliptic-slot free jets", *International Journal of Turbo and Jet Engines*,Vol 15,No 1 (1998), pp. 7-25.

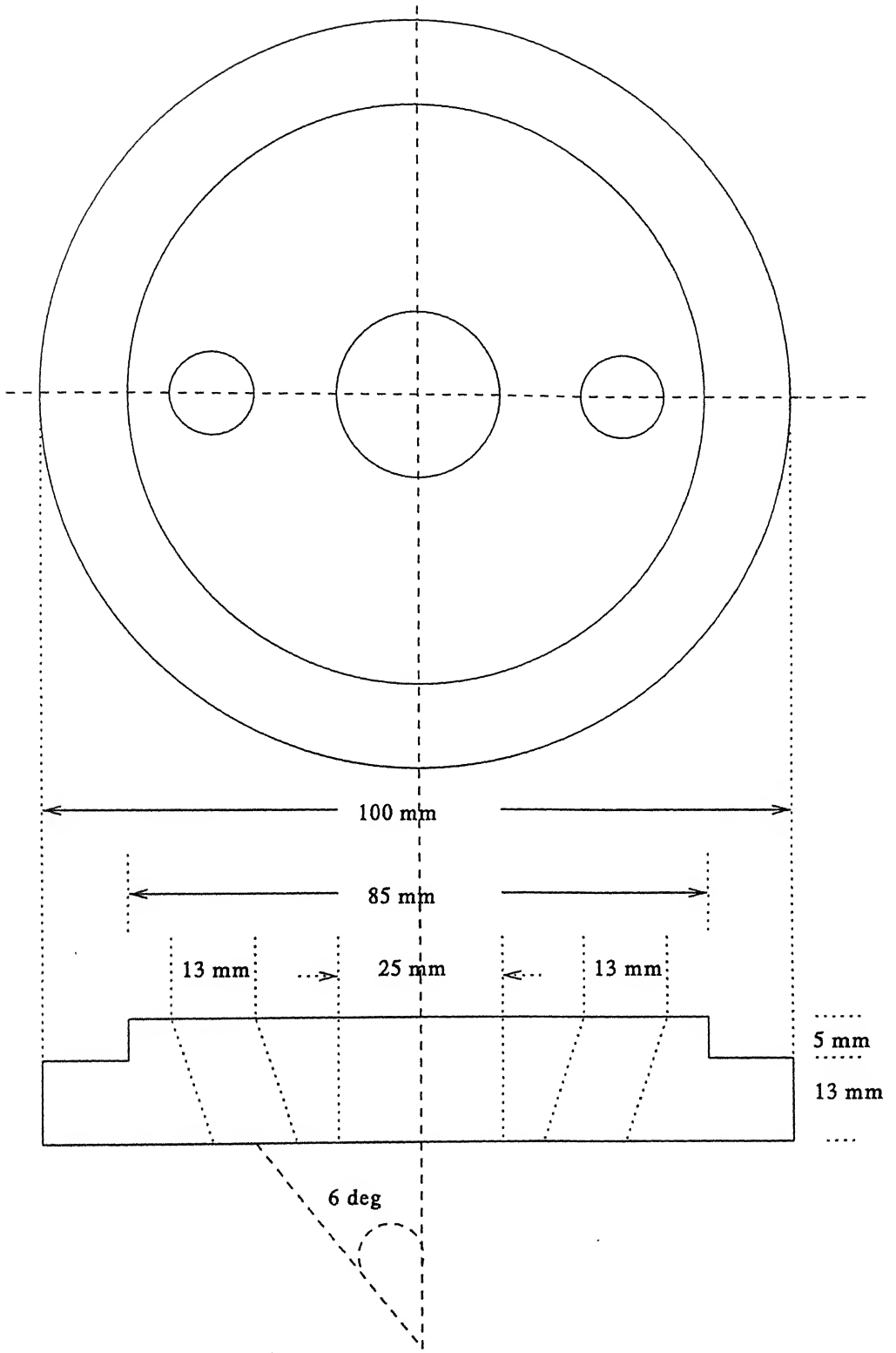

Fig. 1 Multijet configuration

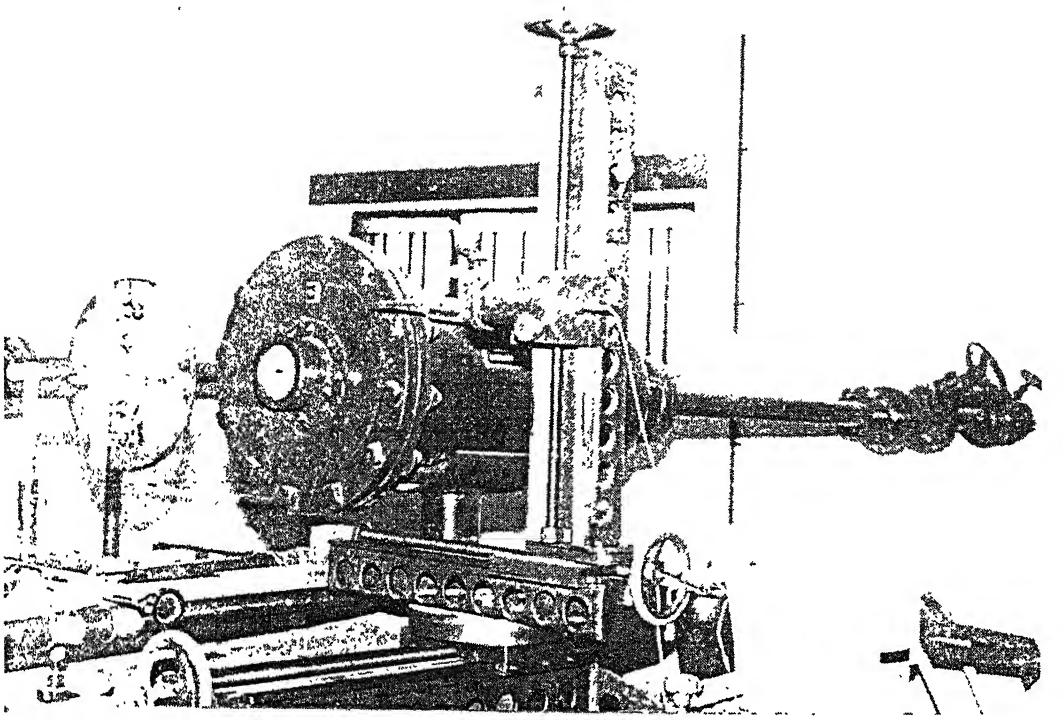

Fig. 2a Setup of jet test facility

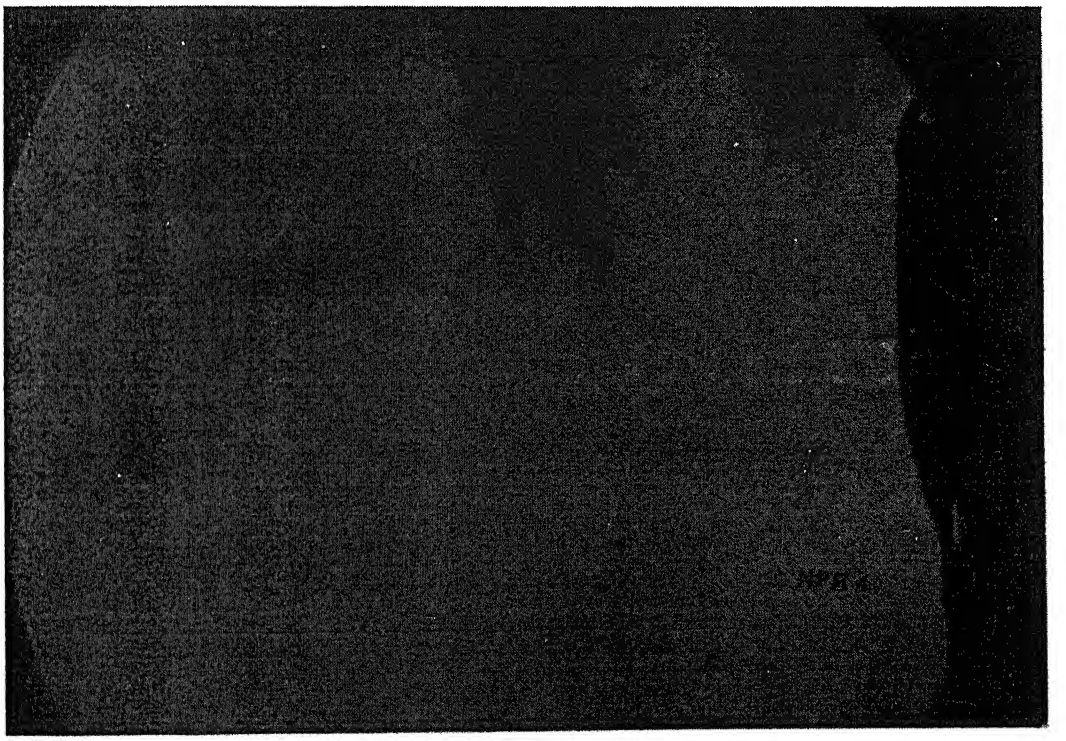

Fig. 2b Shadow graphic view of strapon jet at NPR 4

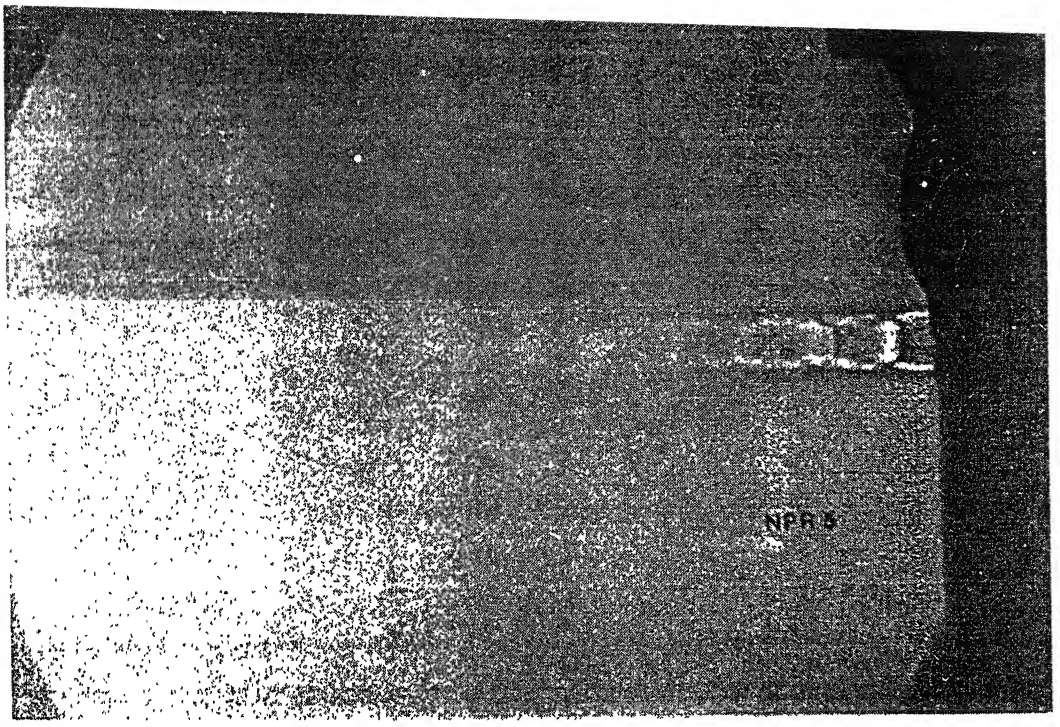

Fig. 2c Shadow graphic view of strapon jet at NPR 5

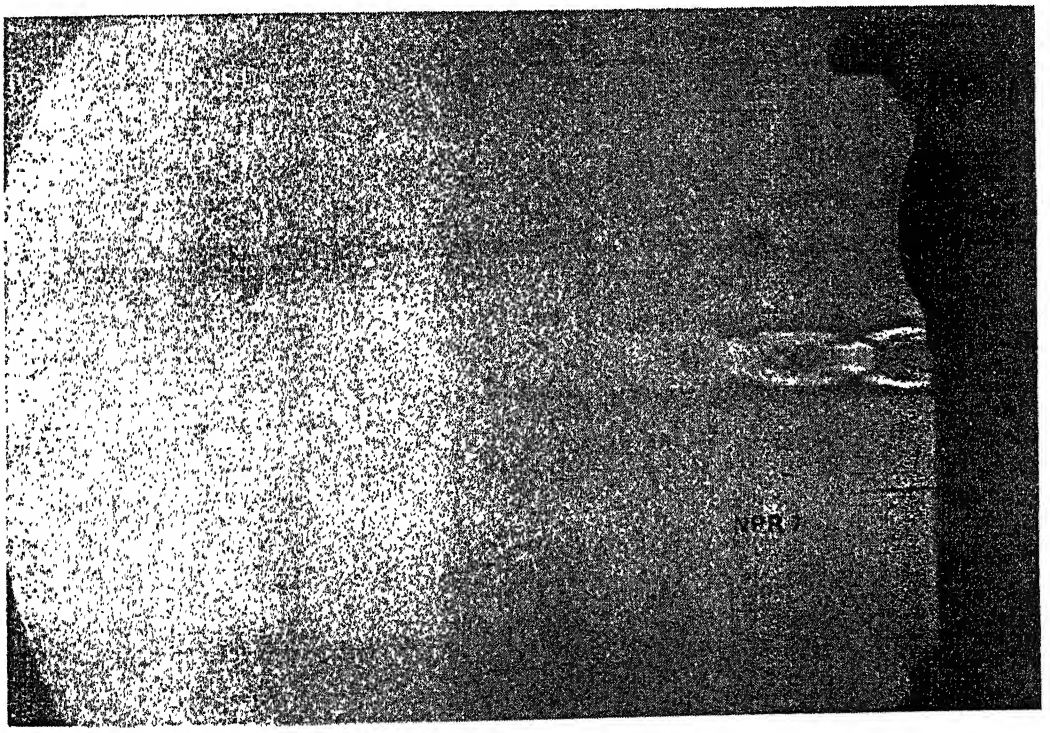

Fig. 2d Shadow graphic view of strapon jet at NPR 7

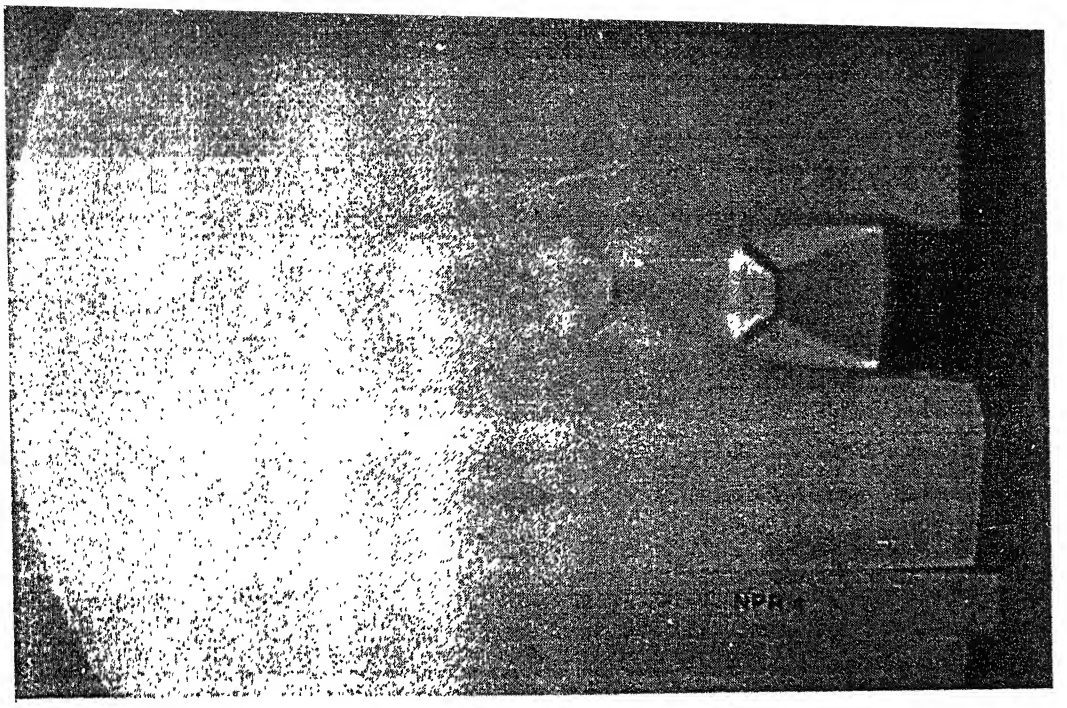

Fig. 2e Shadow graphic view of core jet at NPR4

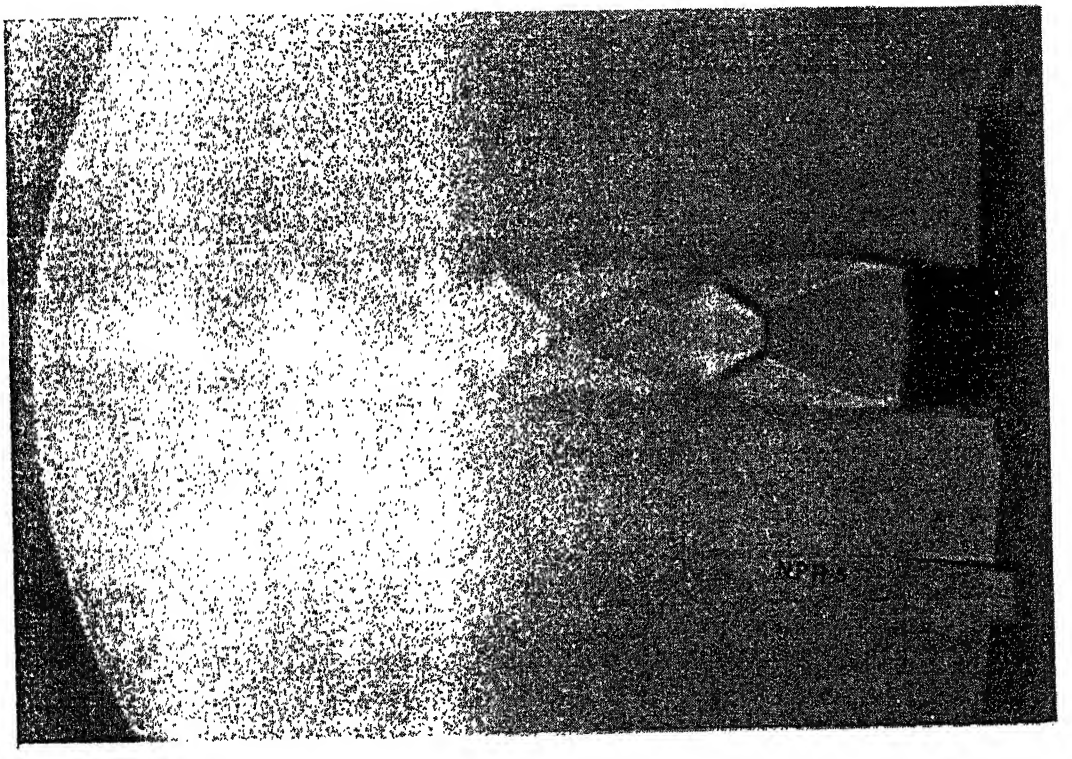

Fig. 2f Shadow graphic view of core jet at NPR5

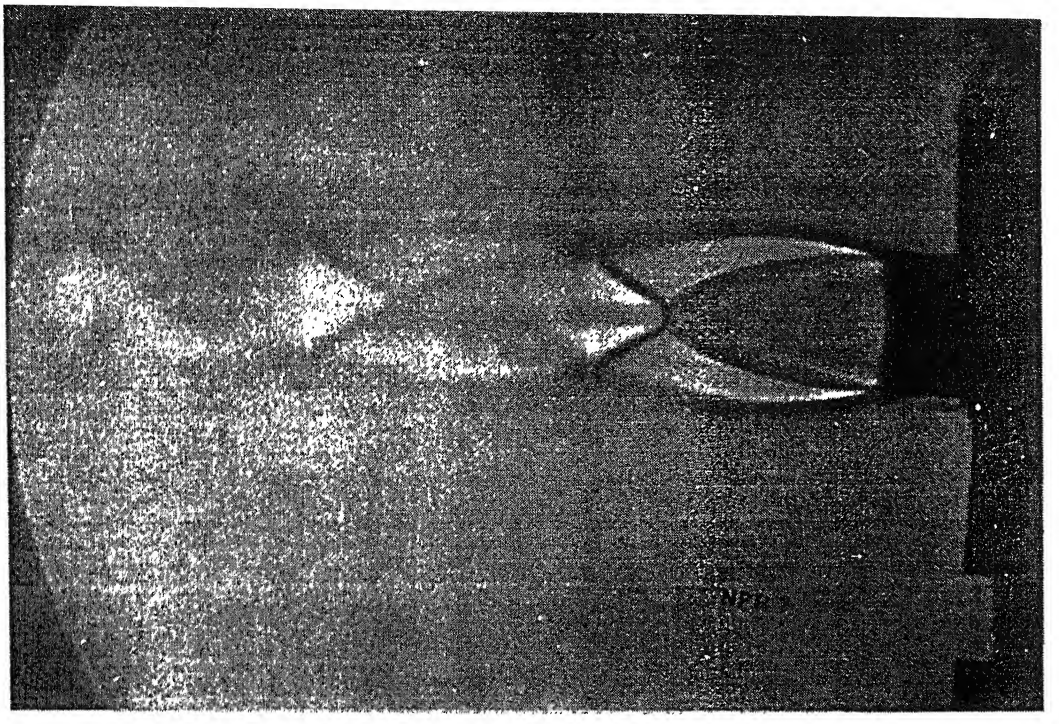

Fig. 2g Shadow graphic view of core jet at NPR 7

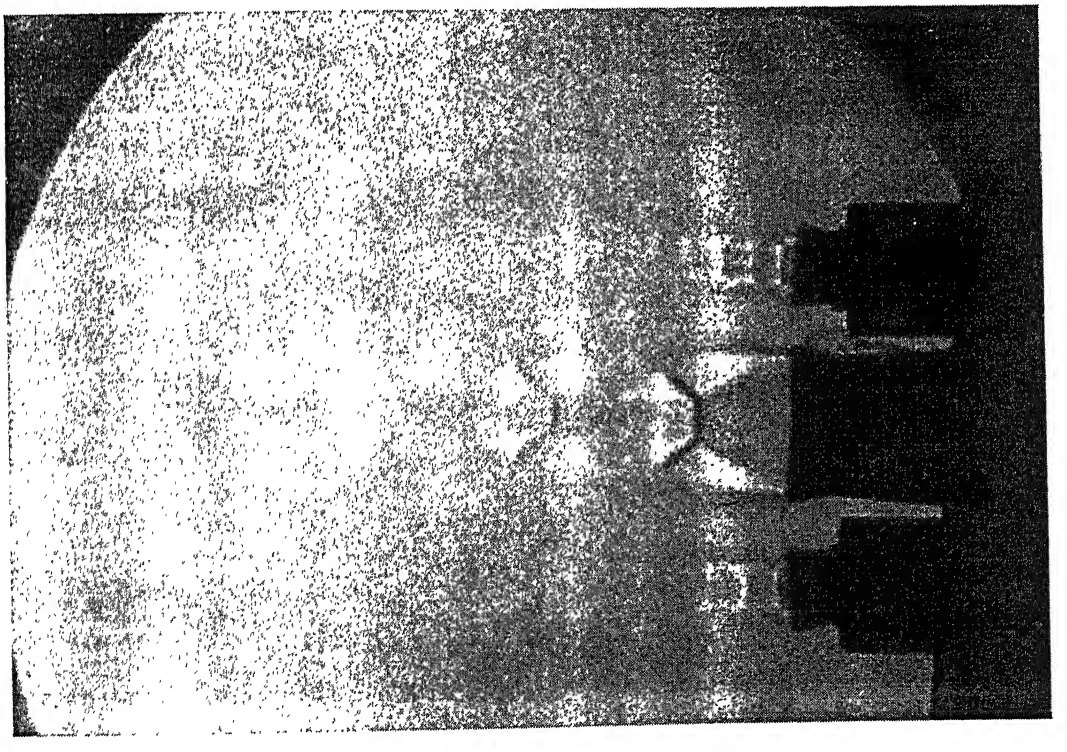

Fig. 2h Shadow graphic view of Multijet at NPR 4

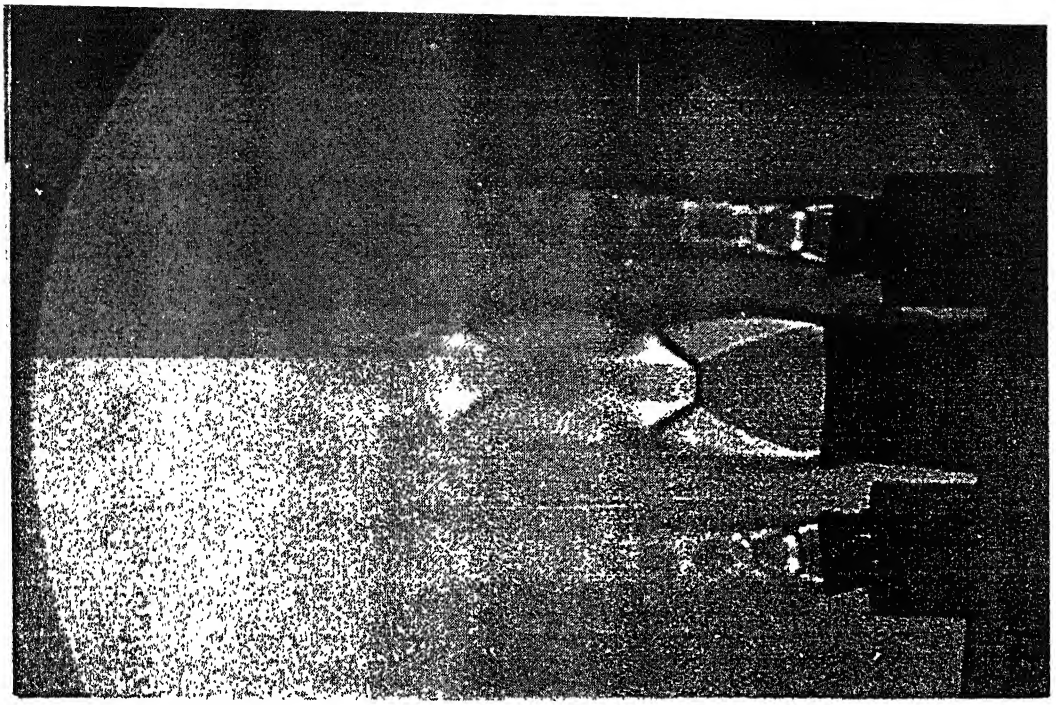

Fig. 2i Shadow graphic view of Multijet at NPR 5

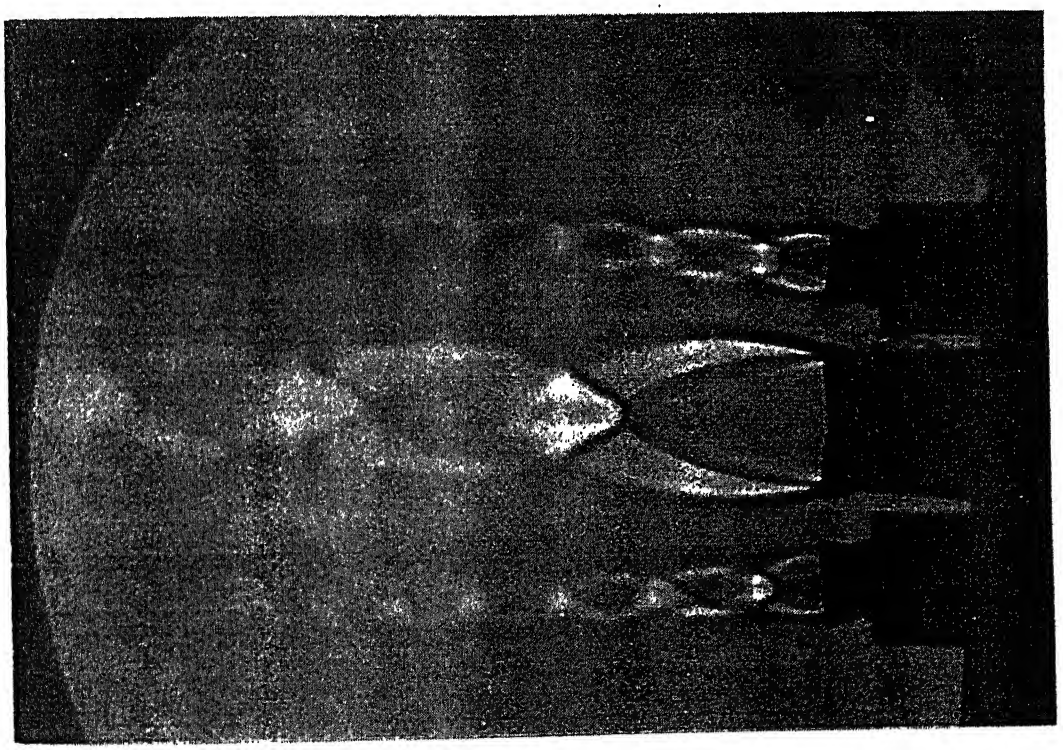

Fig. 2j Shadow graphic view of Multijet at NPR 7

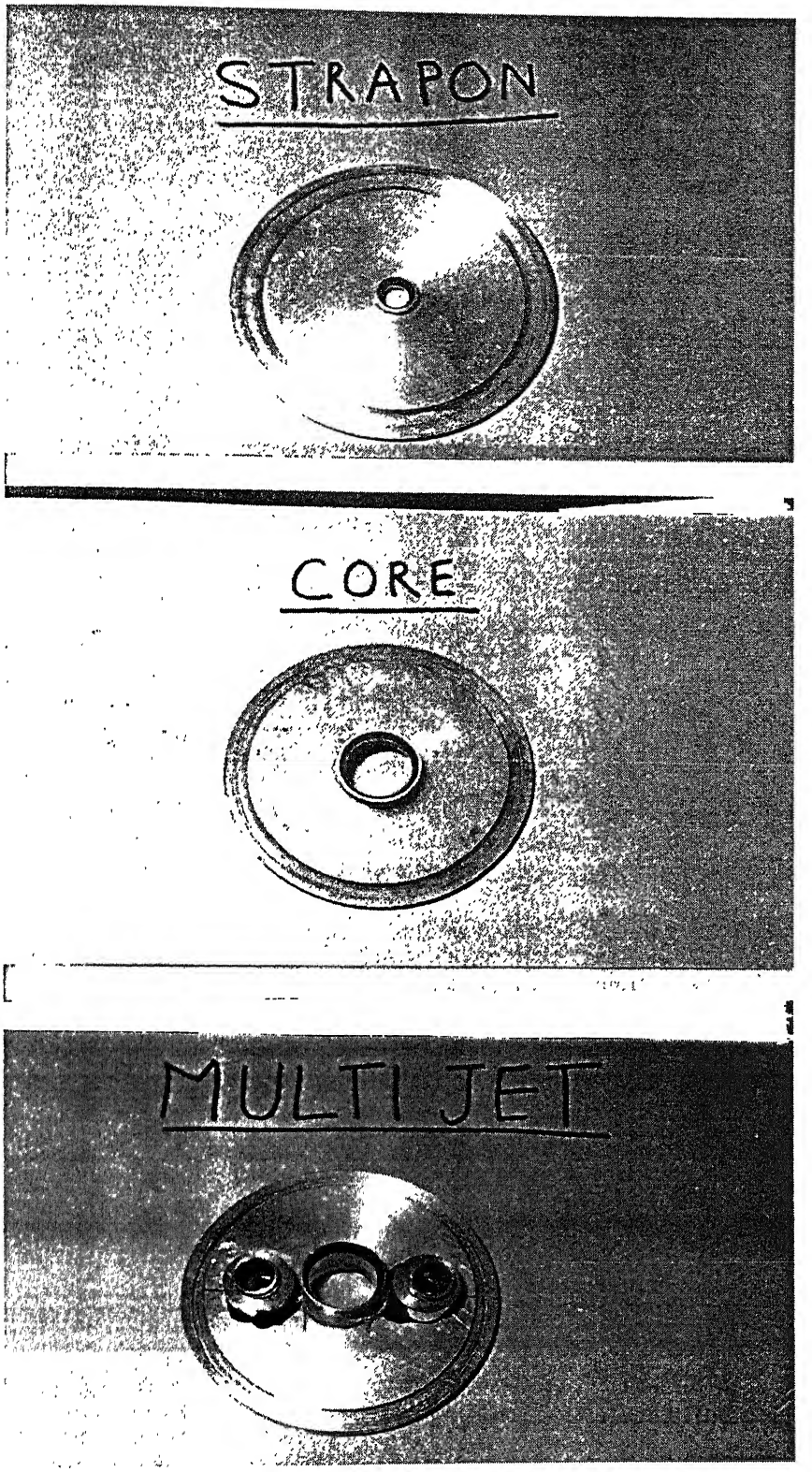

Fig. 2k Photographic view of Strapon, Core and Multijet nozzles

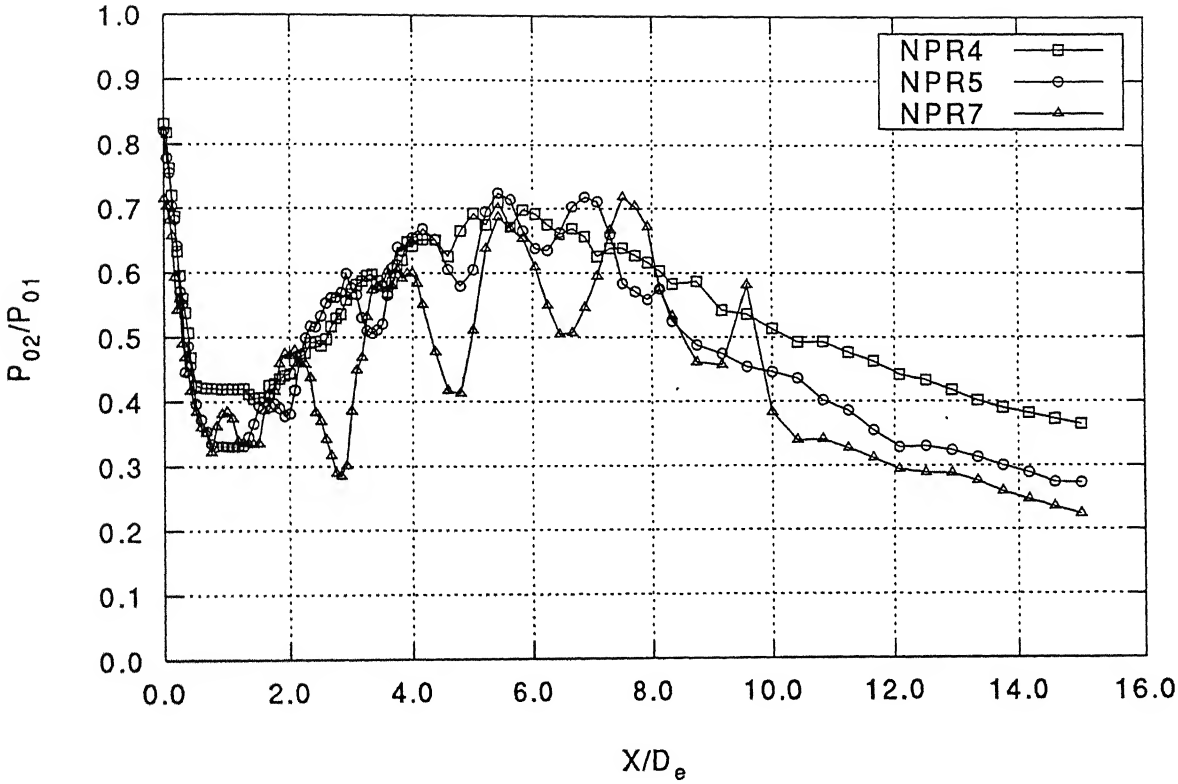

Fig. 3.1 Centerline Decay for Core nozzle

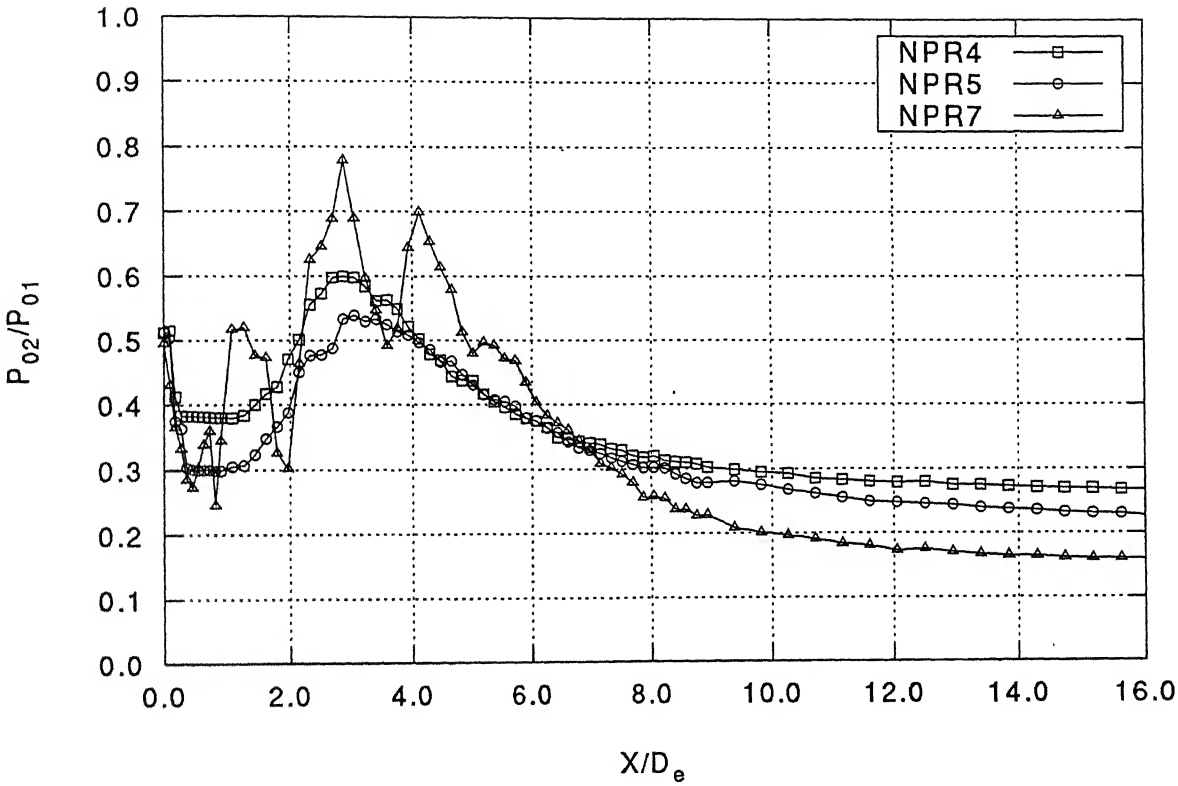

Fig. 3.2 Centerline Decay for Strapon nozzle

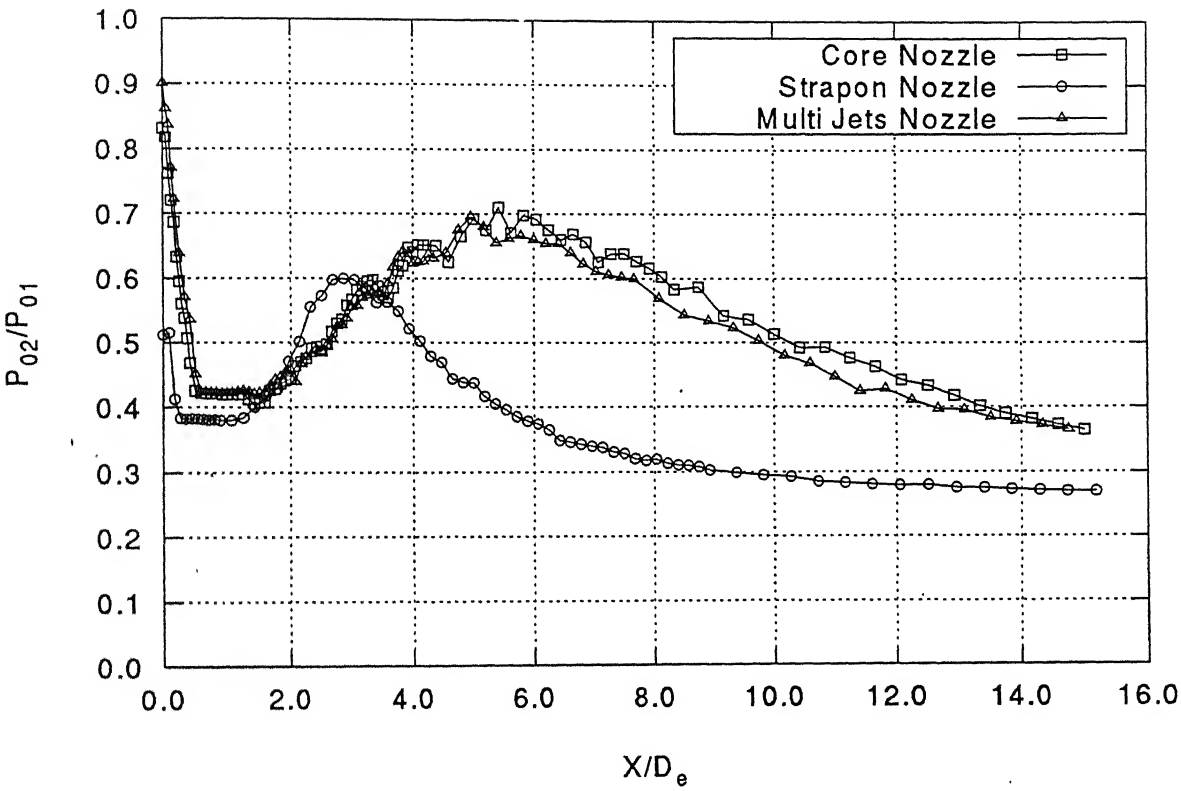

Fig. 3.3 Centerline Decay at NPR4

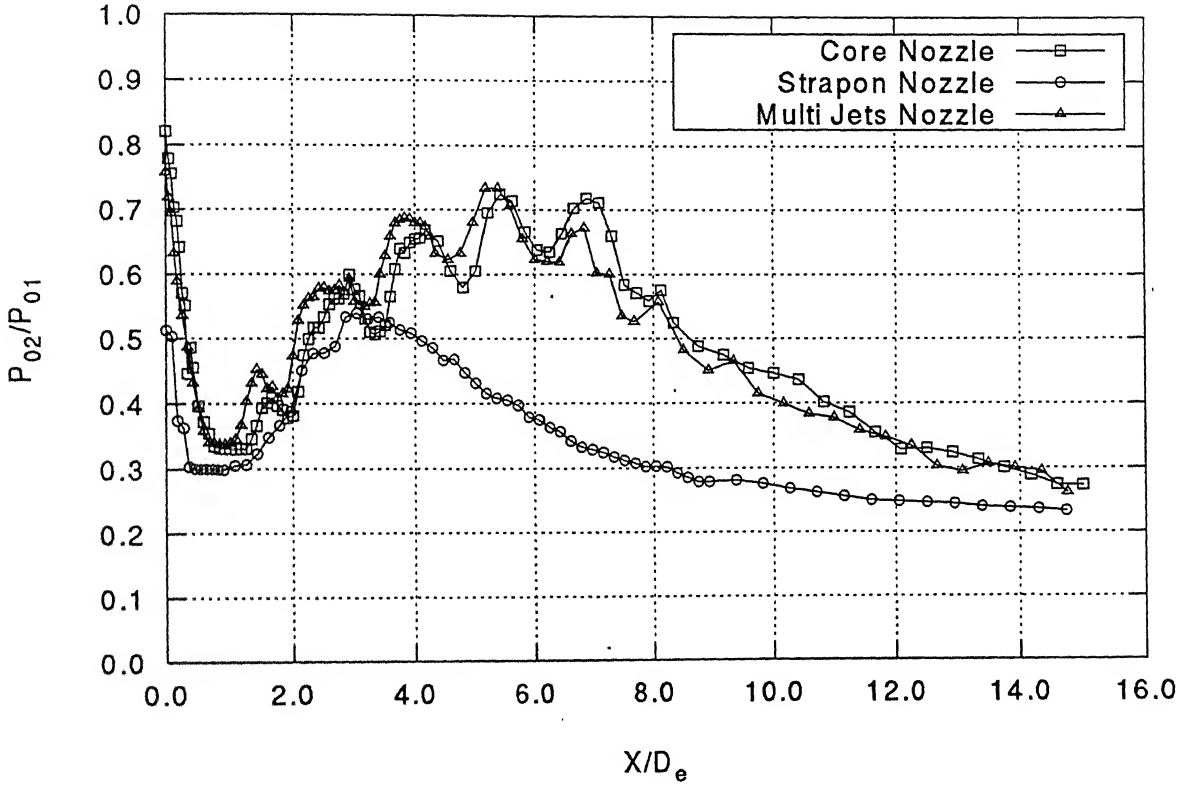

Fig. 3.4 Centerline Decay at NPR5

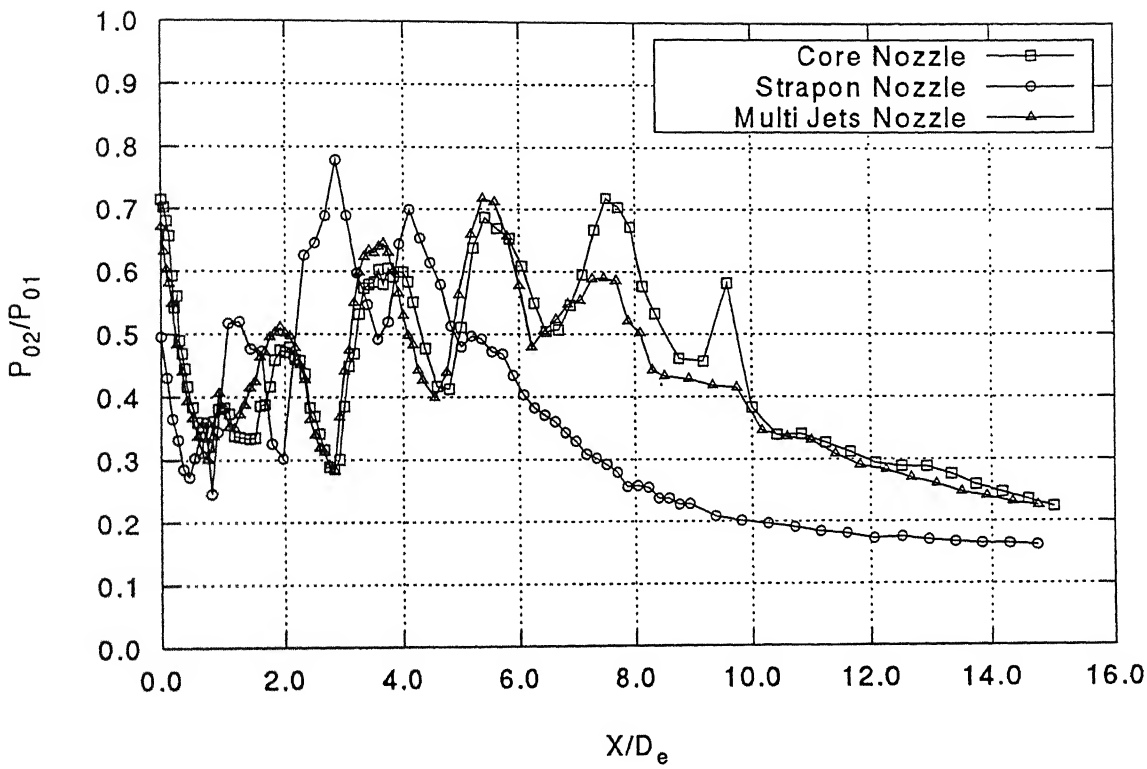

Fig. 3.5 Centerline Decay at NPR7

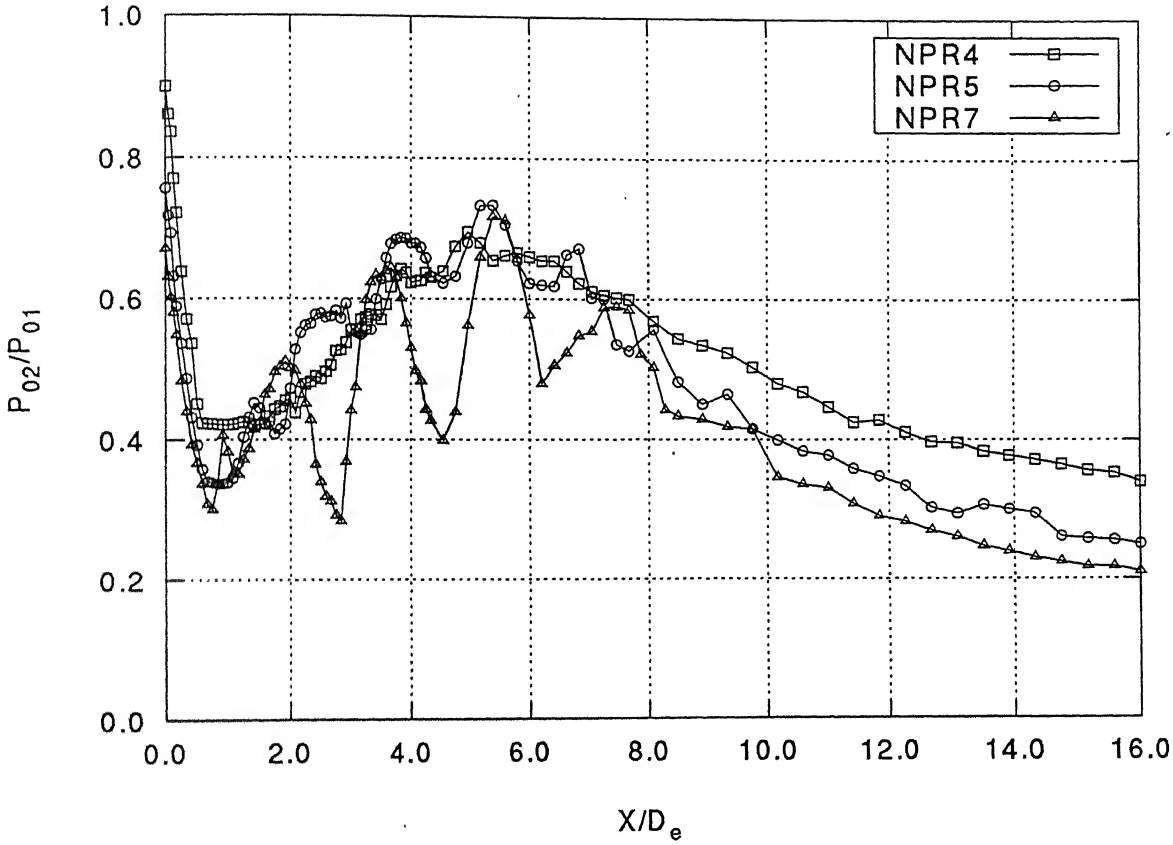

Fig. 3.6 Centerline Decay for Multijet nozzles

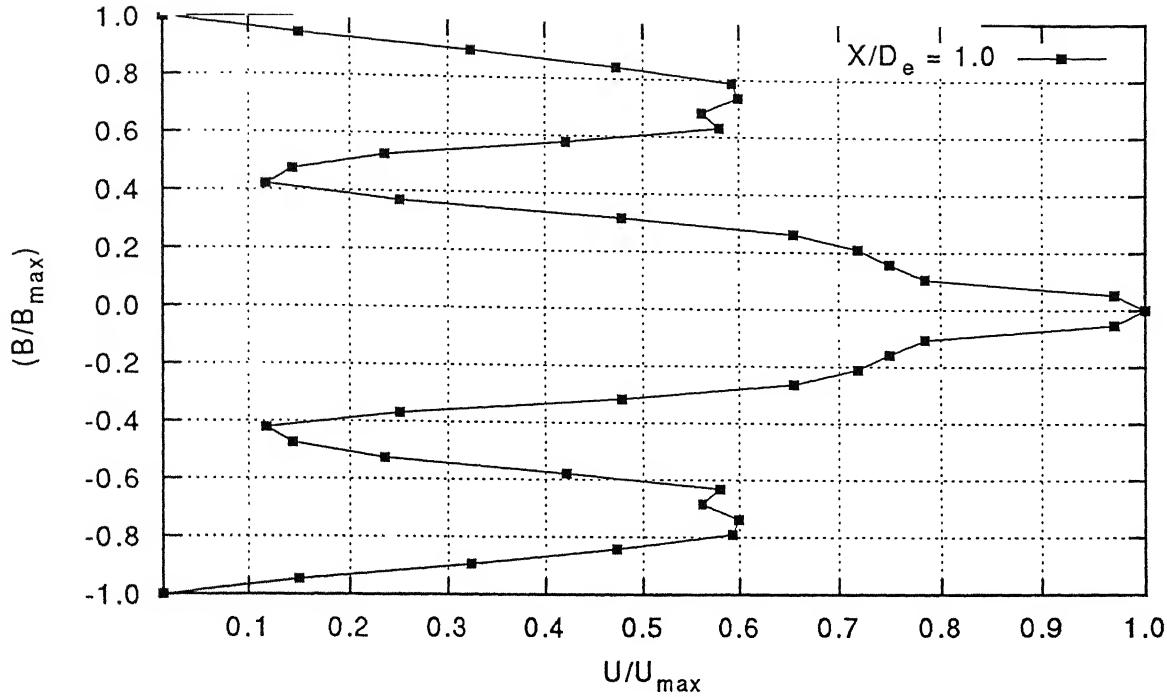

Fig. 3.7a Velocity profile at NPR 4

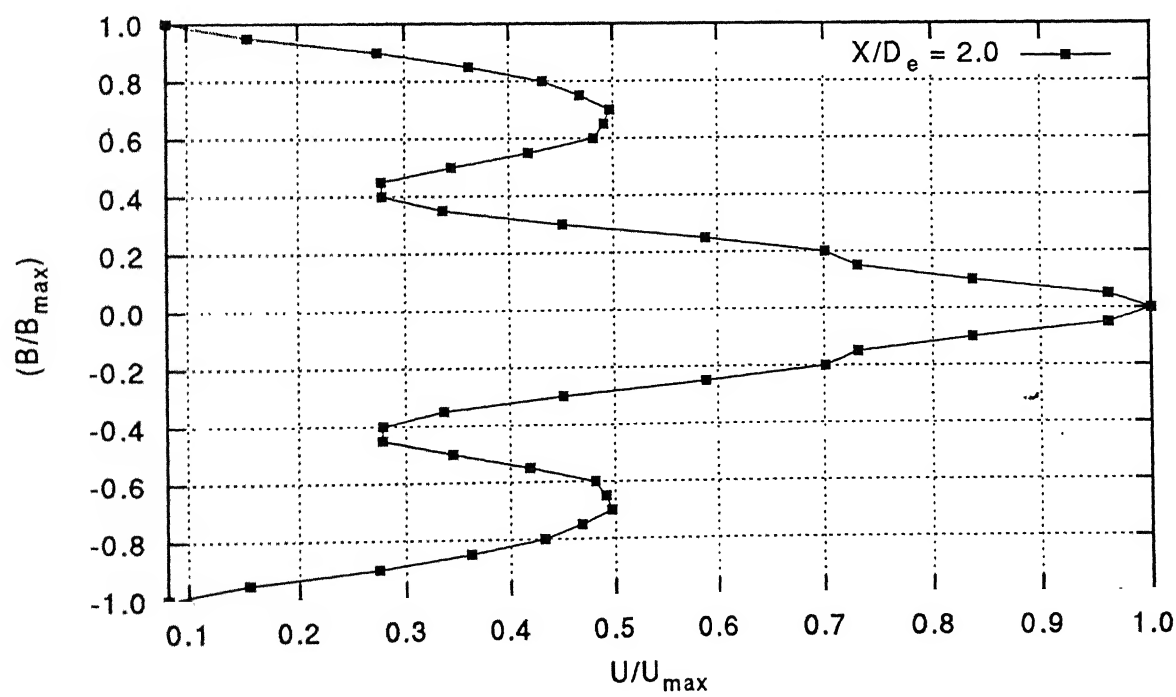

Fig. 3.7b Velocity profile at NPR 4

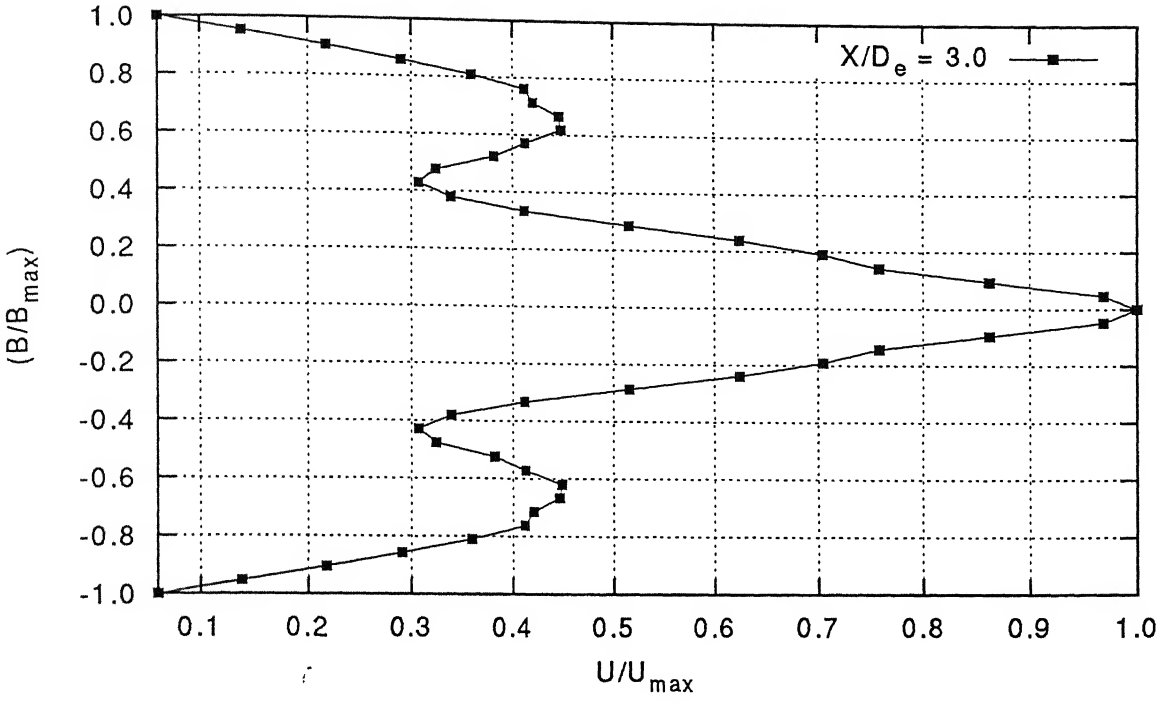

Fig. 3.7c Velocity profile at NPR 4

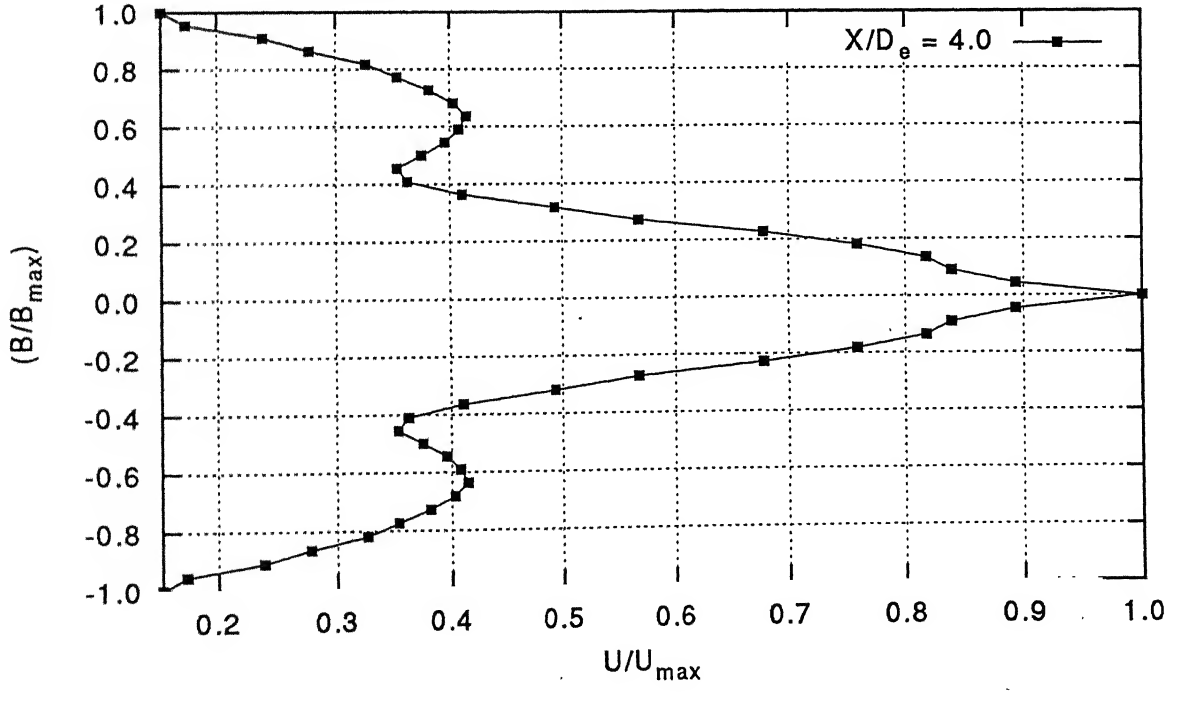

Fig. 3.7d Velocity profile at NPR 4

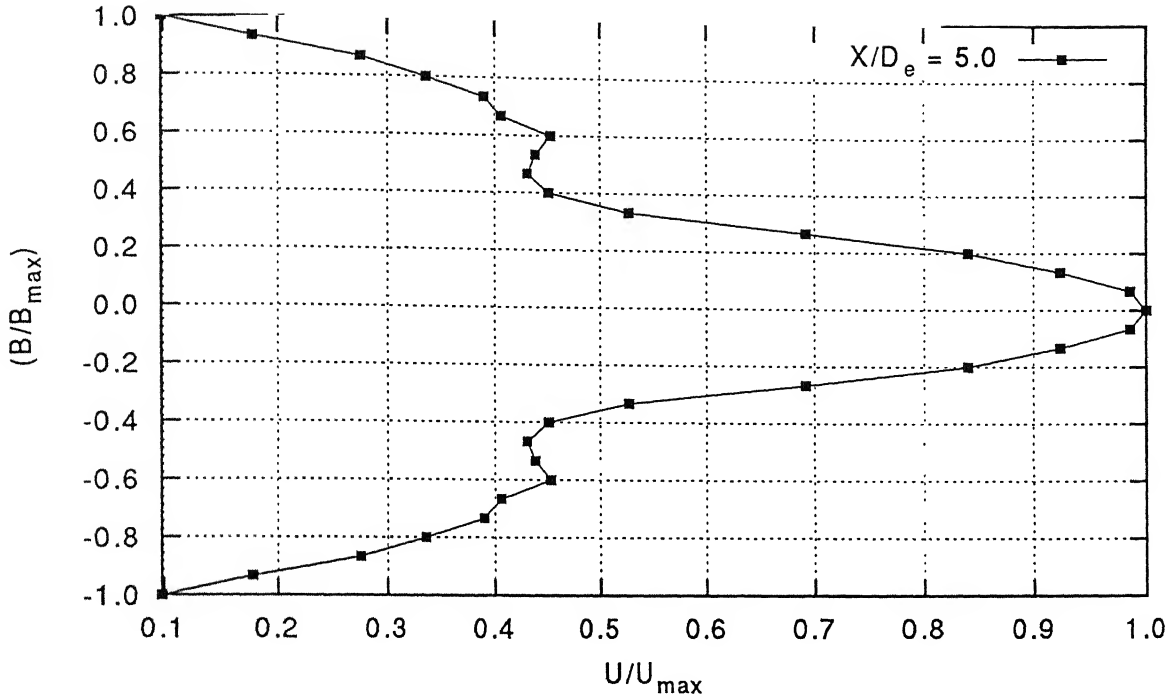

Fig. 3.7e Velocity profile at NPR 4

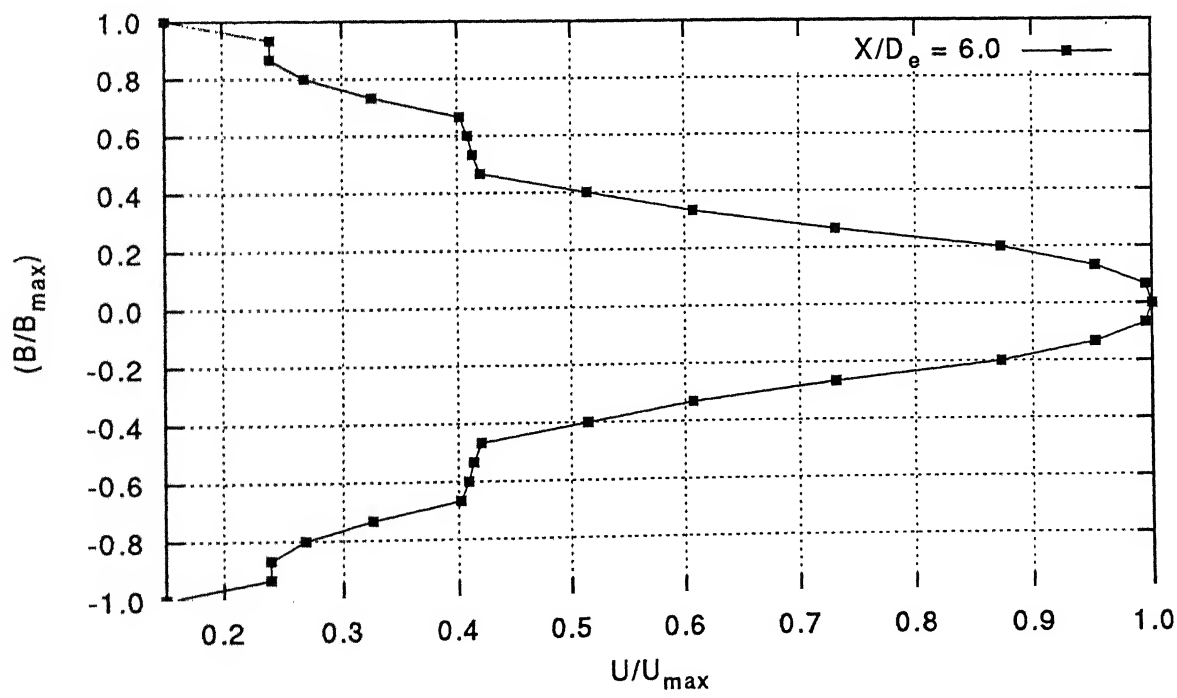

Fig. 3.7f Velocity profile at NPR 4

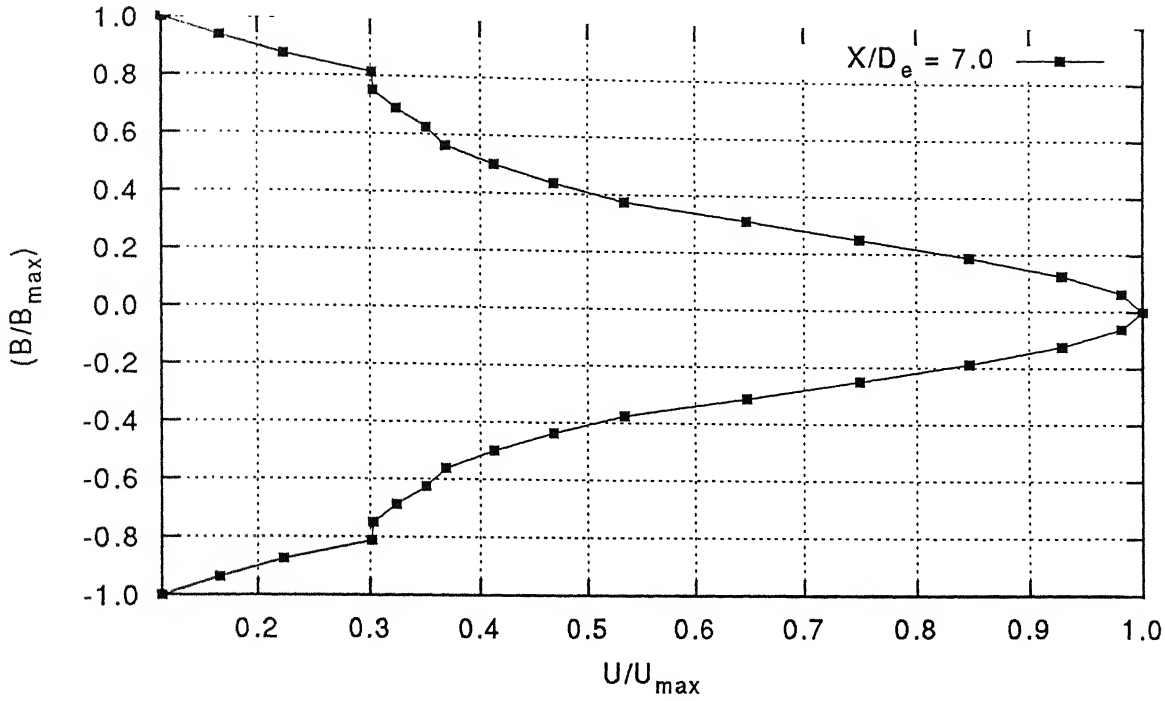

Fig. 3.7g Velocity profile at NPR 4

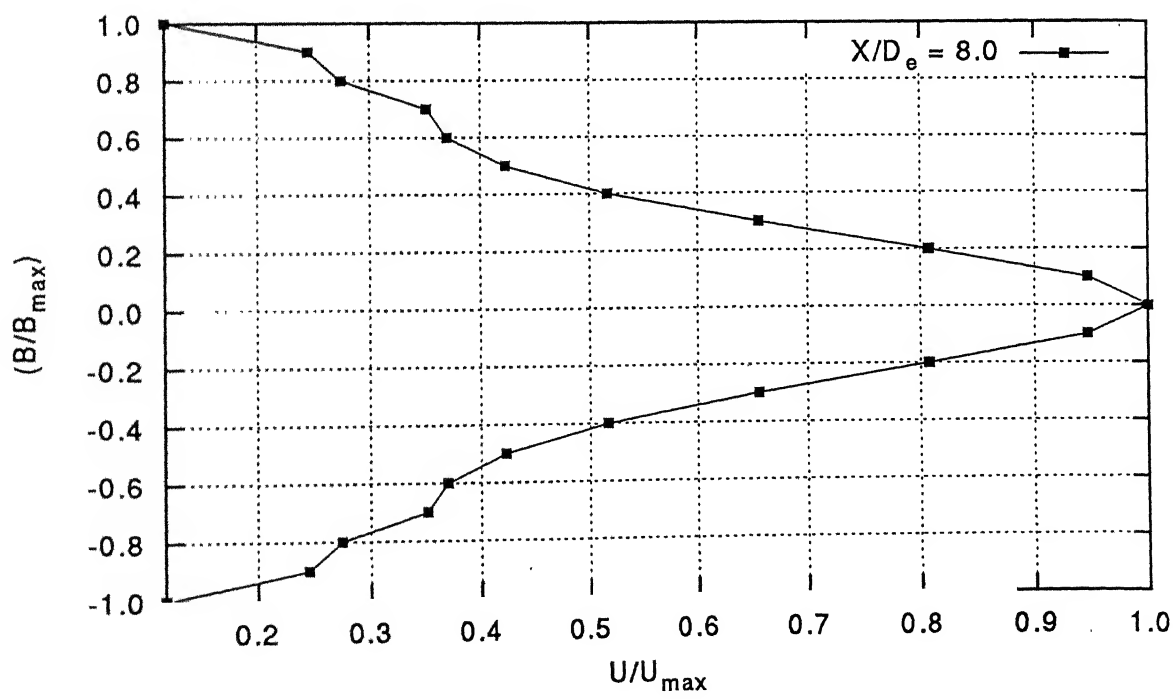

Fig. 3.7h Velocity profile at NPR 4

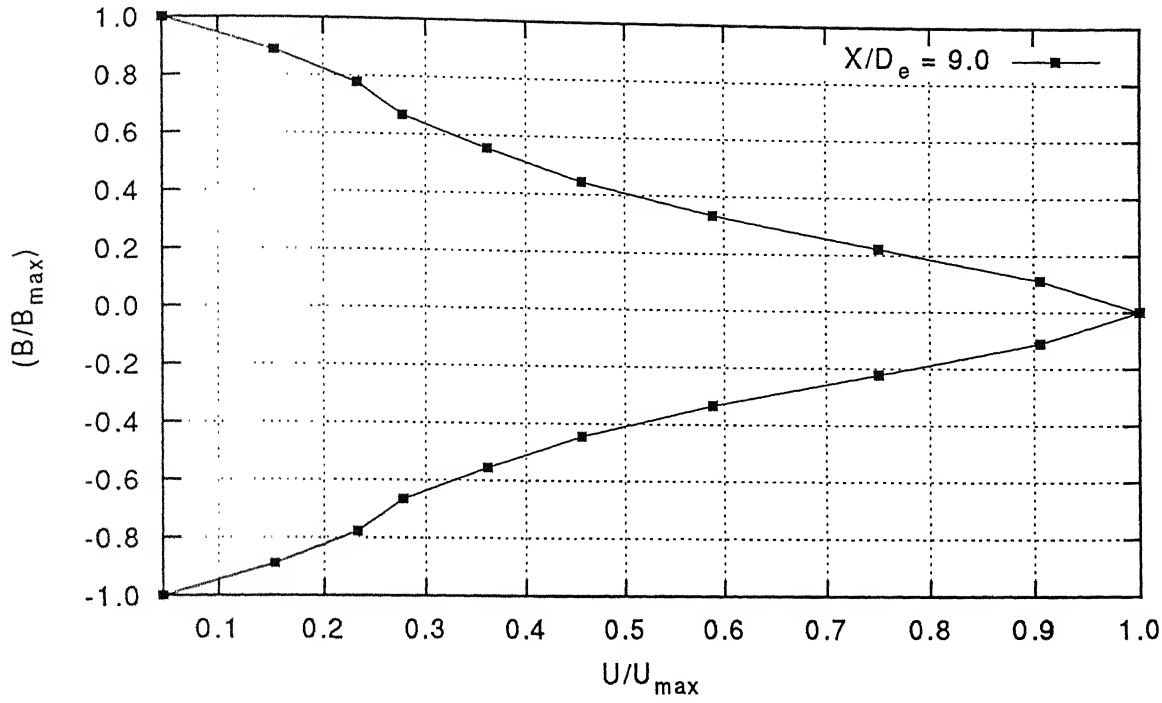

Fig. 3.7i Velocity profile at NPR 4

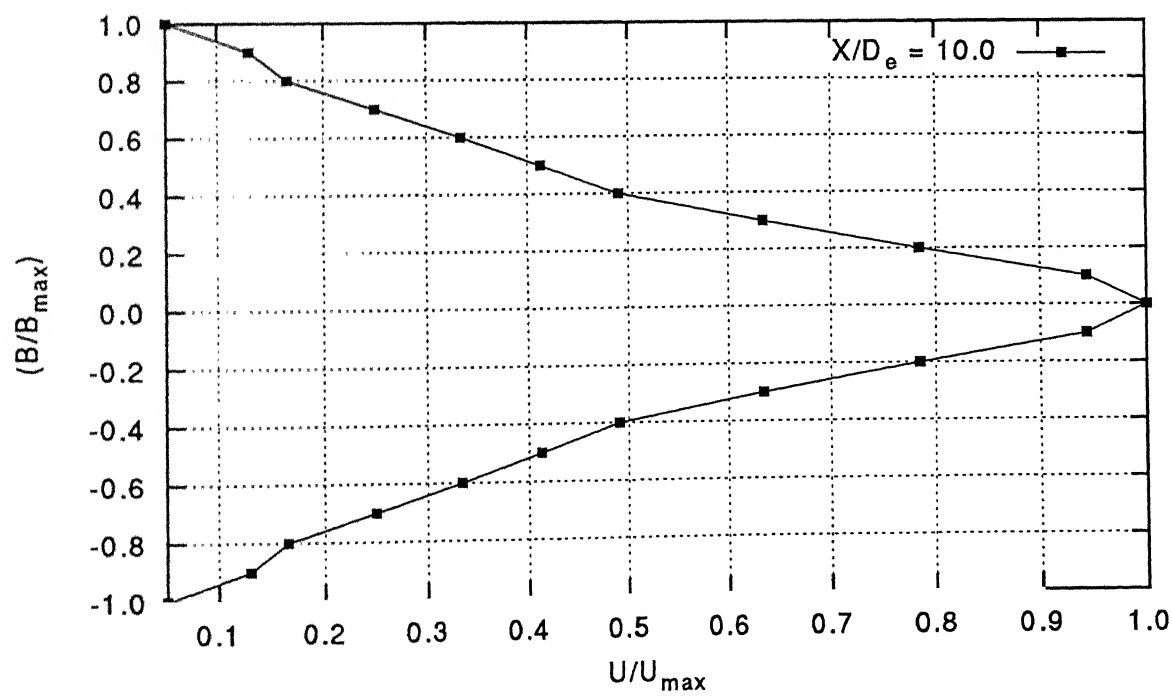

Fig. 3.7j Velocity profile at NPR 4

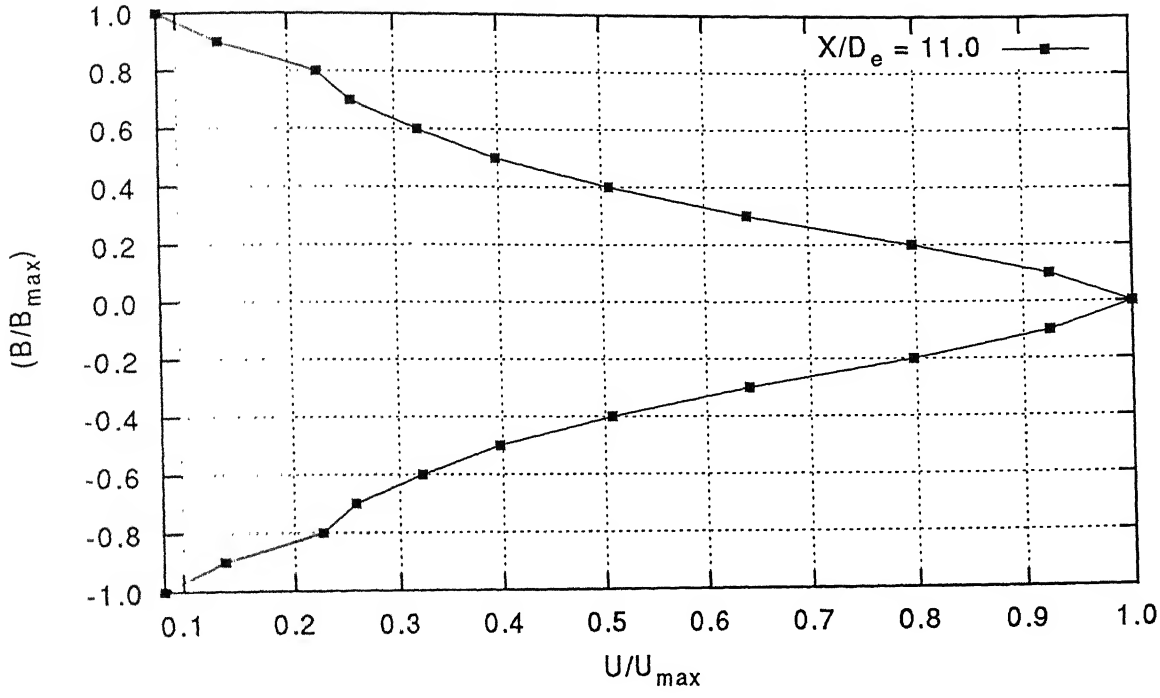

Fig. 3.7k Velocity profile at NPR 4

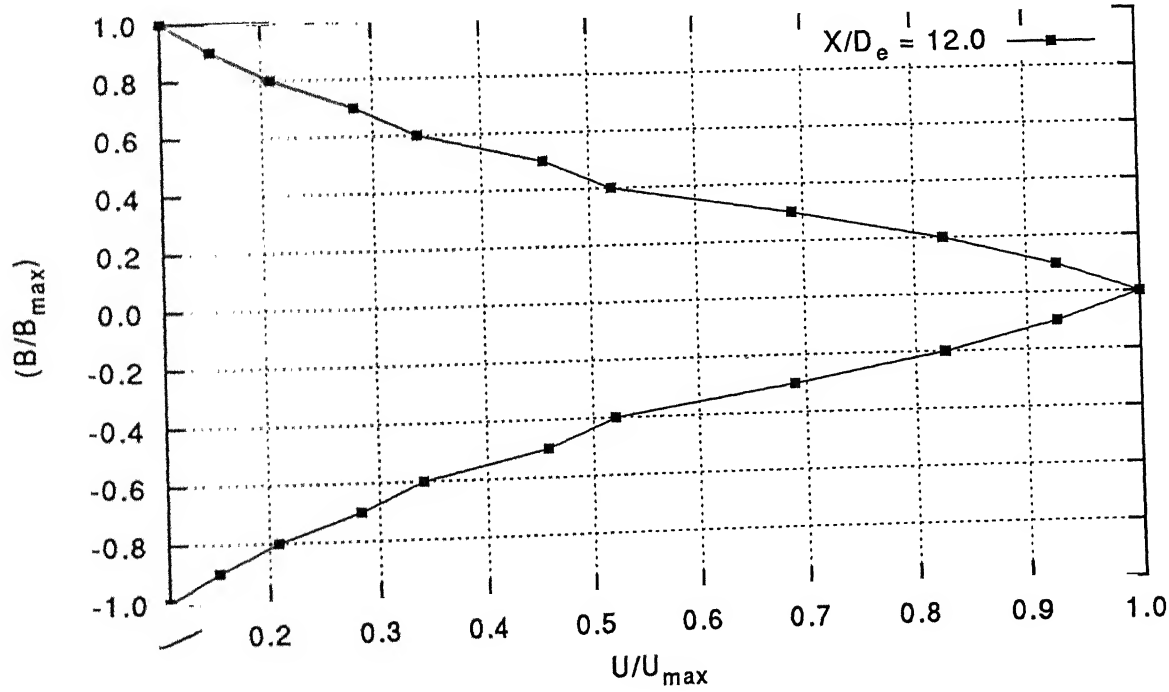

Fig. 3.7l Velocity profile at NPR 4

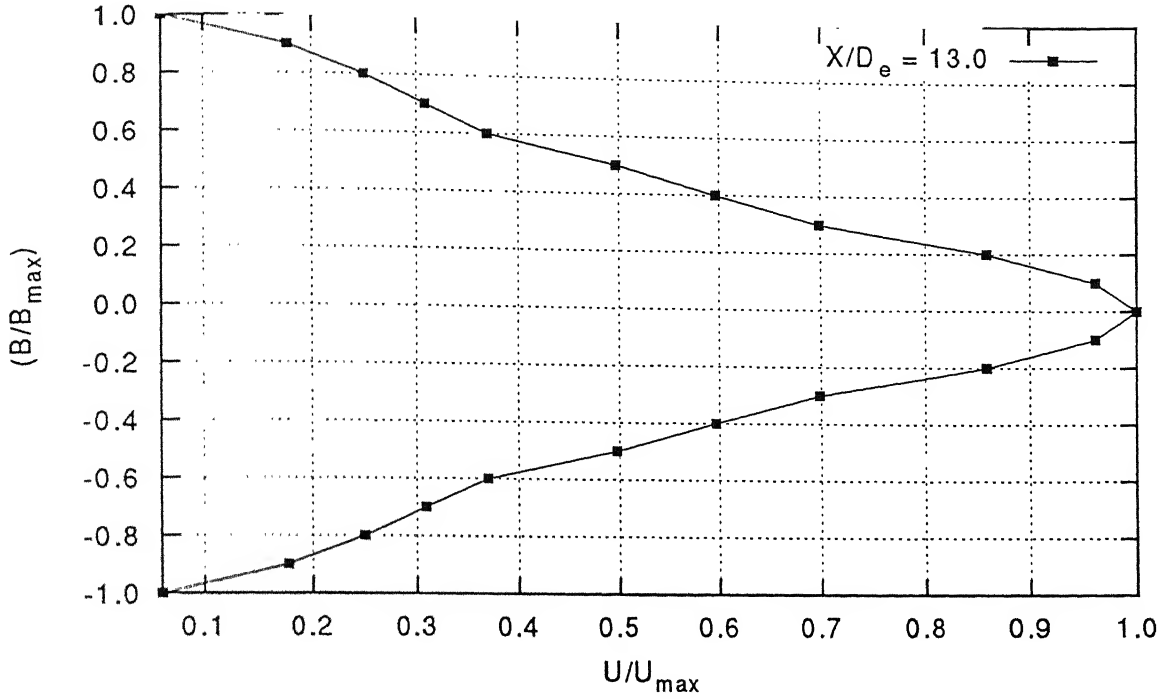

Fig. 3.7m Velocity profile at NPR 4

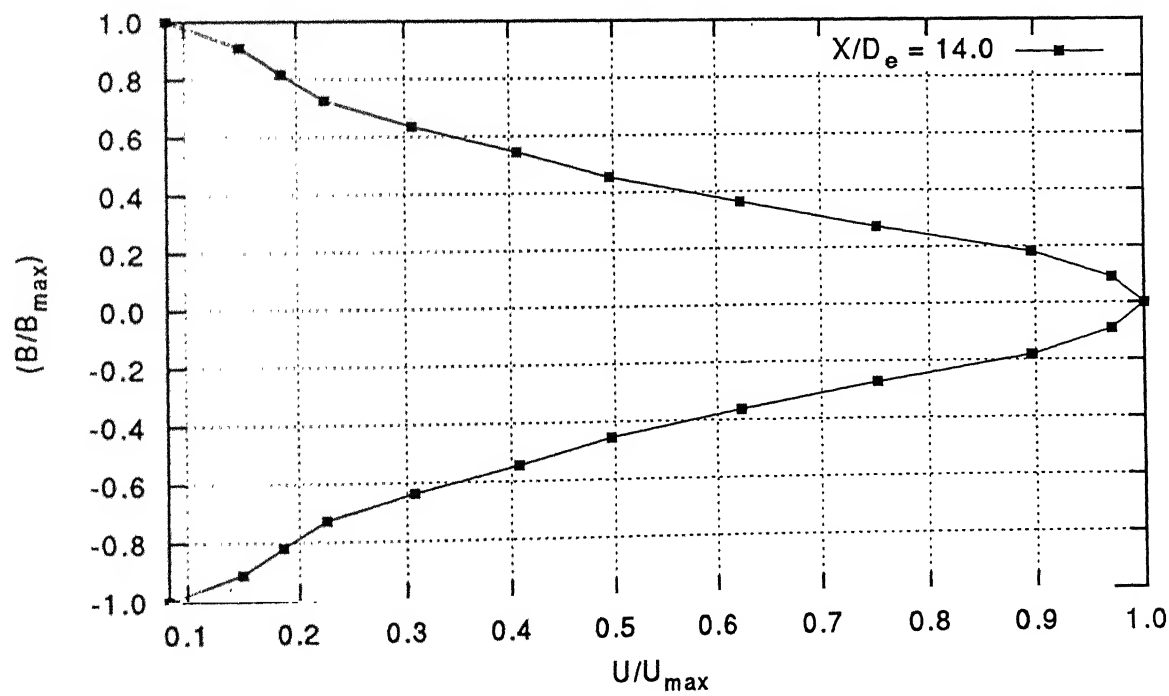

Fig. 3.7n Velocity profile at NPR 4

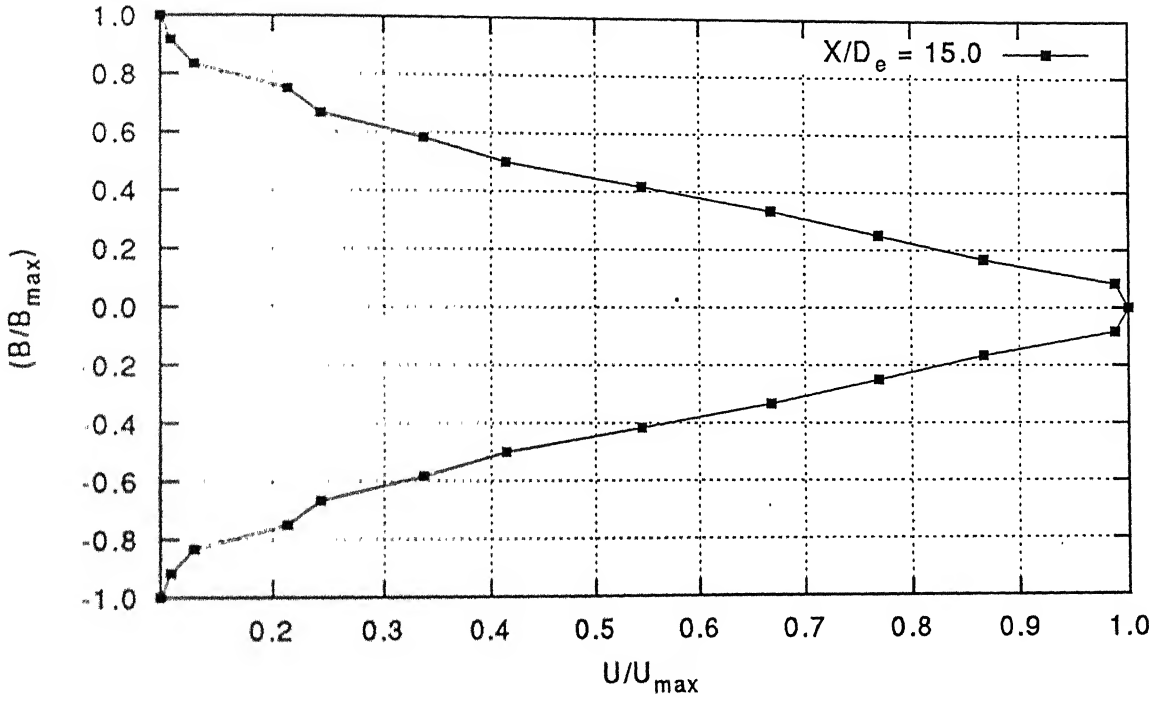

Fig. 3.7o Velocity profile at NPR 4

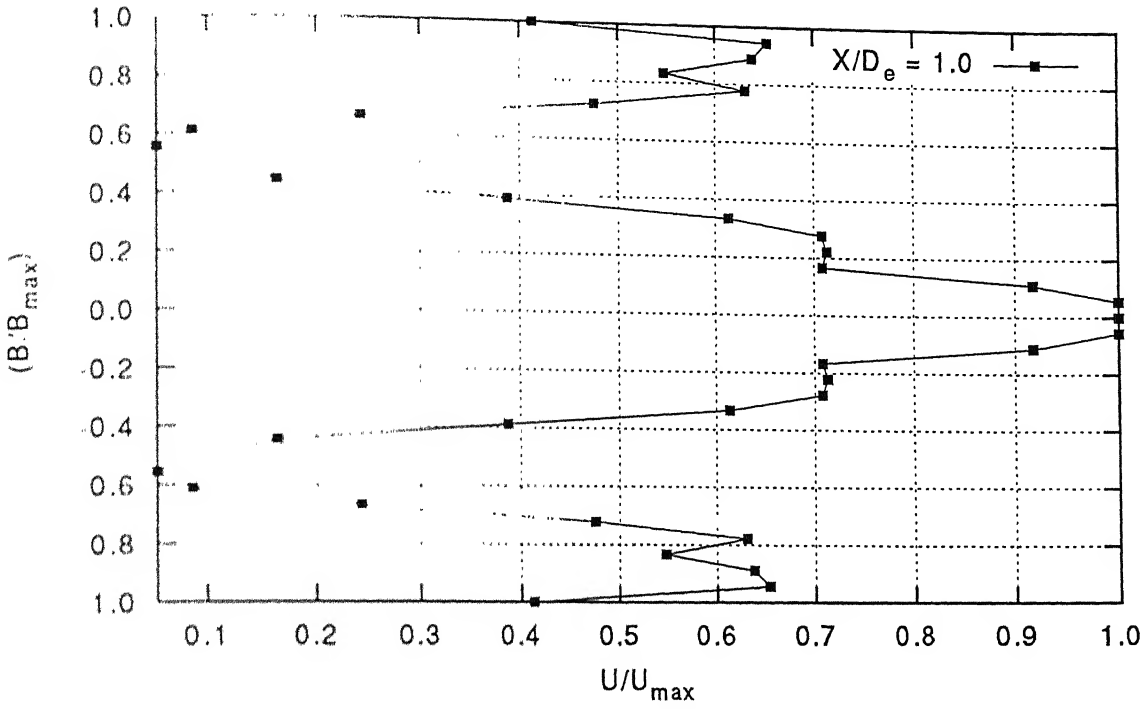

Fig. 3.8a Velocity profile at NPR 5

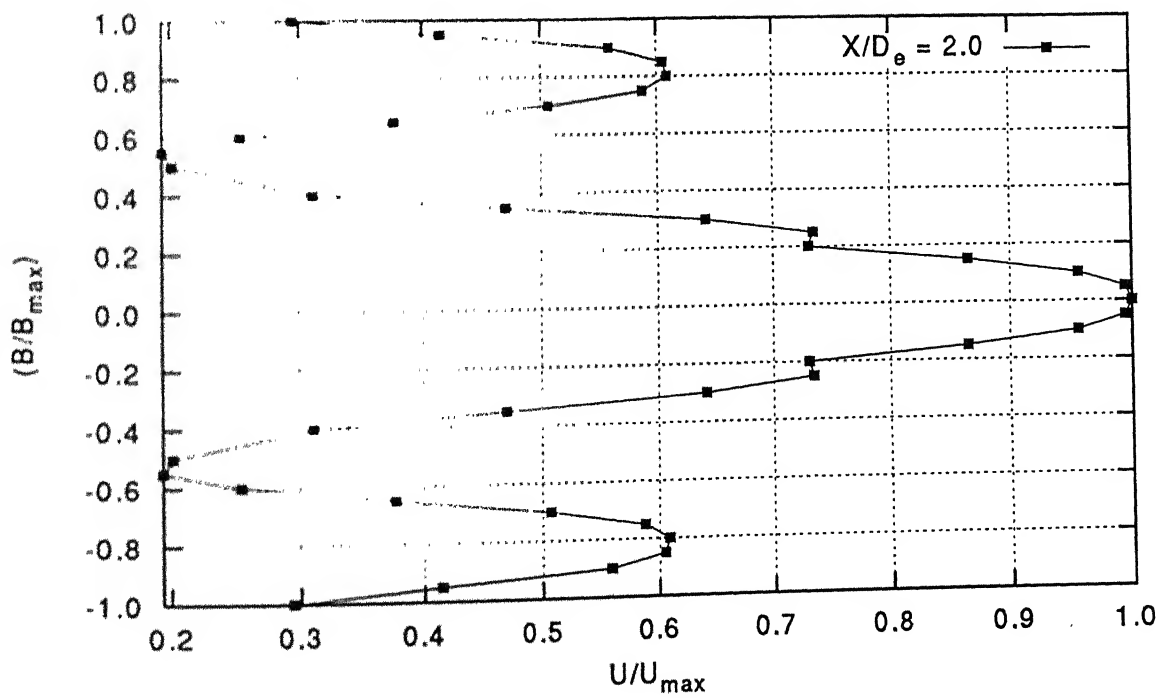

Fig. 3.8b Velocity profile at NPR 5

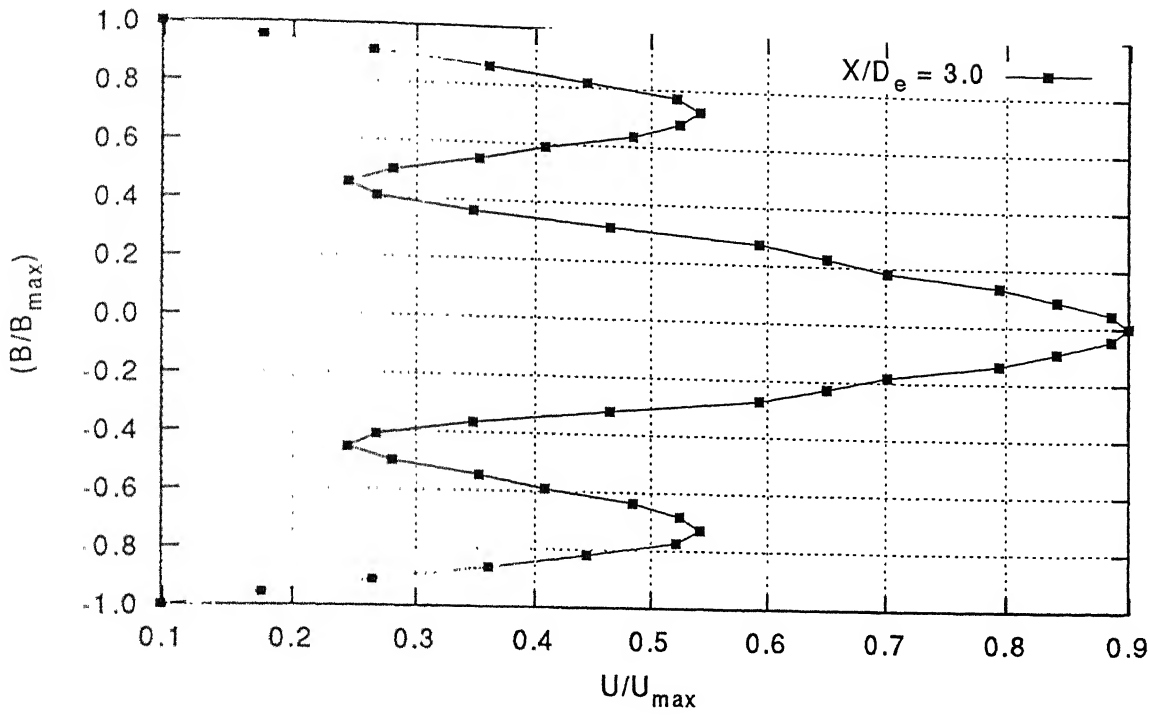

Fig. 3.8c Velocity profile at NPR 5

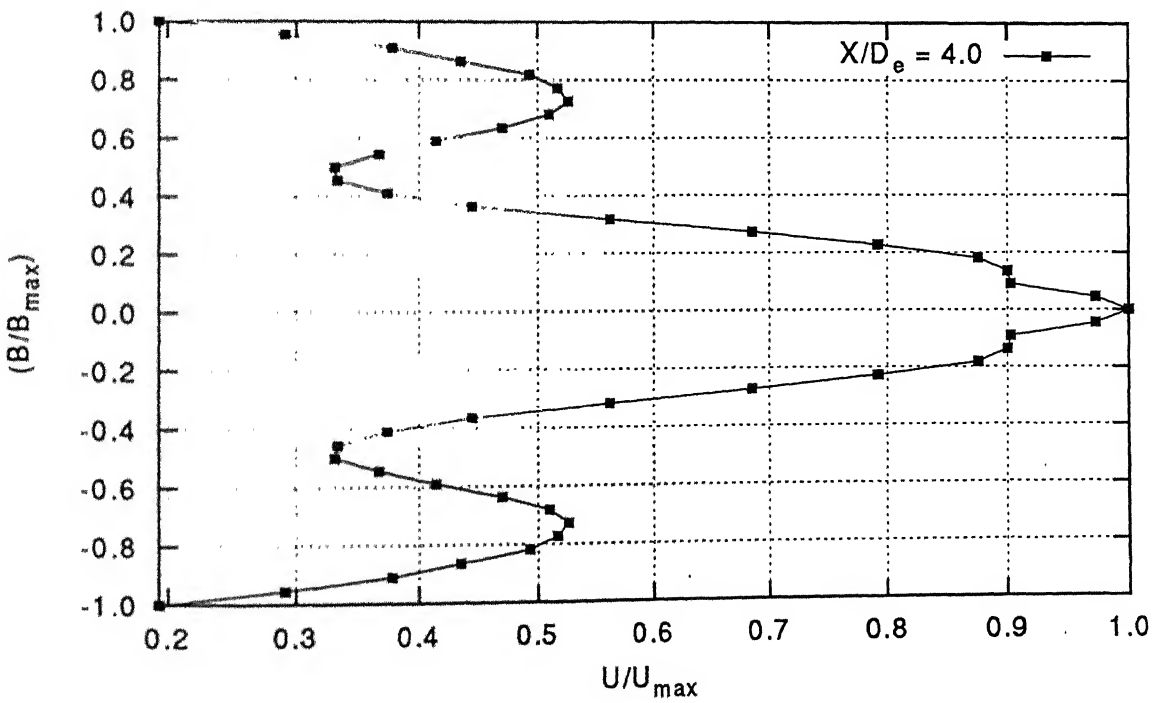

Fig. 3.8d Velocity profile at NPR 5

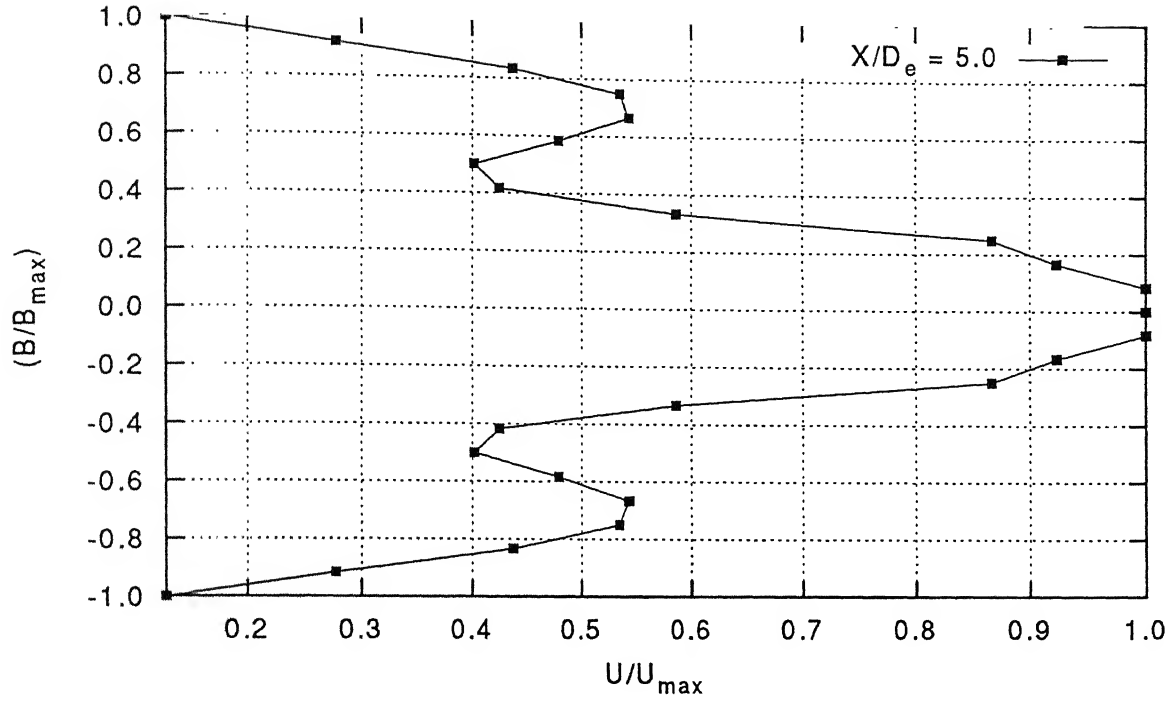

Fig 3.8e Velocity profile at NPR 5

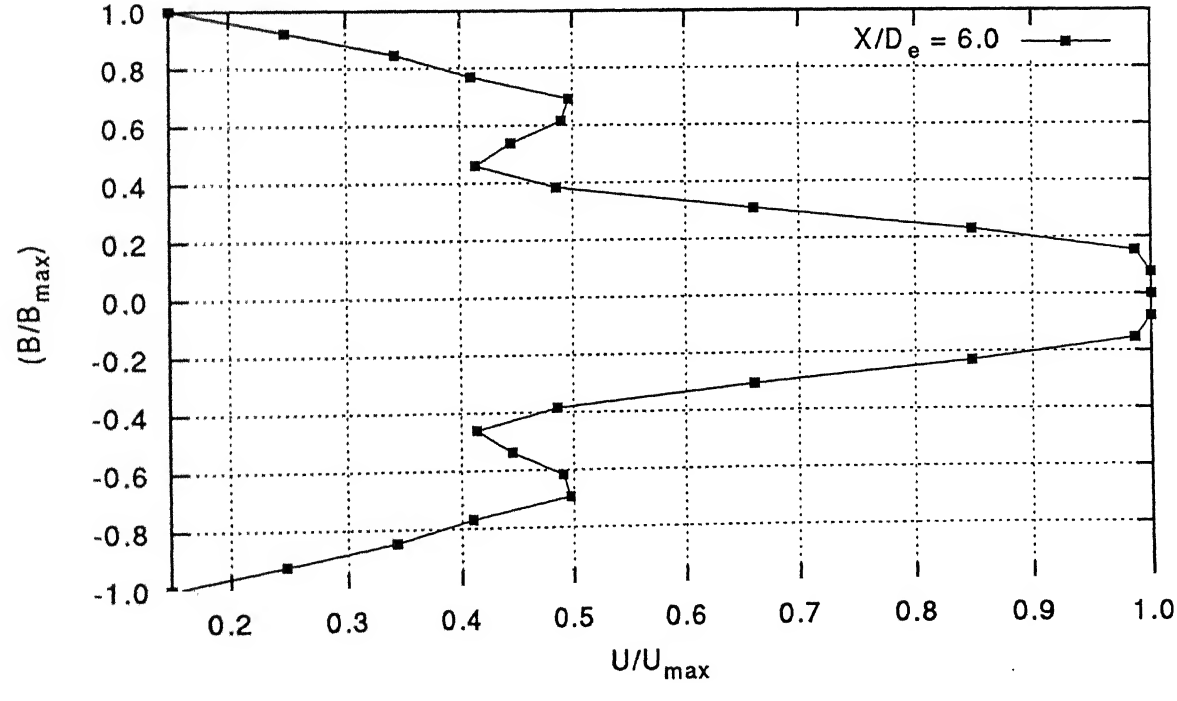

Fig. 3.8f Velocity profile at NPR 5

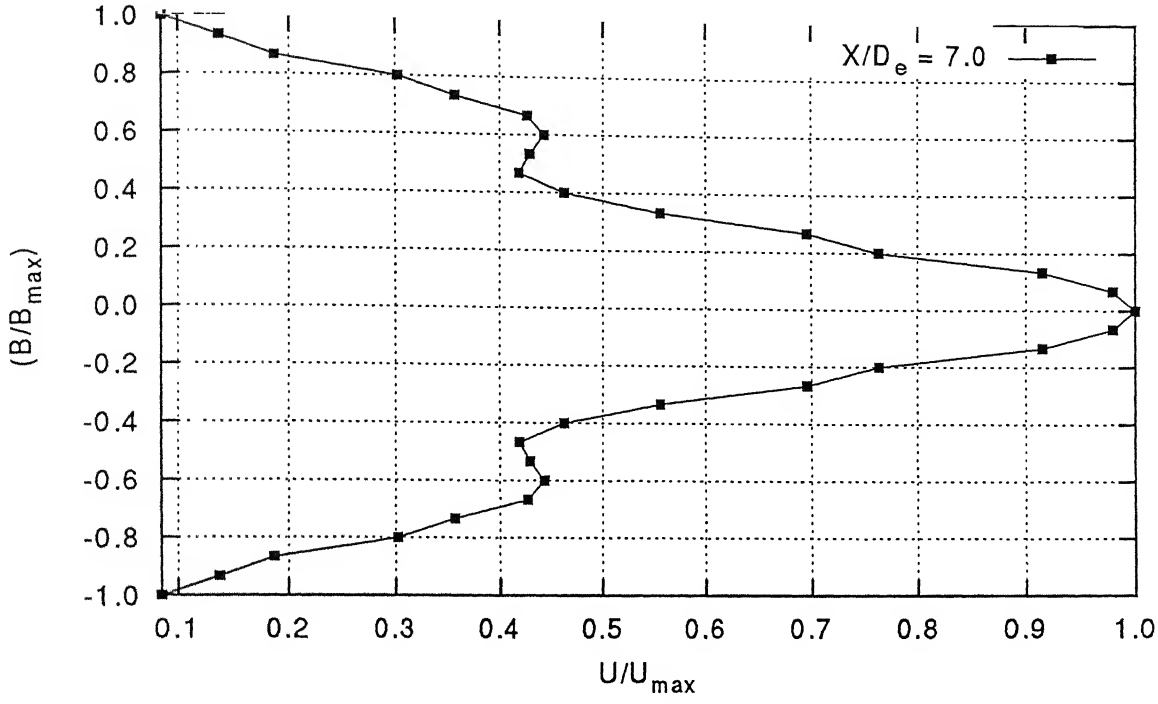

Fig. 3.8g Velocity profile at NPR 5

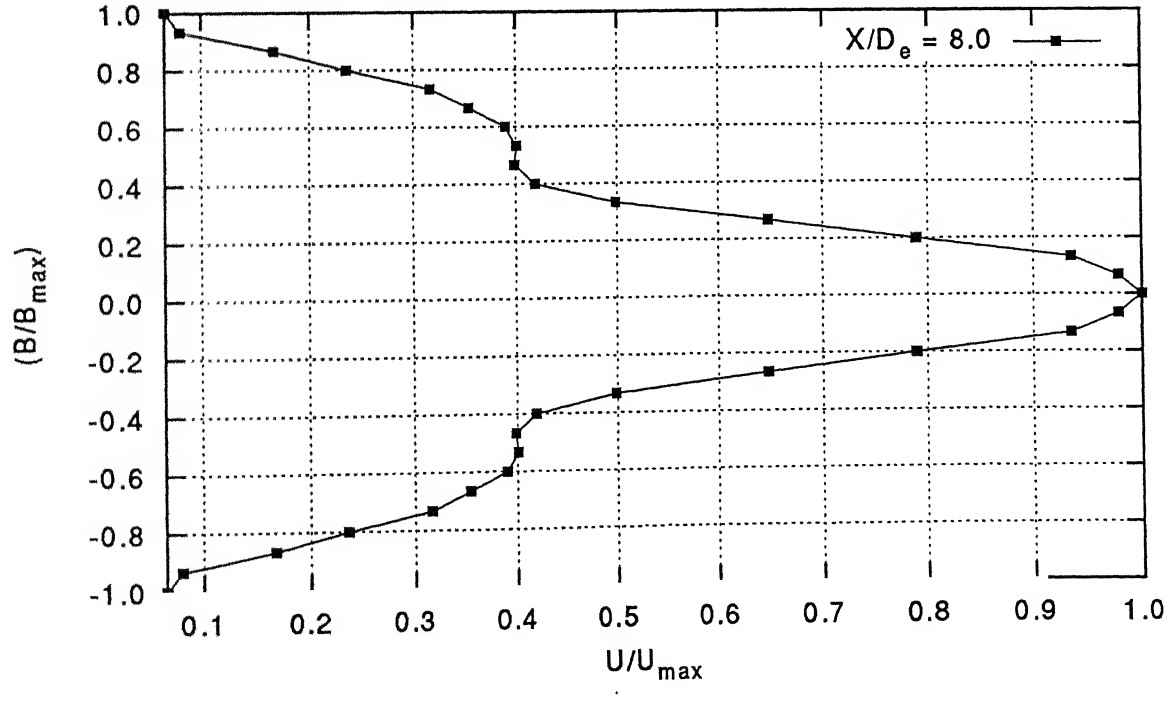

Fig. 3.8h Velocity profile at NPR 5

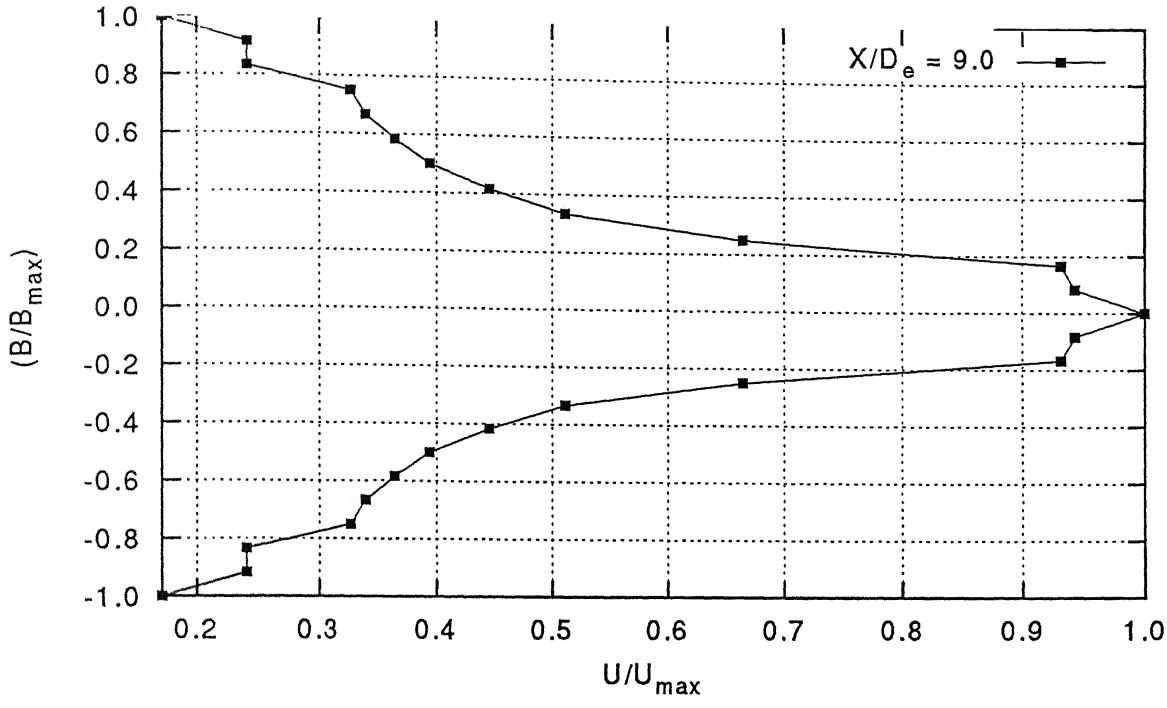

Fig. 3.8i Velocity profile at NPR 5

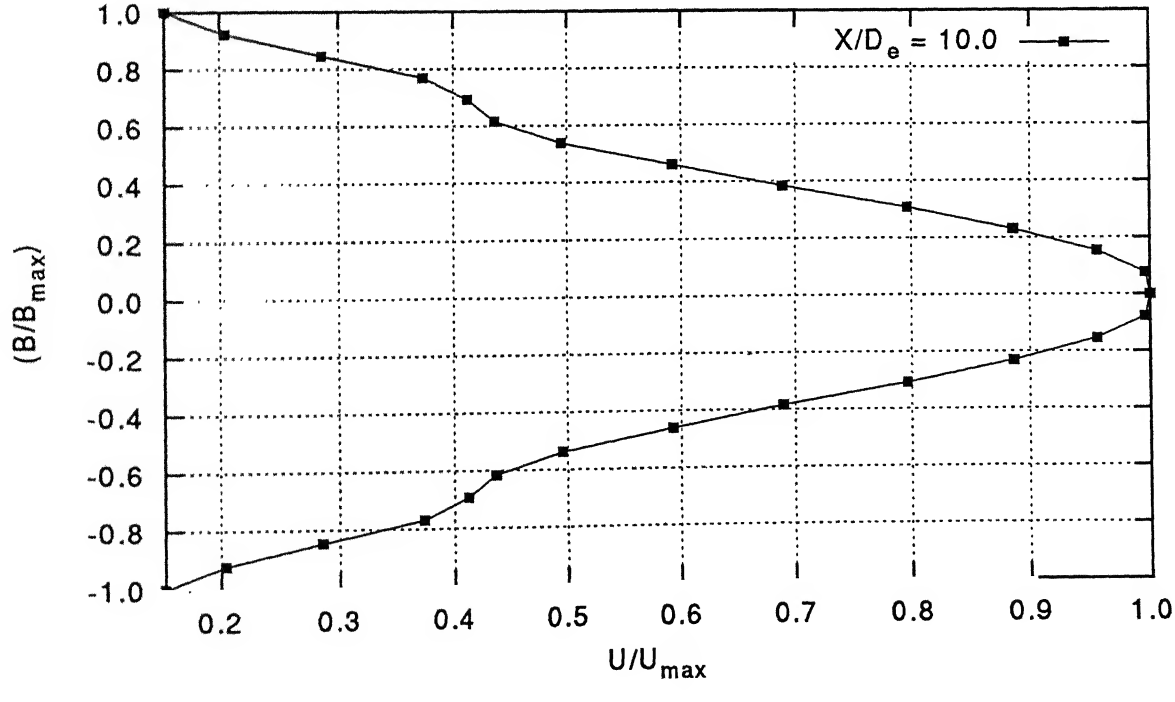

Fig. 3.8j Velocity profile at NPR 5

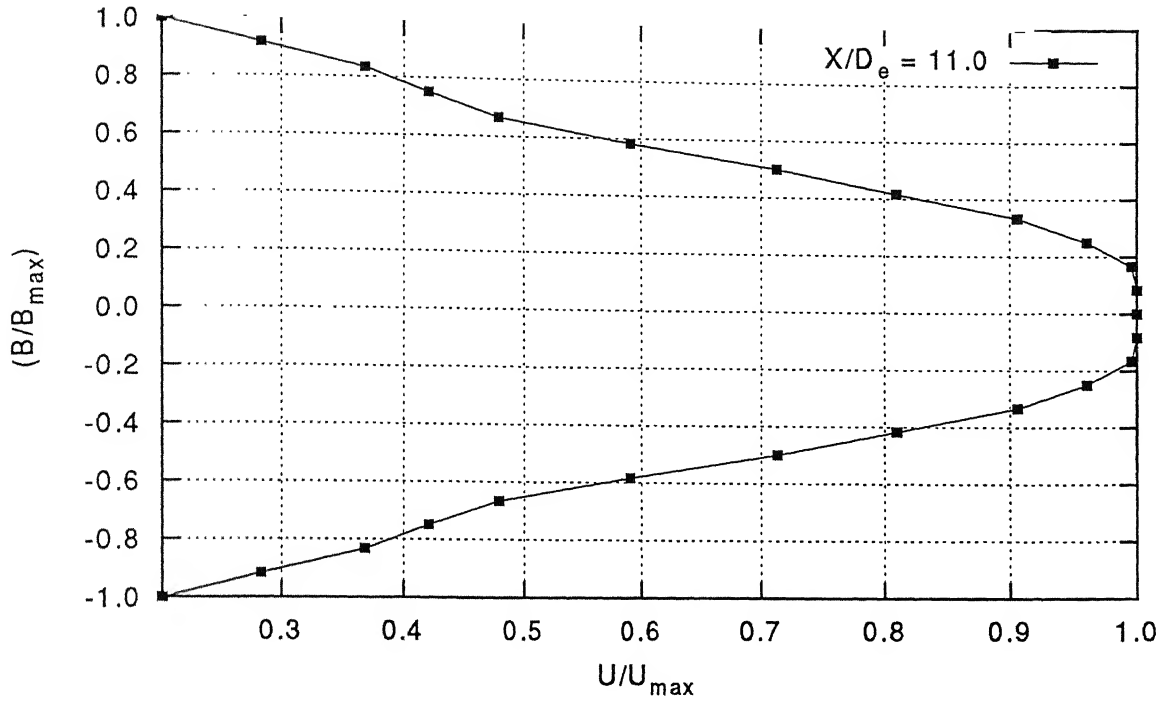

Fig. 3.8k Velocity profile at NPR 5

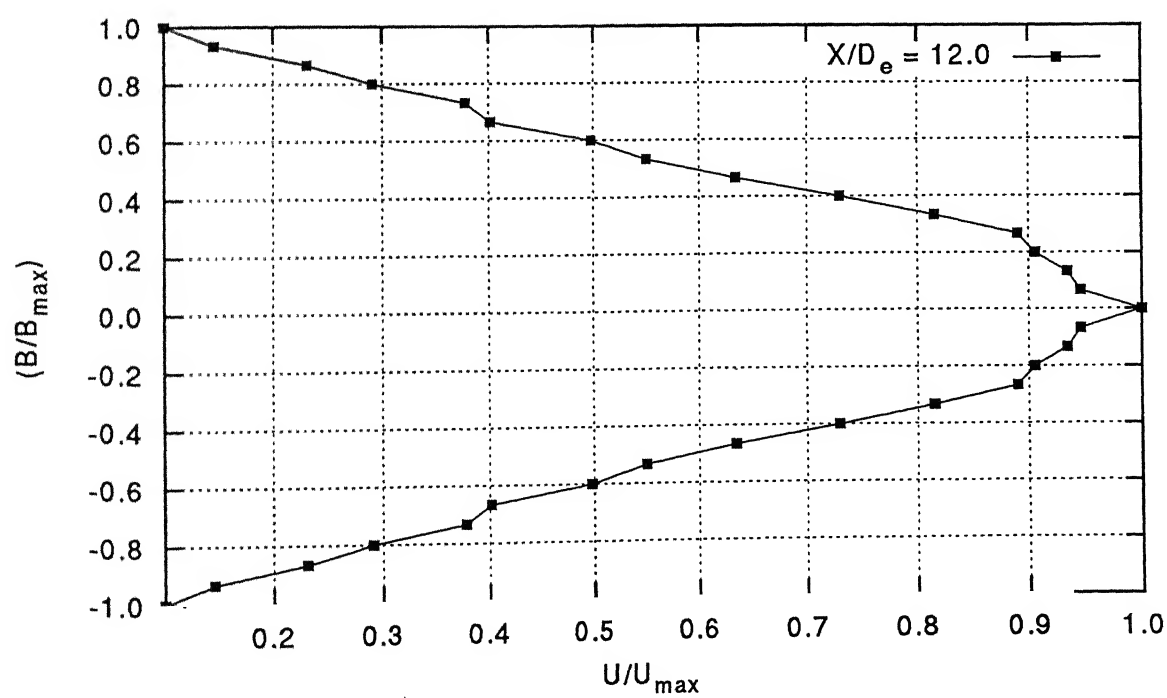

Fig. 3.8l Velocity profile at NPR 5

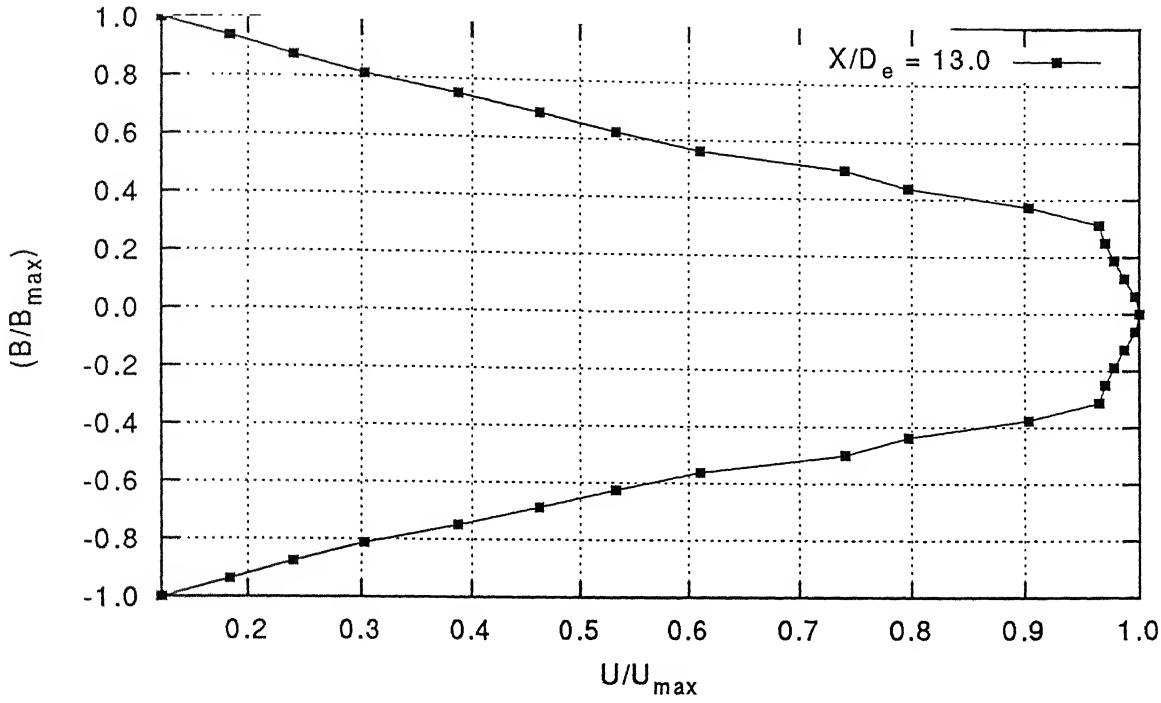

Fig. 3.8m Velocity profile at NPR 5

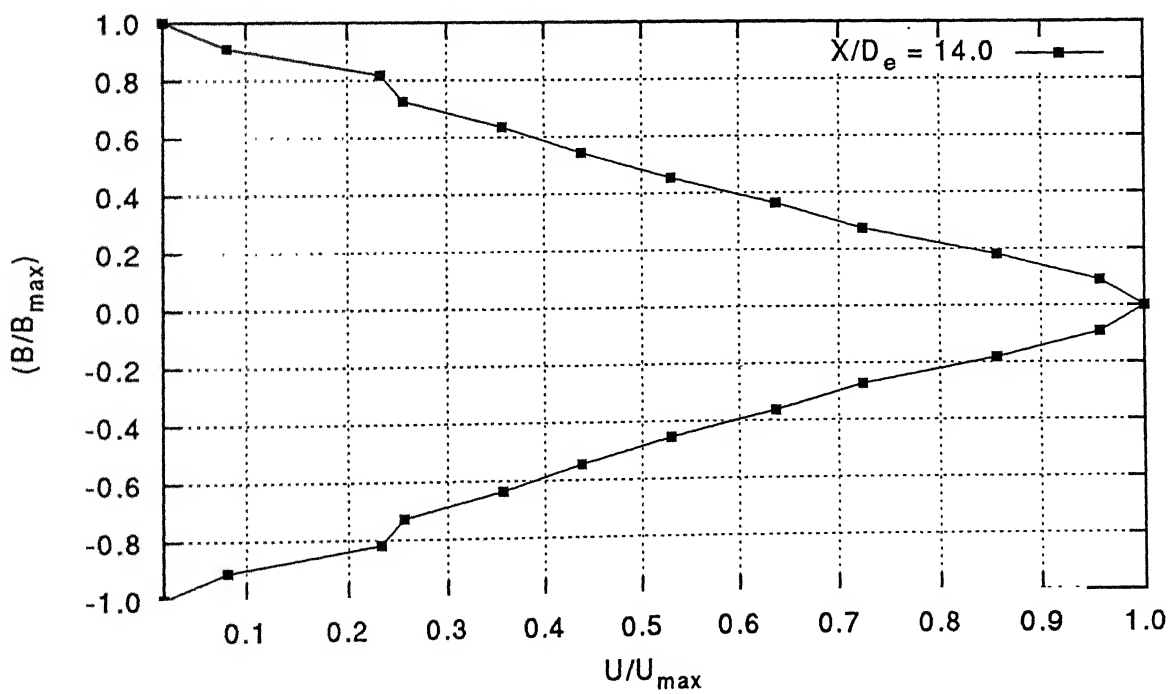

Fig. 3.8n Velocity profile at NPR 5

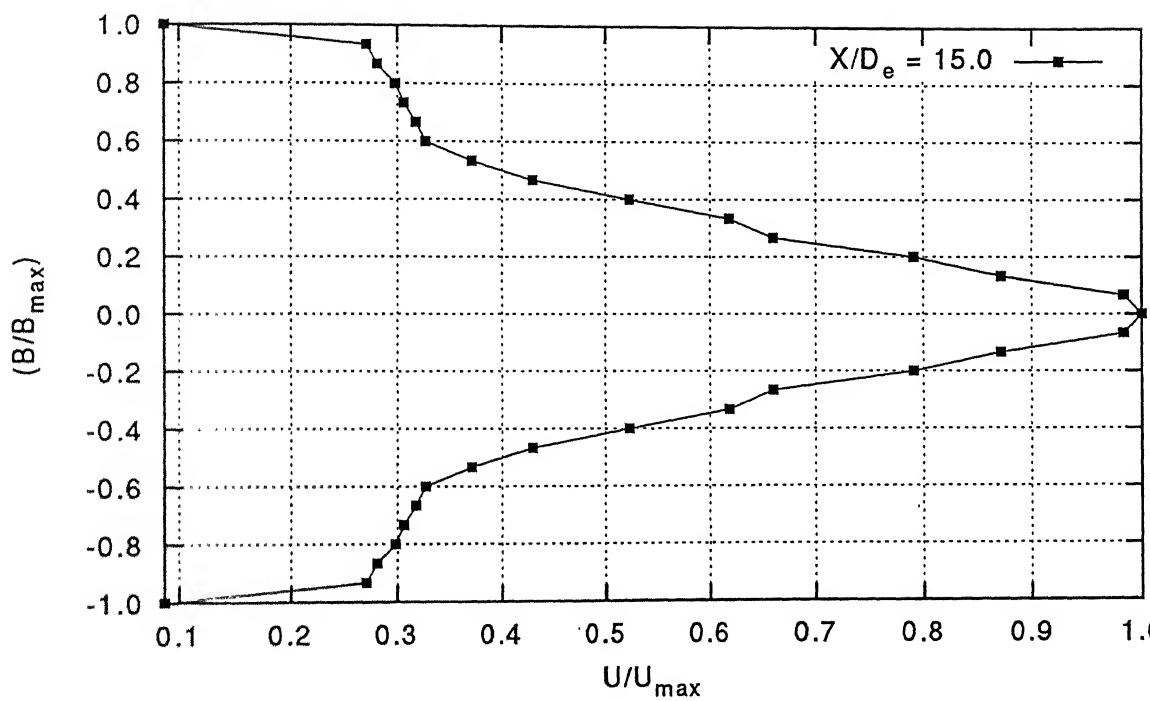

Fig. 3.8o Velocity profile at NPR 5

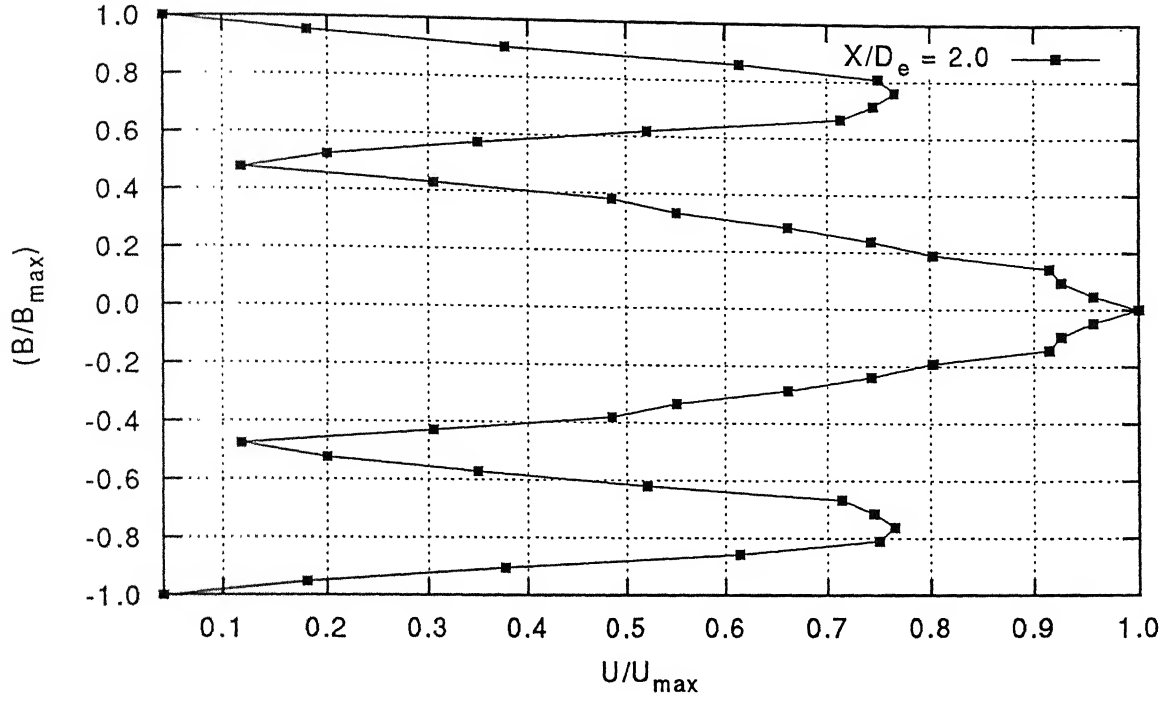

Fig. 3.9a Velocity profile at NPR 7

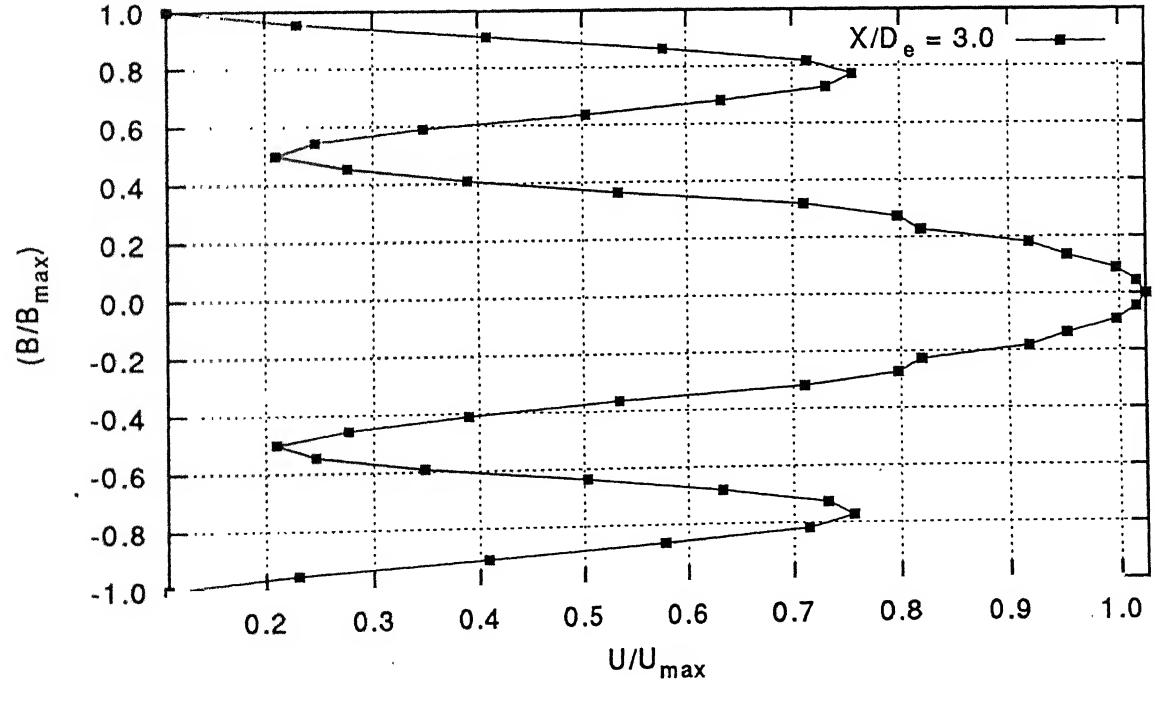

Fig. 3.9b Velocity profile at NPR 7

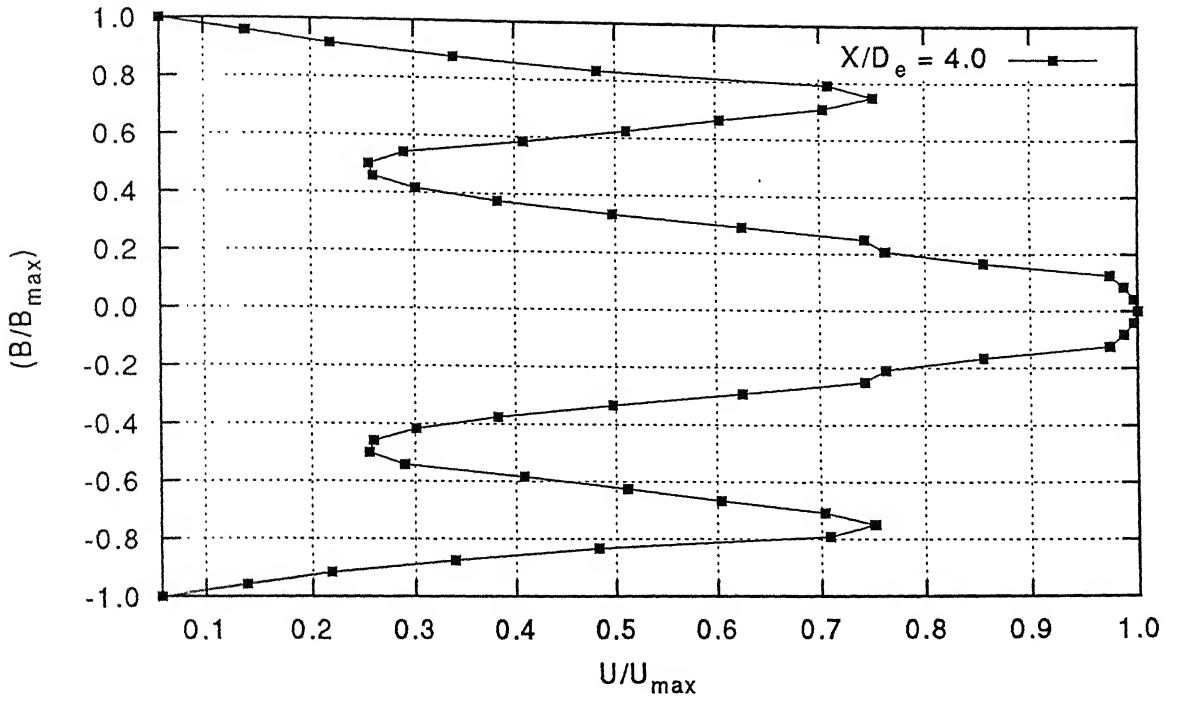

Fig. 3.9c Velocity profile at NPR 7

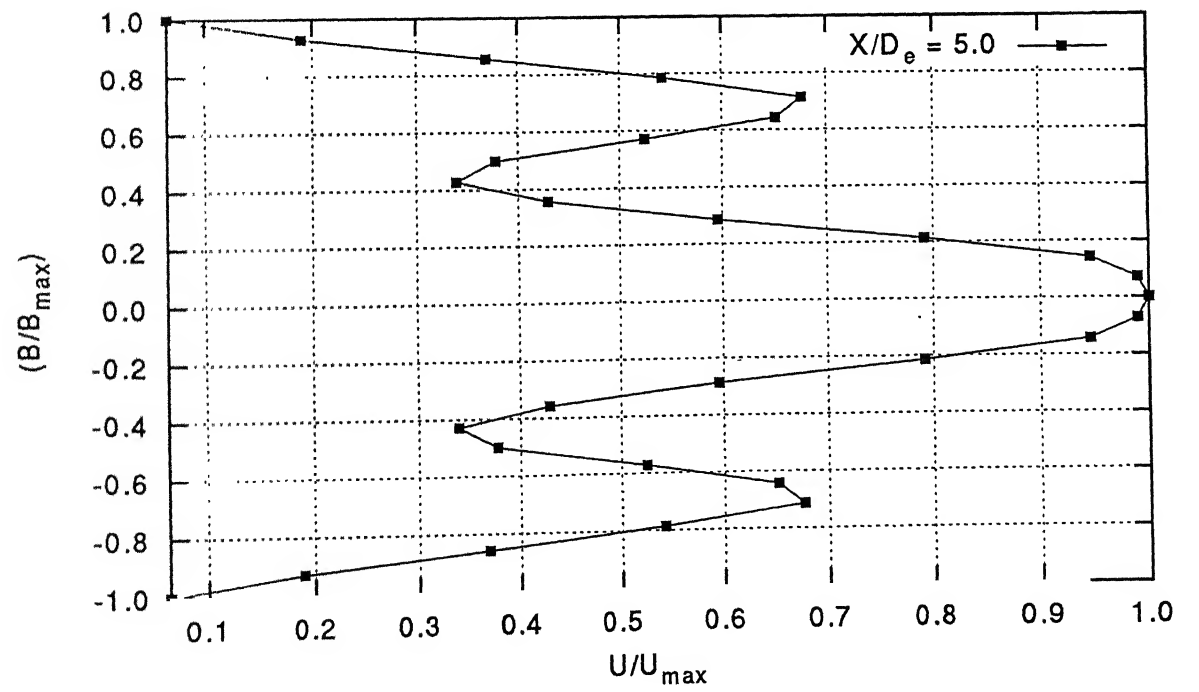

Fig 3.9d Velocity profile at NPR 7

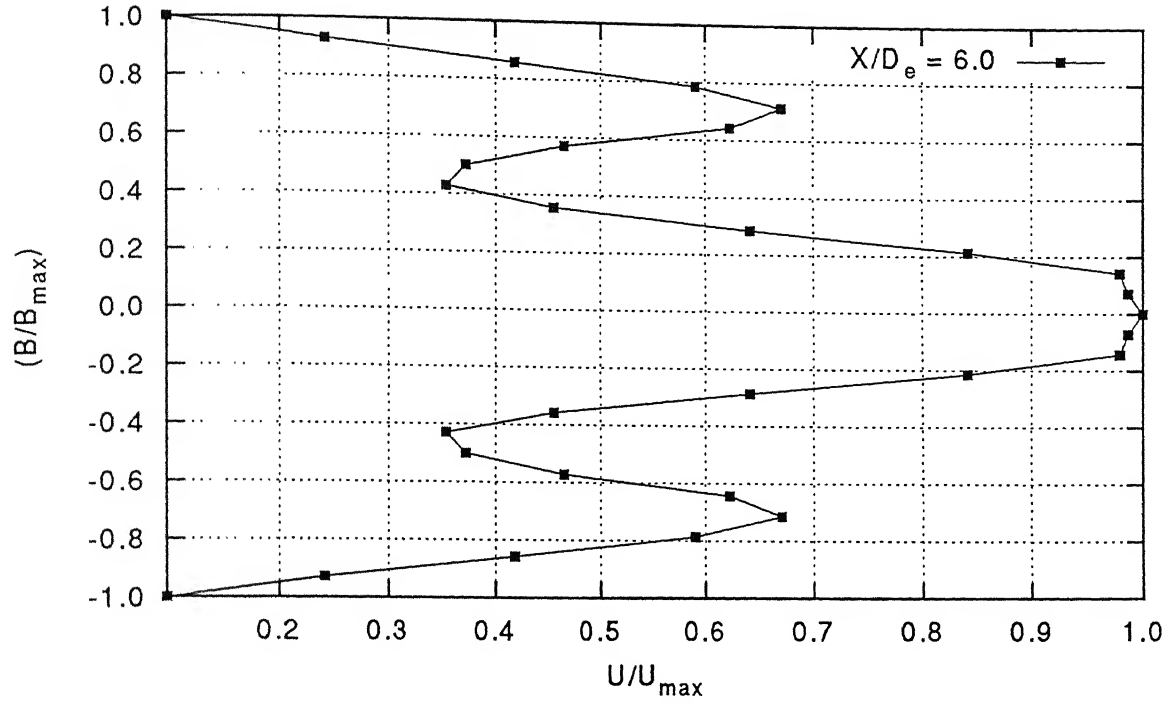

Fig. 3.9e Velocity profile at NPR 7

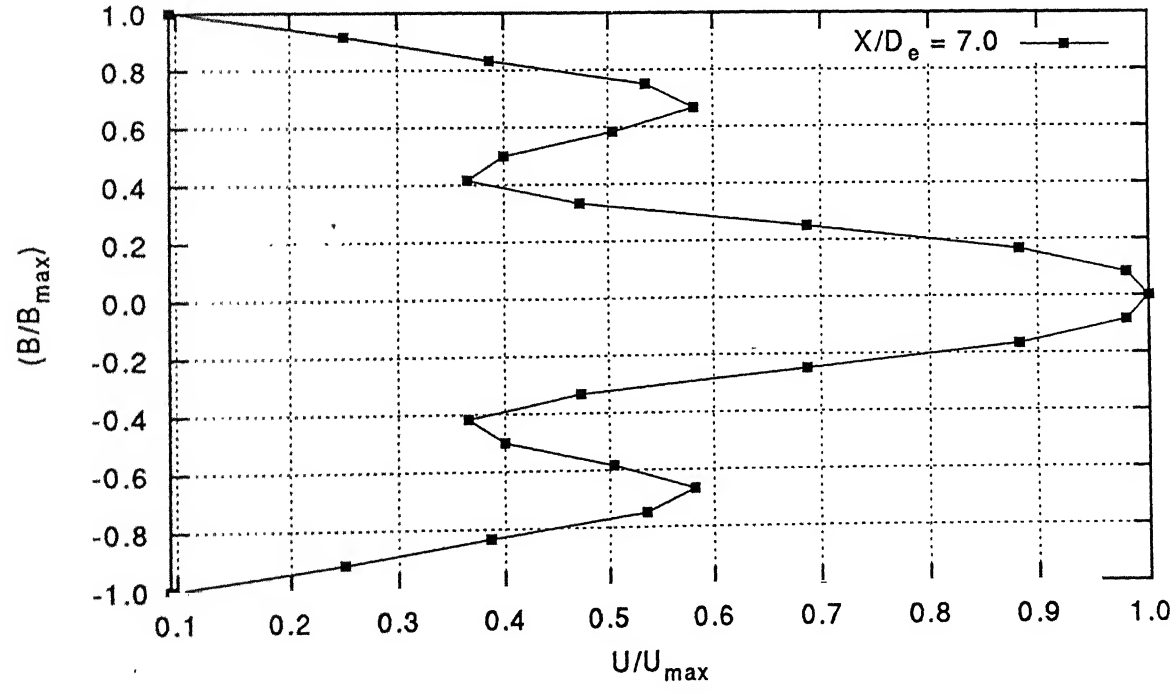

Fig. 3.9f Velocity profile at NPR 7

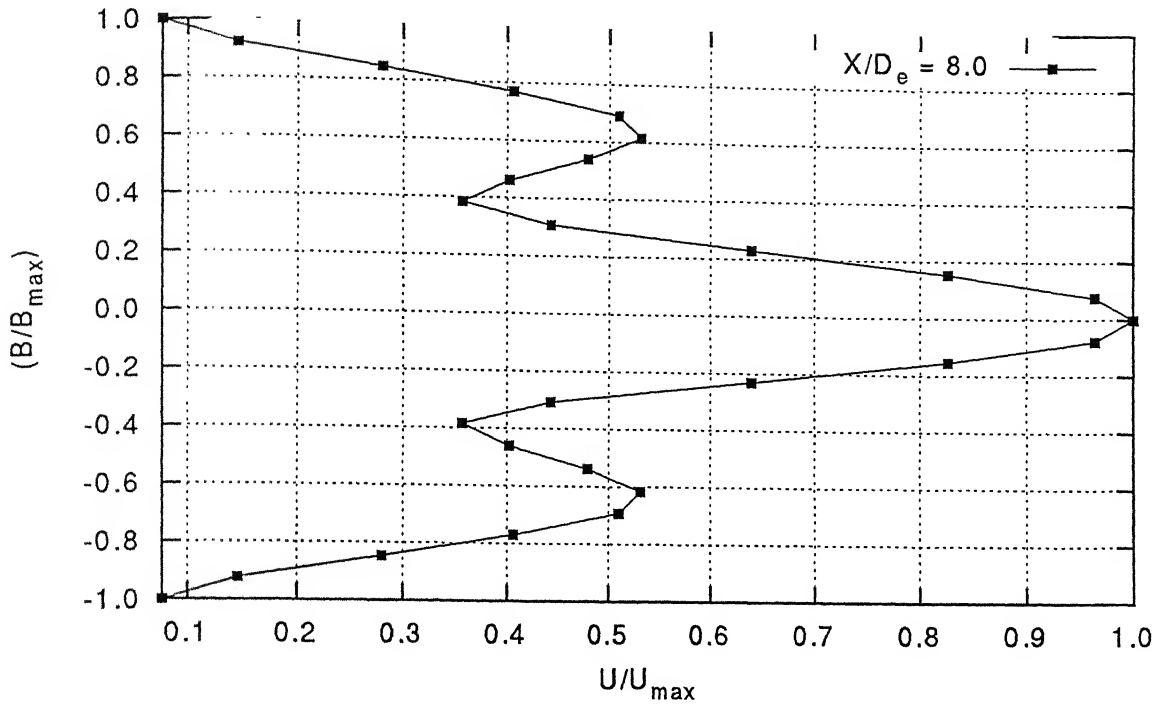

Fig. 3.9g Velocity profile at NPR 7

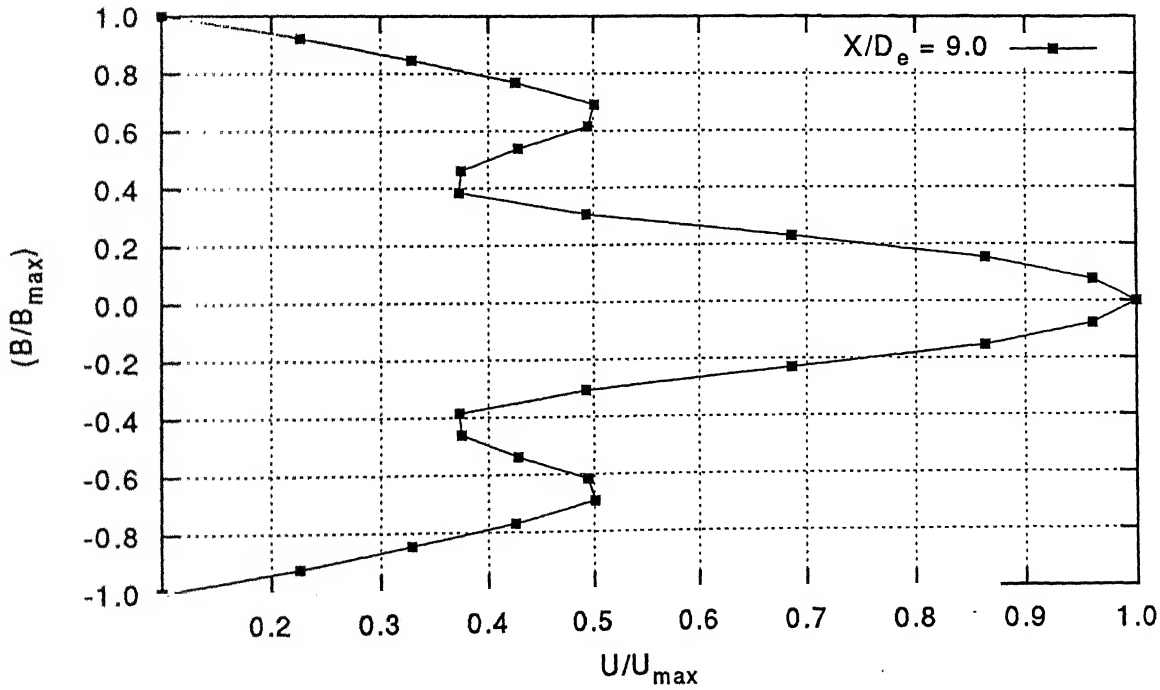

Fig. 3.9h Velocity profile at NPR 7

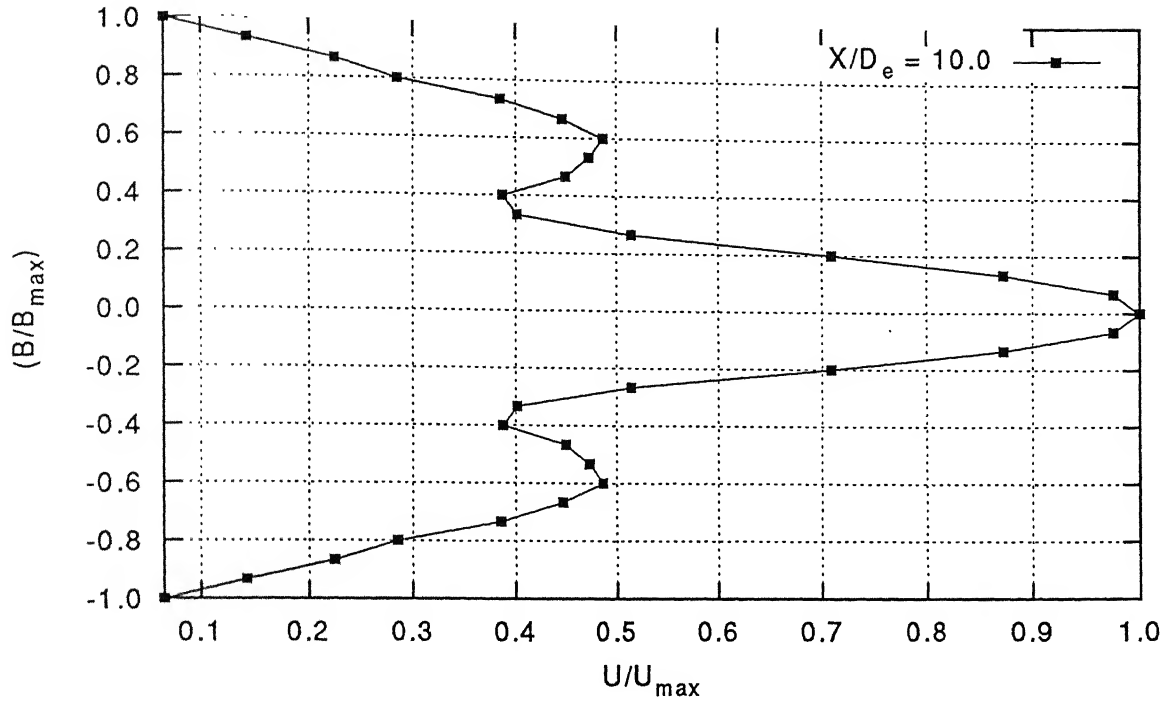

Fig. 3.9i Velocity profile at NPR 7

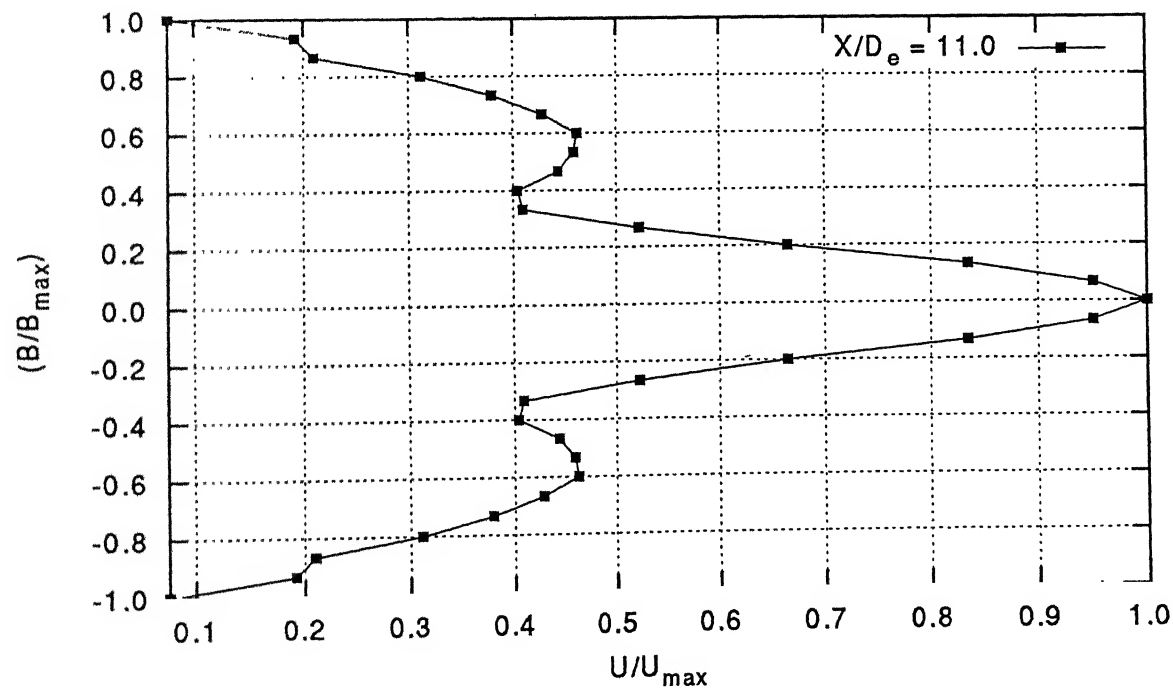

Fig. 3.9j Velocity profile at NPR 7

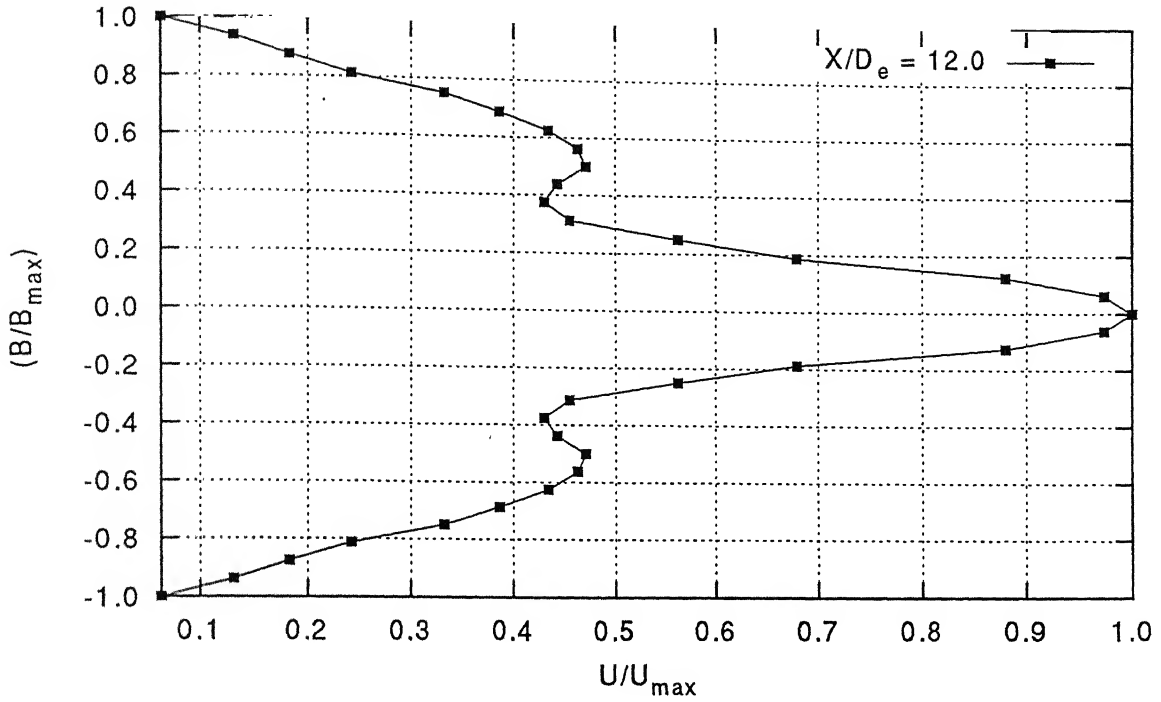

Fig. 3.9k Velocity profile at NPR 7

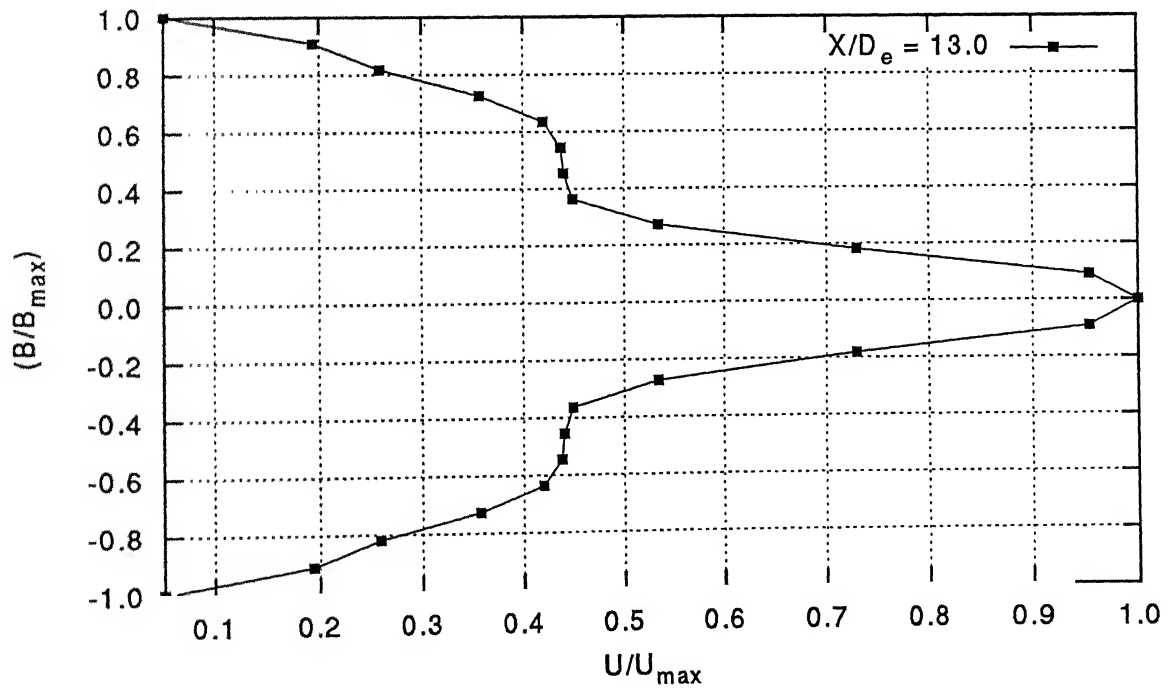

Fig. 3.9l Velocity profile at NPR 7

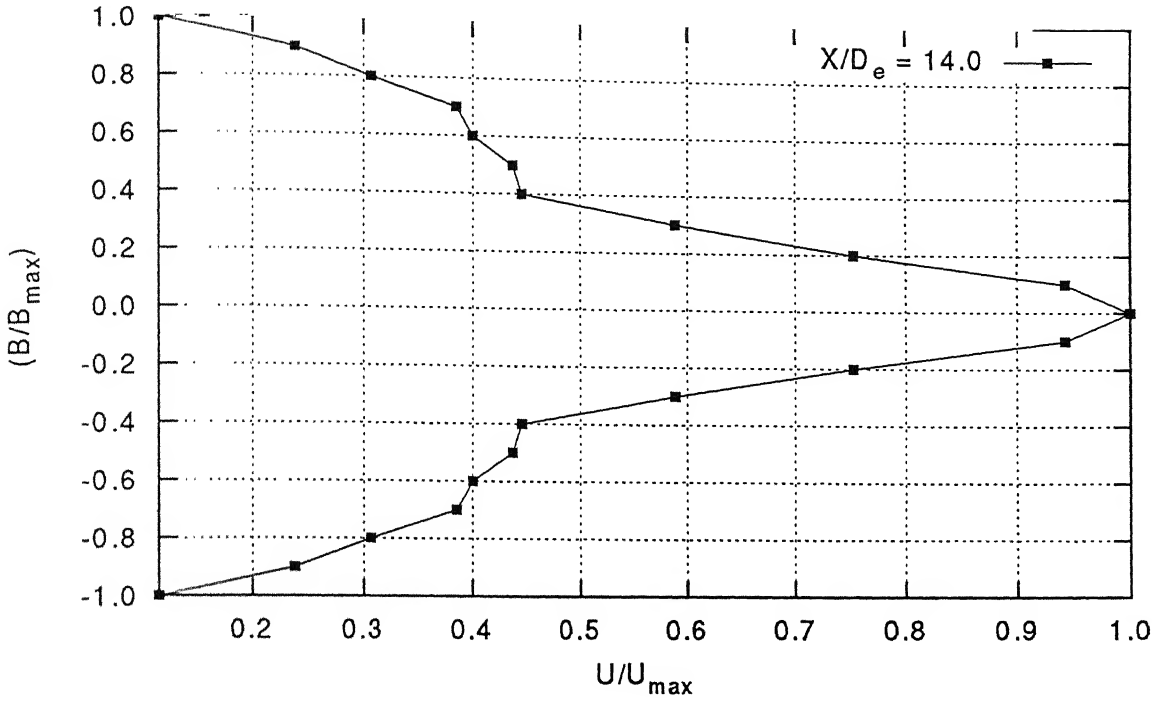

Fig. 3.9m Velocity profile at NPR 7

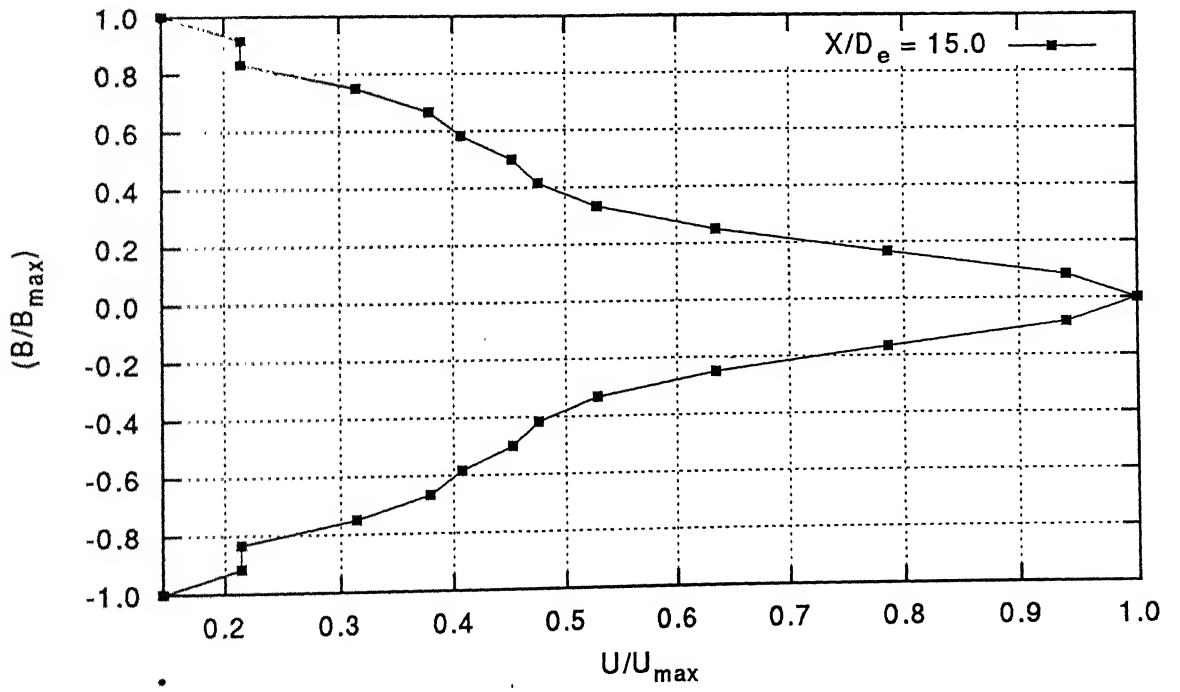

Fig. 3.9n Velocity profile at NPR 7

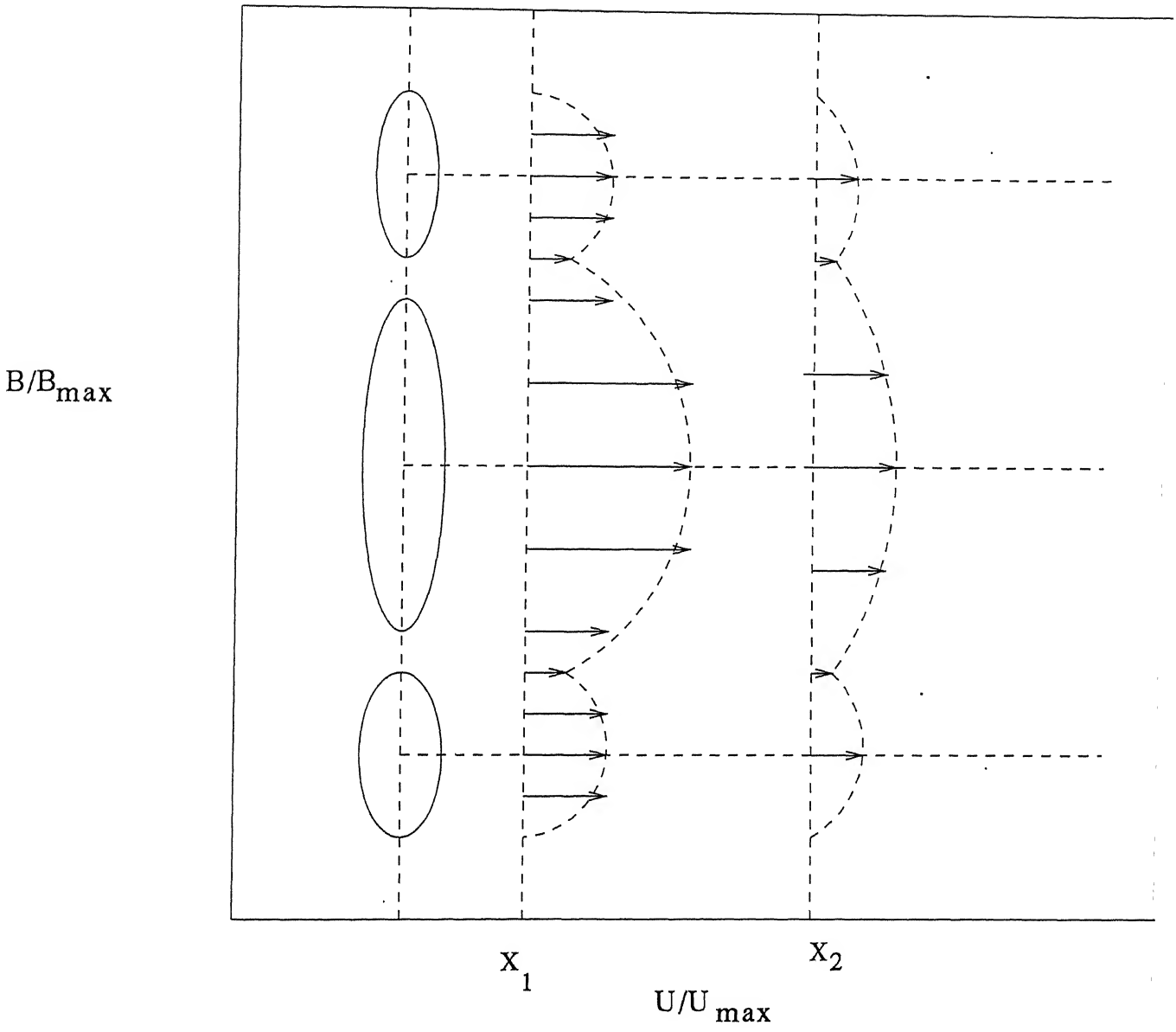

Fig. 3.10 Schematic figure of multijet confluence

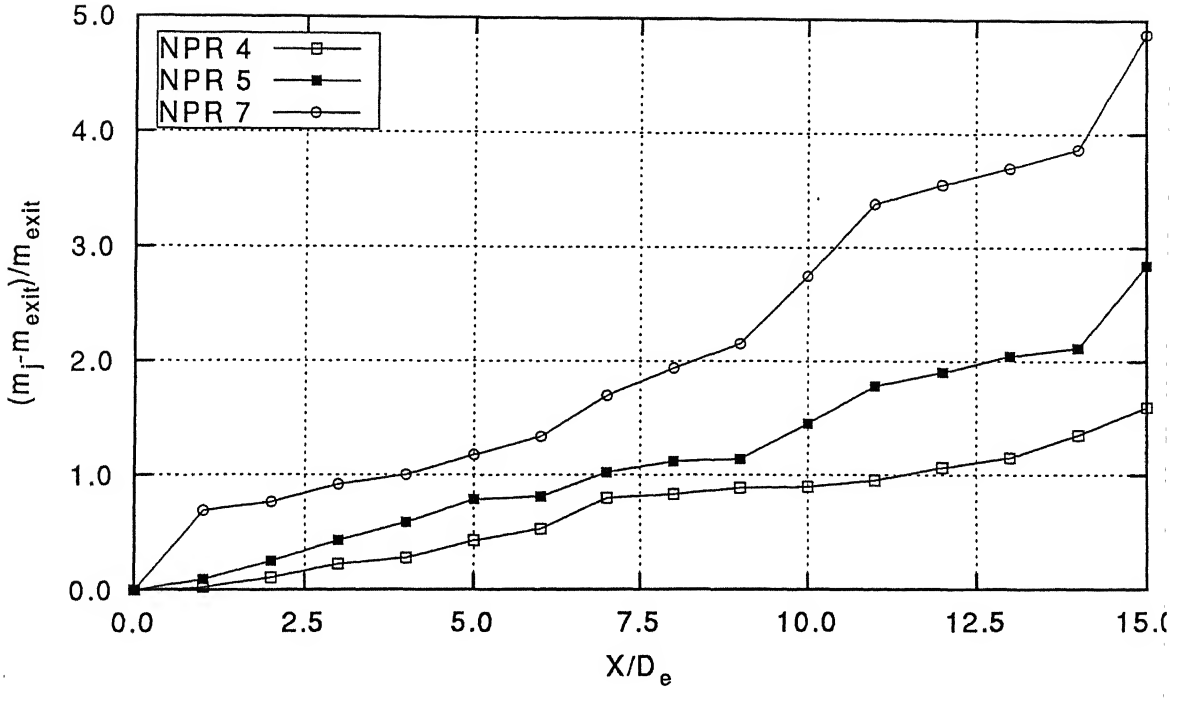

Fig. 3.11 Mass entrainment for core Nozzle

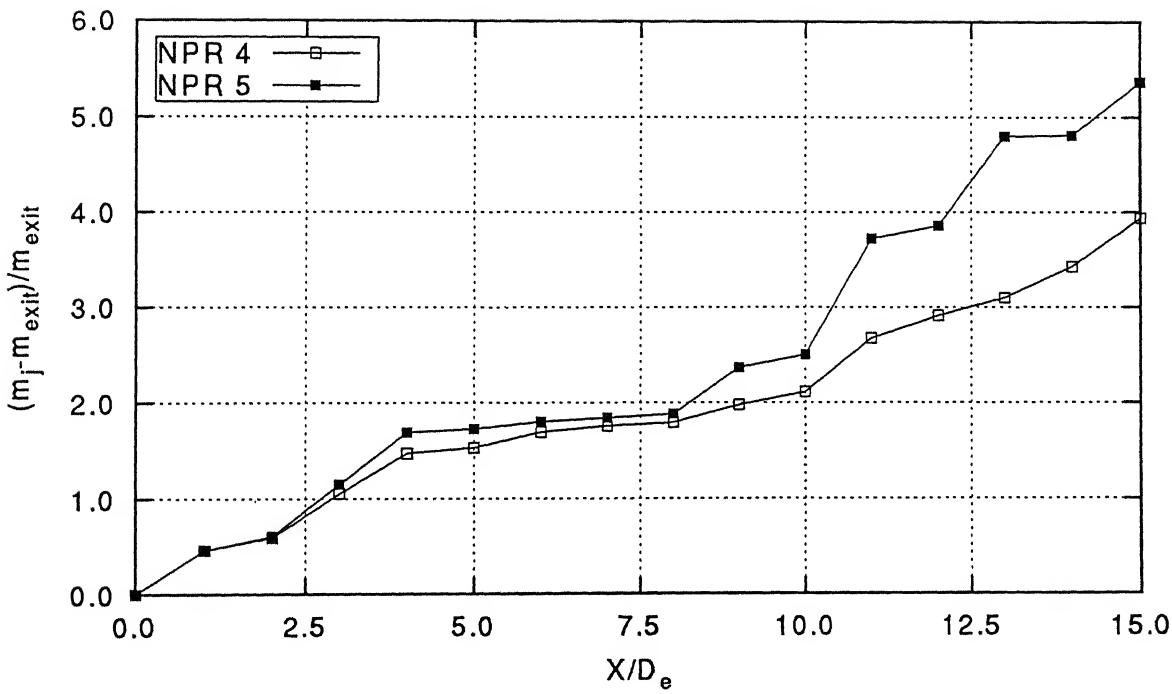

Fig. 3.12 Mass entrainment for Strapon Nozzle

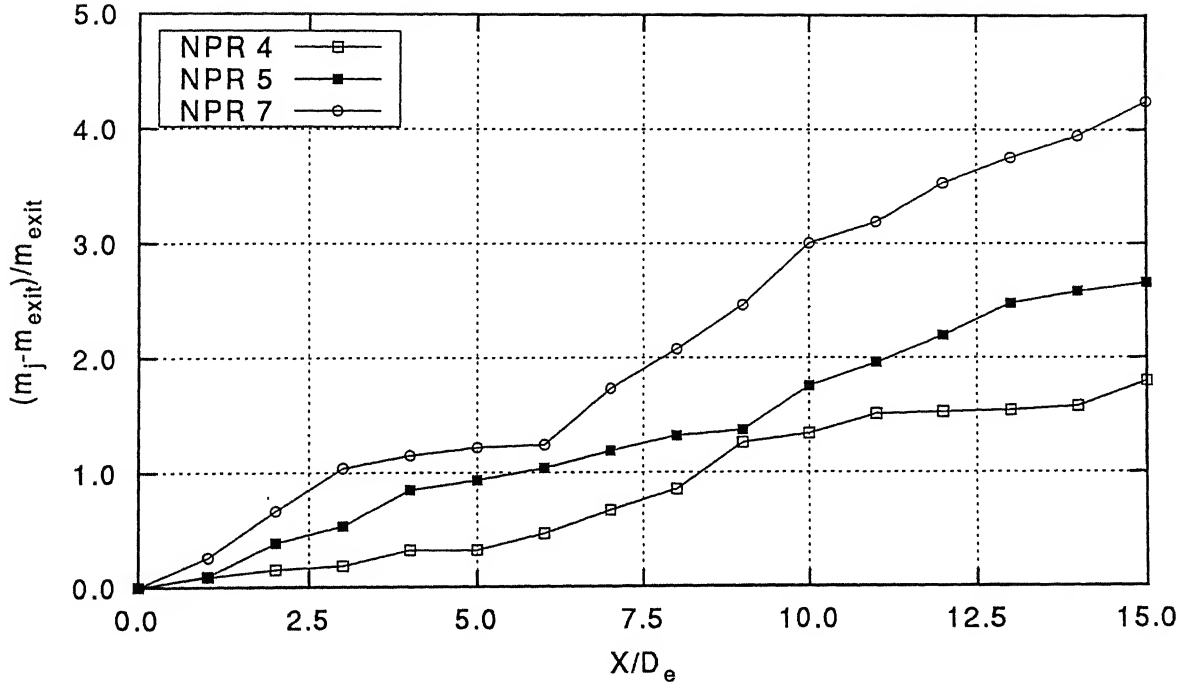

Fig. 3.13 Mass entrainment for Multijet Nozzles

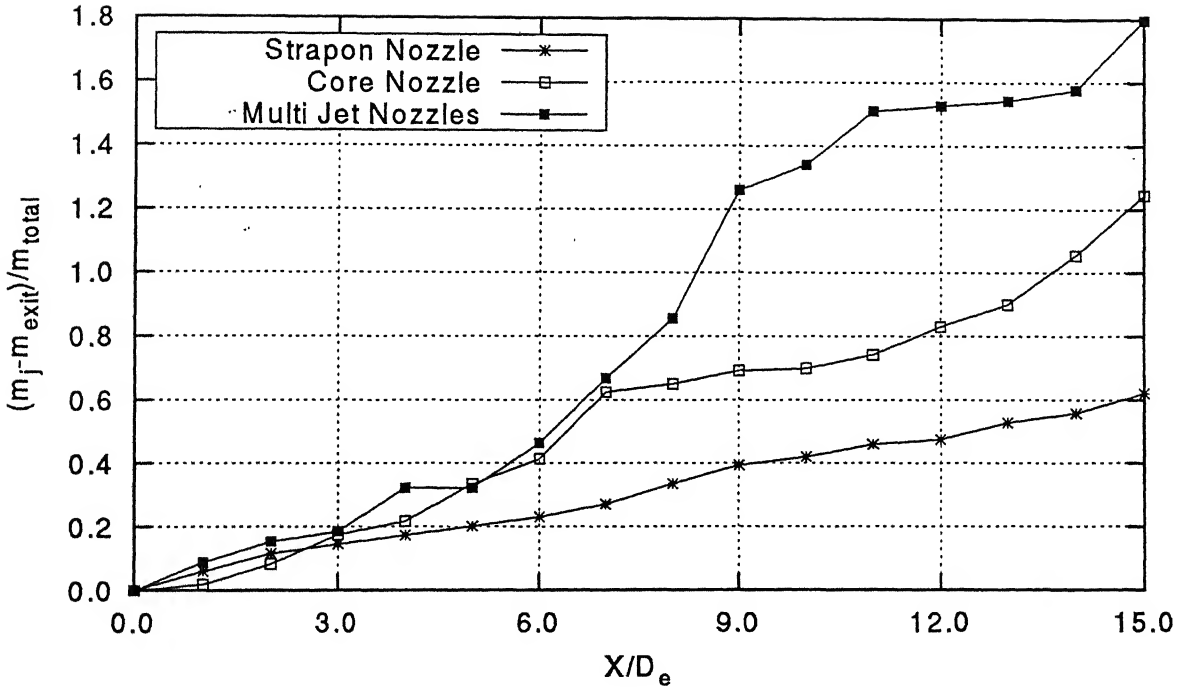

Fig. 3.14 Mass entrainment profile at NPR4

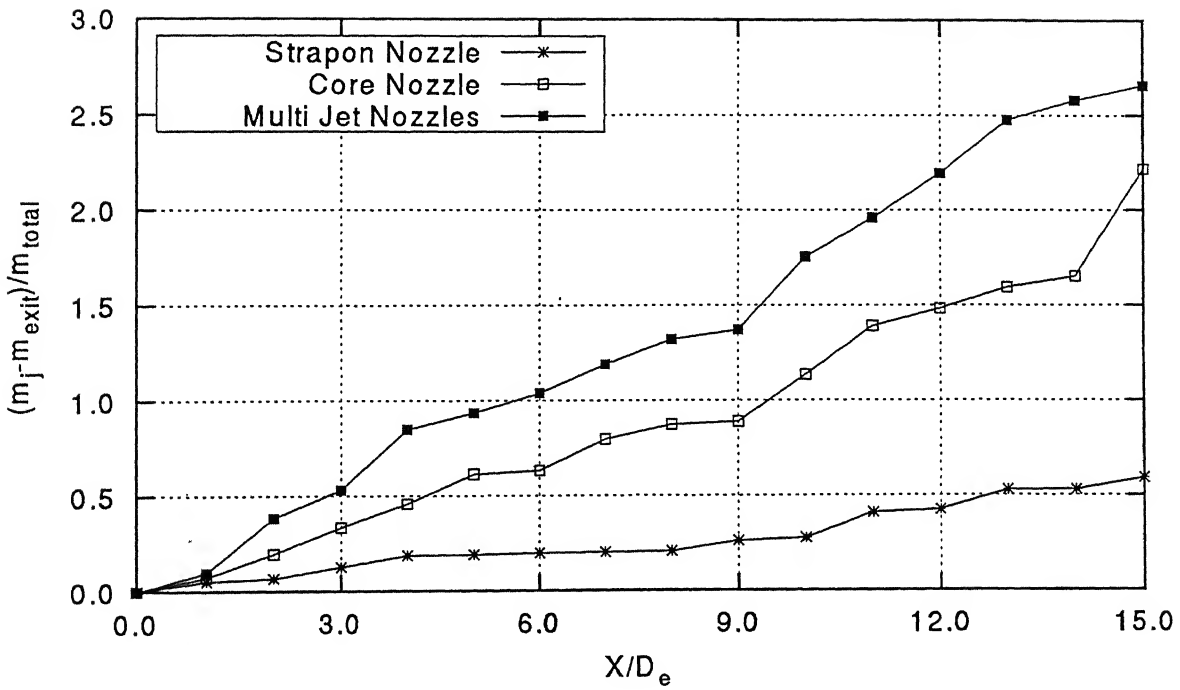

Fig. 3.15 Mass entrainment profile at NPR5

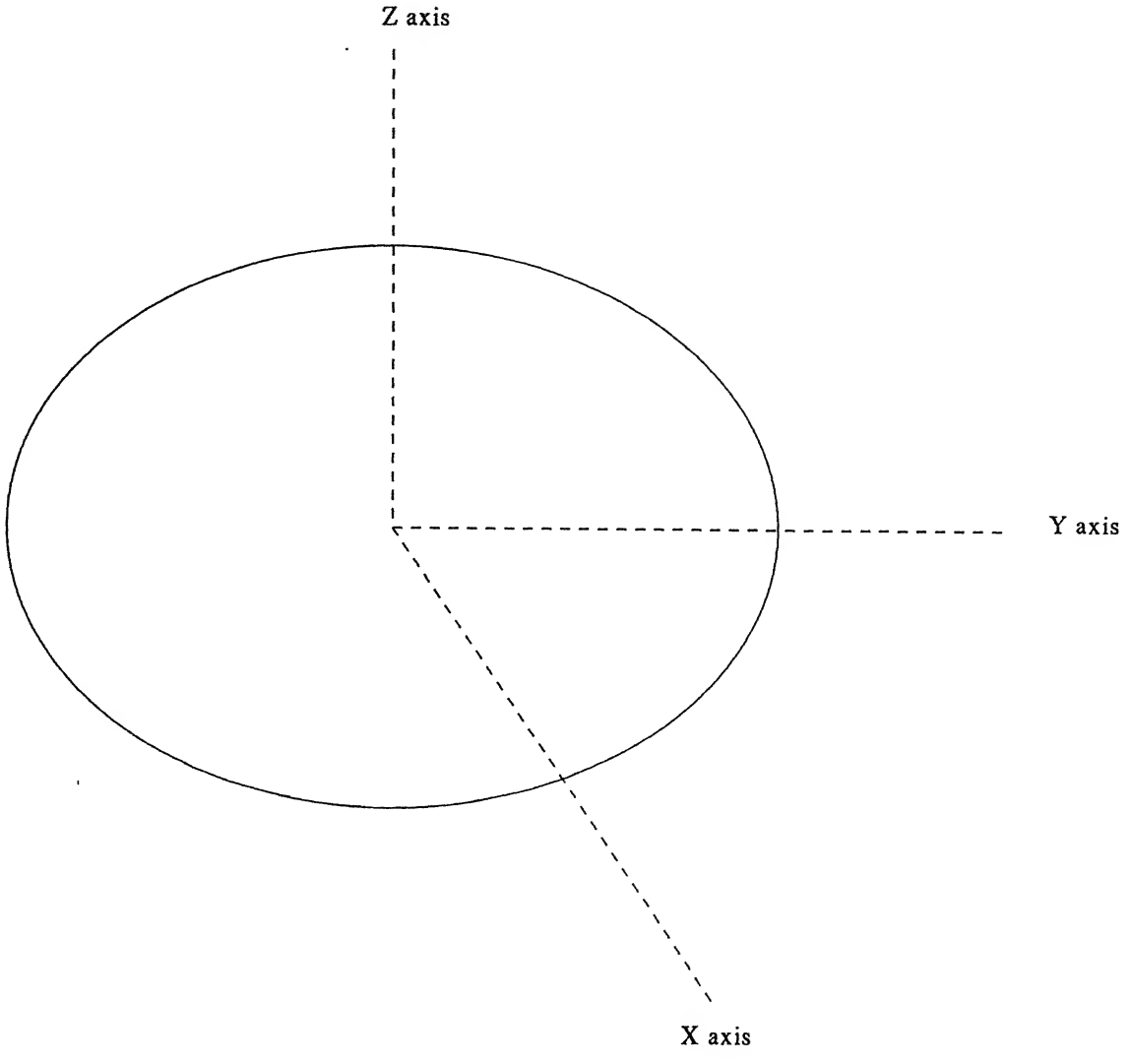

Schematic of coordinate axes

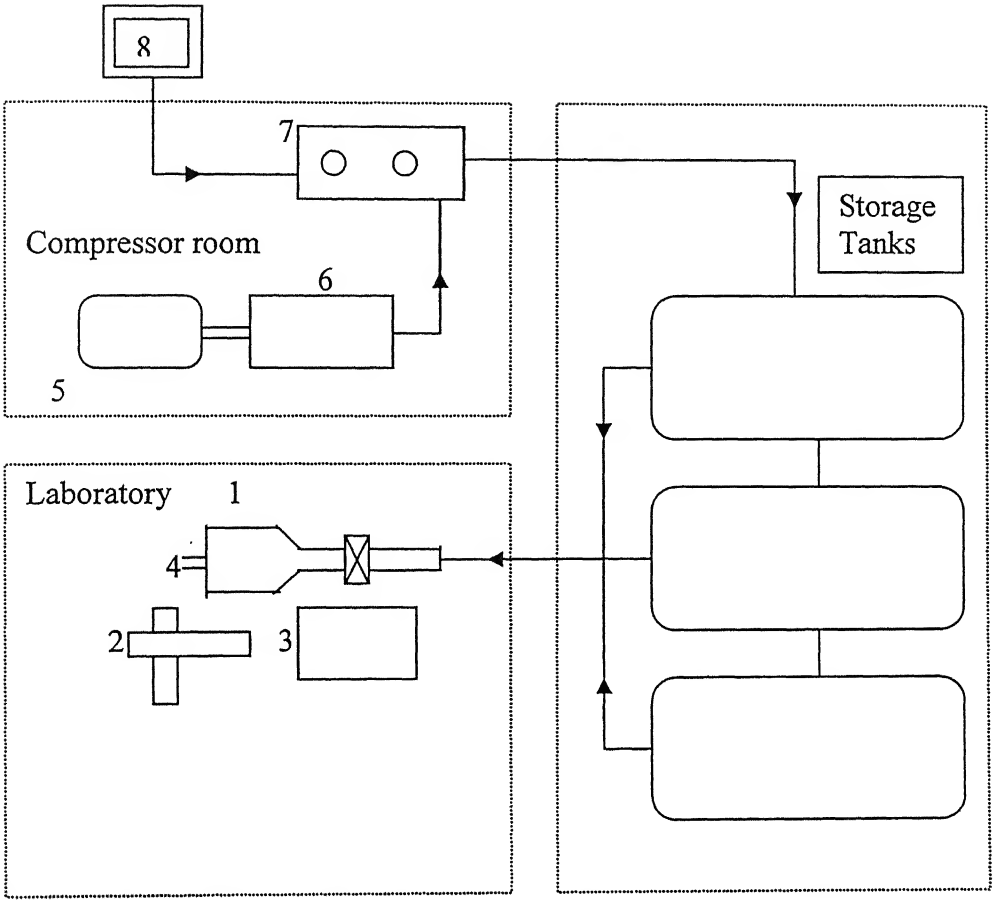

1. Settling chamber
2. Traversing system
3. Pressure measurement instrument (transducer)
4. Model
5. 150hp electric induction motor
6. Ingersoll Rand 2-stage Reciprocating compressor
7. Activated Charcoal Filter and Silica Gel drier units
8. Water-cooling unit

Schematic view of lab facility

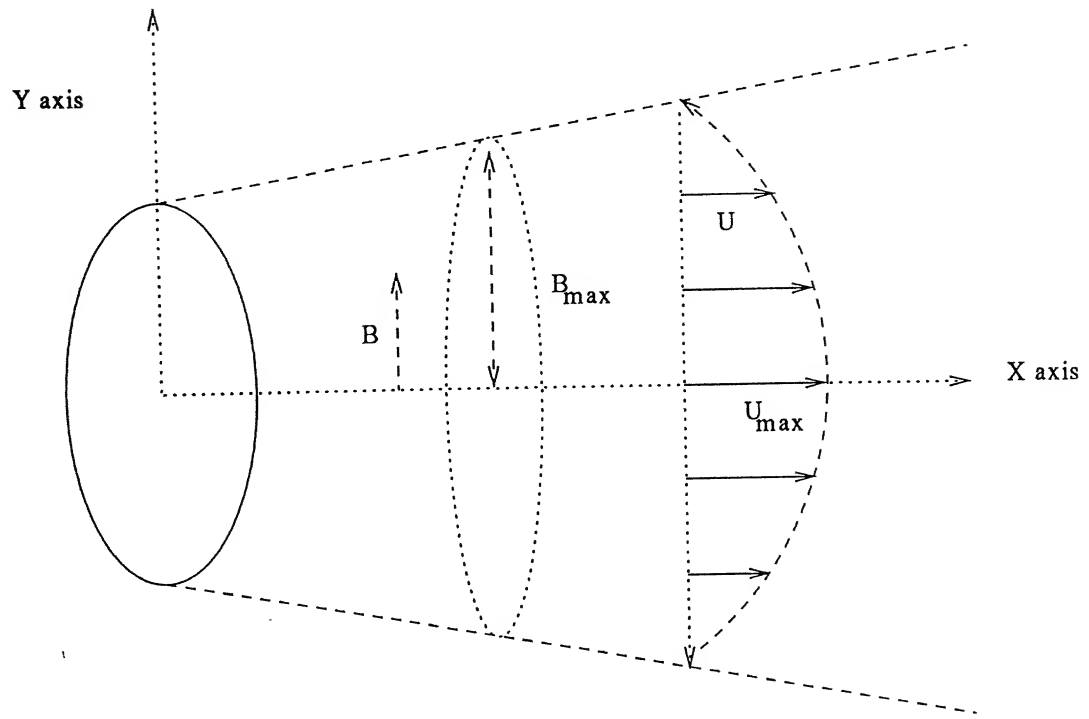

Schematic showing B and B_{max} and U and U_{max}